



Effect of Halite (NaCl) on Sandstone permeability and well injectivity during CO₂ storage in Saline Aquifers

Ramadan Makhzoom Benashor

(B.Sc. Eng., M.Sc.)

School of Computing Science and Engineering
Petroleum Technology and Spray Research Groups
University of Salford
Manchester, UK

Submitted in Partial Fulfilment of the Requirements of the Degree of Doctor of Philosophy, September 2017

Abstract

Carbon dioxide capture and storage (CCS) is one of the widely discussed options for decreasing CO₂ emissions. This method requires the techniques for capturing purification of anthropogenic CO₂ from fossil-fuel power plants, subsequent compression and transport, and, ultimately, its storage in deep geological formations. Due to the high formation salinity, there is a substantial concern about the near well bore formation dry out as a result salt precipitation in the form of halite (NaCl). The focus was on one of the important physical mechanisms of CO₂ injection into deep saline aquifers. The salt (mainly halite) will eventually fully saturate the brine causing the salt to start precipitating as solids. This solid precipitation could significantly decrease the porosity and permeability of the porous medium.

The investigations, in this study, were carried out in three distinct parts: (i) core flooding tests for different sandstone core samples (Bentheimer, Castlegate and Idaho Gray) which were saturated with different brine concentrations to measure the CO₂ flow rate for different injection pressures, (ii) utilising simulated experimental apparatus to estimate the porosity and permeability of the core samples and (iii) Qualitative analysis of porosities using CT scanner.

In Part (i), it was found that the CO₂ flow rates vary from 0.4 to 6.0 l/min when using brine solution concentrations of 10, 15, 20 and 26.4% for core flooding tests of the studied sandstone core samples before diluting concentrations with sea water (3.5%), and after diluting by sea water the flow rates vary from 0.6 to 7.0 l/min. The flow rate increase indicates that the injectivity will increase.

In part (ii), Helium Gas Porosimeter was used to calculate the porosity of each core sample and the results showed for Bentheimer, Castlegate and Idaho Gray 20.8 %, 25.6 % and 23.4 % respectively. Liquid saturating method was also used to calculate the porosity of each core sample and the results showed 23.6% for Bentheimer, 24.4% for Castlegate and 22.4% for Idaho Gray. Regarding the permeability impairment investigations for both brine permeability and gas permeability, the permeability damage took place due to the salt precipitation (NaCl) phenomenon. For brine permeability, the damage percentage of Bentheimer, Castlegate and Idaho Gray was 40%, 42% and 47%. For gas permeability the reduction due to dry out of saturated samples with 20% brine solution were calculated as 34.5% for Bentheimer, 42% for Castlegate and 50.2% for Idaho Gray.

Finally, in part (iii), CT Scann was used to determine each core sample porosity and the results showed 20.7% for Bentheimer, 24.3% for Castlegate and 24.6% for Idaho Gray

Acknowledgements

I would like to express my gratitude and sincere thanks to Dr Amir Norian and Prof G.G. Nasr for their helpful advice, endless support and help throughout the course of this work. Their guidance has been fruitful in steering the direction of this project.

My wife was my greatest support during the last few years. Her loyalty, faithfulness, patience and positive enthusiasm provided the much-needed strength during the preparation of this thesis. I am extremely grateful for everything she did including spending much of her time taking care of our lovely children Abedalbadie, Reham and Fatima so to allow me the time for my research. My acknowledgement goes to the scholarship from Libyan High Educational studies through the cultural section of Libyan embassy in London, UK.

In addition, I would like to thank all the staff members and my colleagues at the Petroleum and Gas Engineering department, particularly Dr Enyi Godpower, Dr A.J. Abbas, Mr Aminu Abba Yahaya and Mr Alan Mapin for their valuable and constant support.

Declaration

I, Ramadan Makhzoom Benashor, declare that this dissertation report is my original work, and has not been defer to elsewhere for any award. Any section, part or phrasing that has been used or copied from other literature or documents copied has been clearly referenced at the point of use as well as in the reference section of the thesis work.

Signature

Date / /

Approved by

Dedication

This work is dedicated to

My remarkable wife, Nesren Flah

And

My smart children

Abedalbadie, Reham and Fatima

And my wonderful mother, Fatima Ali

List of Publications

- 1- Benashor, R. M. Z., Nourian, A., Nasr, G., & Enyi, G. C. (2016). The Effects of Dissolved Sodium Chloride (NaCl) on Well Injectivity during CO₂ Storage into Saline Aquifers, 6 (2), 11–22.
- 2- Benashor, R. M. Z., Nourian, A., Nasr, G., & Abbas, A. J. (2016). Well Injectivity Management during Geological Carbon Sequestration Activity, 6(2), 11–22.
- 3- R .M. Benashor, A. Nourian and G G Nasr, University of Salford, UK. Experimental investigations to study the effects of halite (NaCl) precipitation on sandstone permeability and injectivity during CO₂ storage into saline aquifers. 6th International Conference on Petroleum Engineering ,June 29-30, 2017 ,Madrid, Spain

List of symbols and abbreviations

CCS	Carbon dioxide capture and storage
GHG	Greenhouse gases
IPCC	Intergovernmental panel on climate change
IEA	International energy agency
CO ₂	Carbon dioxide
PPM	part per million
Ppg	Ib/gallon
Gt	Giga ton
Mt	Mega ton
EOR	Enhanced Oil Recovery
MPa	Mega Pascale
mD	Milli Darcy
CAB	CO ₂ alternating brine
CBM	coal bed methane
Mt	mega tonnes
t/day	ton /day
Mt/yr	mega tonne per year
NaCl	Sodium chloride
H ₂ S	Hydrogen sulphide
ROI	Region of interest
CT	Computed Topography
NOX	Nitrous oxide
CH ₄	Methane
V _p	Pore volume of the core sample
V _b	Bulk volume of the core sample
V _g	Grain volume of the core sample
K	Rock permeability
ϕ	Rock porosity

Conversion Table

1 D	1000 millidarcy
1 ton	one metric ton = 1000 kg
1 mt	one mega ton = 10^6 ton
1 Gt	one giga ton = 1000 mt = 10^9 ton
1 atm	14.6959 psi
1 atm	101325.01 Pascal
1 atm	1.0132501 bar
1 bar	14.50377 psi
Poise	100 cp
1 m	100 cm
1 ft	30.48 cm
1 inch	2.54 cm

Table of Contents

Abstract	i
Acknowledgements	ii
Declaration	iii
Dedication	iv
List of Publications	v
List of symbols and abbreviations	vi
Table of Contents	ix
List of Figures	xiii
List of Tables	xvi
Chapter 1: Introduction	1
1.1. Risks associated with CO ₂ underground storage	3
1.3. Overall Aim	4
1.4. Objectives	4
1.5. Thesis structure	4
Chapter 2: Literature Review	6
2.1 Overview.....	6
2.2 Sources of CO ₂	7
2.3 Global Warming and CO ₂ Emissions.....	7
2.4 CO ₂ Storage Options.....	9
2.5 CO ₂ Storage into Saline Aquifer.....	9
2.5.1 Why Saline Aquifers.....	10
2.5.2 Reservoir Properties of Saline Aquifers.....	11
2.6 Trapping Mechanism	12
2.7 CO ₂ Injection Approaches	13
2.8 Present and Scheduled CO ₂ Projects.....	13

2.9	Risks Posed by CO ₂ Geological Storage.....	13
2.9.1	Salt Precipitation and Dry out in the near- Wellbore.....	14
2.10	Approaches to Restore the Well Injectivity	16
2.10.1	Fracture managements	17
2.10.2	Perforation.....	17
2.10.3	Acid management	18
2.11	Optimisation of CCS Costs.....	18
2.12	Rock properties	19
2.13	Classification of Porosity	19
2.13.1	Effective Porosity.....	20
2.13.2	Absolute Porosity.....	20
2.14	Permeability	21
2.15	Saturation	22
2.16	Well Injectivity	22
2.17	CT scan	24
2.18	Summary.....	25
Chapter 3: Experiment Apparatus and Methodology of Data Processing		26
3.1.1	Salinity Measurement	30
3.1.2	Viscosity Measurement.....	31
3.1.3	Density	33
3.1.4	Errors and Accuracy	35
3.2	PHASE-I: Core Flooding Tests	35
3.2.1	Experimental set up.....	37
3.2.2	Methodology of measurement	39
3.2.3	Errors and Accuracy.....	41
3.3	Phase-II: Porosity and Permeability.....	41

3.3.1	Description of Apparatus	41
3.3.2	Methodology of Measurement	44
	Measurement of Bulk Volume	46
	Measurement of Pore Volume	46
	Measurement of Grain Volume.....	46
3.4	PHASE-III: CT scan	57
3.4.1	Equipment description and principles of X-Ray inspection	57
3.4.2	Methodology of measurement	60
3.4.3	Errors and Accuracy.....	66
3.5	Chapter Summary	67
Chapter 4: Results and Discussion		68
4.1	Sample preparation	68
4.1.1	Salinity	69
4.1.2	Viscosity	69
4.1.3	Density	69
4.1.4	Density, Viscosity and Salinity relationships.....	70
4.2	PHASE – I Core flooding tests	72
4.2.1	Core flooding tests for Bentheimer sandstone	72
4.2.2	Core flooding tests for Castlegate sandstone	78
4.2.3	Core flooding tests for Idaho gray sandstone.....	83
4.3	PHASE-II Porosity & Permeability	89
4.3.1	Porosity	89
4.3.2	Permeability	93
4.3.3	Effect of Salinity on liquid Permeability	94
4.3.4	Effect of Salinity on gas Permeability	98
4.4	The Porosity and the Brine Permeability Relationship	103

4.4.1	The Porosity and the Brine Permeability Relationship	104
4.4.2	The Porosity and the gas Permeability Relationship.....	105
4.5	PHASE III: CT scanning	106
4.5.1	CT scan of Bentheimer sandstone.....	106
4.5.2	CT scan of Castlegate sandstone.....	106
4.5.3	CT scan of Idaho gray sandstone	108
4.5.4	Images and visualisation of the scanned core sample.....	109
4.5.5	CT Scan Visualisation and Quantification of Salt Precipitation.....	111
4.5.6	Porosity determination summary	112
4.6	Summary.....	113
Chapter 5: Conclusion and Recommendations		115
5.1	Conclusions.....	115
5.2	Future work and recommendation	116
References.....		117
APPENDIX – A: Journal Publications		120

List of Figures

Figure 2.1 : The CCS process	7
Figure 2.2 : Origin of anthropogenic CO ₂ emissions	8
Figure 2.3 : Options for CO ₂ storage in deep geological underground formations [1]	9
Figure 2.4 : Trapping mechanisms for CO ₂ storing in deep saline aquifers A) structural trapping, B) capillary trapping, C) dissolution and D) mineral trapping	12
Figure 2.5 : Schematic of CO ₂ /water mutual dissolution in porous media [39]	15
Figure 2.6 : Pressure and time relationship under various CO ₂ injection rates	17
Figure 2.7 : the scheme of cost optimisation of CCS[30]	18
Figure 2.8 : (a) Cubical packing, (b) rhombohedra, (c) cubical packing with two grain sizes, and (d) typical sand with irregular grain shape	19
Figure 2.9 : Permeability is an indication of how easy it is for the fluids to flow through the medium [47]	22
Figure 3.1: thesis work plan	27
Figure 3.2: Different Types of Sandstones (a) Bentheimer, (b) Castlegate and (c) Idaho Gray	29
Figure 3.3: Brine solutions in (wt %)	30
Figure 3.4 : Refractometer gives the salinity in (wt %)	31
Figure 3.5 : Electronic Rotational Viscometer	32
Figure 3.6 : Mud Balance scale device	34
Figure 3.7 : the experimental set up diagram	37
Figure 3.8 : Experimental set up	38
Figure 3.9 : Shows the fancher core holder (1"x1")	39
Figure 3.10 : PORG – 200	42
Figure 3.11 : PERL – 200	43
Figure 3.12 : PERG – 200	44
Figure 3.13: Definition of Darcy's law	52
Figure 3.14 : Microfocus – nanofocus	58
Figure 3.15 : CT scanner at Salford University	59
Figure 3.16 : Histogram and scan optimiser for Bentheimer sandstone	61
Figure 3.17 : Properties of defect detection analysis for Bentheimer sandstone core sample	62
Figure 3.18 : Flow chart of sectioning to obtain 3D images of porous media [54]	65
Figure 4.1: Brine density and brine viscosity	71

Figure 4.2: Brine salinity and brine density	71
Figure 4.3 :Brine salinity and brine density	72
Figure 4.4: Core flow test results for Bentheimer sandstone (10 % NaCl + saturated with 3.5 %).....	74
Figure 4.5: Core flow test results for Bentheimer sandstone (15 % NaCl + saturated with 3.5 %).....	75
Figure 4.6 : Core flow test results for Bentheimer sandstone (20 % NaCl + saturated with 3.5 %).....	76
Figure 4.7: Core flow test results for Bentheimer sandstone (10 % NaCl + saturated with 3.5 %).....	78
Figure 4.8 : Core flow test results for Castlegate sandstone (10 % NaCl + saturated with 3.5 %).....	79
Figure 4.9 : Core flow test results for Castlegate sandstone (15 % NaCl + saturated with 3.5 %).....	81
Figure 4.10 : Core flow test results for Castlegate sandstone (20 % NaCl + saturated with 3.5 %).....	82
Figure 4.11 : Core flow test results for Castlegate sandstone (26 % NaCl + saturated with 3.5 %).....	83
Figure 4.12 : Core flow test results for Idaho gray sandstone (10 % NaCl + saturated with 3.5 %)	85
Figure 4.13: Core flow test results for Idaho gray sandstone (15 % NaCl + saturated with 3.5 %	86
Figure 4.14 : Core flow test results for Idaho gray sandstone (20 % NaCl + saturated with 3.5 %)	87
Figure 4.15 : Core flow test results for Idaho gray sandstone (20 % NaCl + saturated with 3.5 %)	88
Figure 4.16: Porosity Measurement using PORG- 200	90
Figure 4.17 : Porosity Measurement using Liquid Saturating Method	93
Figure 4.18: NaCl concentration % & permeability Damage % (Bentheimer sandstone).....	95
Figure 4.19: NaCl concentration % & permeability Damage % (Castlegate sandstone).....	96
Figure 4.20: NaCl concentration % & permeability Damage % (Idaho gray sandstone)	97
Figure 4.21: the permeability alteration and NaCl % for Bentheimer sandstone	100
Figure 4.22: the permeability alteration and NaCl % for Castlegate sandstone	101
Figure 4.23 : the permeability alteration and NaCl % for Idaho gray sandstone	102
Figure 4.24: the relationship between the porosity and brine permeability	104
Figure 4.25: the relationship between the porosity and gas permeability of the studied rocks.....	105
Figure 4.26: Histogram and scan optimiser for Castlegate sandstone.	107
Figure 4.27: Properties of defect detection analysis for Castlegate sandstone core sample.	107
Figure 4.28: Histogram and scan optimiser for Idaho gray sandstone.....	108
Figure 4.29: Properties of defect detection analysis for Idaho gray sandstone core sample.....	109
Figure 4.30: Visualisation of the pore spaces for porosity calculation (Bentheimer sandstone), Porosity = 20.7 %	110
Figure 4.31: Visualisation of the pore spaces for porosity calculation (Castlegate sandstone), Porosity = 24.3 %	110

Figure 4.32: Visualisation of the pore spaces for porosity calculation (Idaho gray) sandstone),
Porosity = 24.6 %..... 111
Figure 4.33: Wall thickness and 3D image of the saturated brine Idaho gray core sample 112

List of Tables

Table 2.1 : Main criteria for site selection[16].....	11
Table 2.2 : the worldwide storing capacities evaluations[17].....	12
Table 2.3 : Storage rates of three industrial-scale CO ₂ sequestration projects[20].....	13
Table 2.4 : Classification of reservoir permeability.....	21
Table 3.1 : Water salinity based on dissolved salts.....	33
Table 3.2 : treatment specifications[37].....	36
Table 3.3: Sample data of core flooding tests.....	40
Table 3.4 : Errors and accuracy of the rig components	41
Table 3.5 : Spread sheet for grain volume calculation.....	47
Table 3.6 : porosity determination by liquid saturating method (Bentheimer sandstone	48
Table 3.7: Liquid permeability spread sheet for Idaho gray sandstone sample	53
Table 3.8: Gas permeability spreadsheet for Idaho gray sandstone sample.....	54
Table 3.9: Porosity and permeability sample results	55
Table 3.10 : initial Brine Permeability and Initial Gas permeability	55
Table 4.1: Dimensions of the core samples used in the study	68
Table 4.2 : Brine Salinity (wt %).....	69
Table 4.3: Brine viscosity	69
Table 4.4 : Brine density and specific gravity	70
Table 4.5: Brine viscosity and density.....	71
Table 4.6: Brine salinity and density	71
Table 4.7: Brine viscosity and salinity.....	72
Table 4.8 : Core flooding test results for Bentheimer sandstone (10 % NaCl + saturated with 3.5 %) 73	
Table 4.9: Core flow test results for Bentheimer sandstone (15 % NaCl + saturated with 3.5 %).....	74
Table 4.10 : Core flow test results for Bentheimer sandstone (20 % NaCl + saturated with 3.5 %)....	75
Table 4.11: Core flow test results for Bentheimer sandstone (26 % NaCl + saturated with 3.5 %).....	77
Table 4.12: Core flow test results for Castlegate sandstone (10 % NaCl + saturated with 3.5 %).....	79
Table 4.13: Core flow test results for Castlegate sandstone (15 % NaCl + saturated with 3.5 %).....	80
Table 4.14: Core flow test results for Castlegate sandstone (20 % NaCl + saturated with 3.5 %).....	81
Table 4.15 : Core flow test results for Castlegate sandstone (26 % NaCl + saturated with 3.5 %).....	82
Table 4.16: Core flow test results Idaho gray sandstone (10 % NaCl + saturated with 3.5 %).....	84
Table 4.17: Core flow test results Idaho gray sandstone (15 % NaCl + saturated with 3.5 %).....	85

Table 4.18 : Core flow test results Idaho gray sandstone (20 % NaCl + saturated with 3.5 %)	86
Table 4.19 : Core flow test results Idaho gray sandstone (26 % NaCl + saturated with 3.5 %)	87
Table 4.20 : core samples porosities by Helium gas porosimeter	90
Table 4.21 : porosity determination spread sheet by liquid saturating method	92
Table 4.22 : Bentheimer sandstone core samples brine permeability	95
Table 4.23 : Castlegate sandstone core samples brine permeability	96
Table 4.24 : Idaho gray core samples brine permeability	97
Table 4.25 : effect of NaCl concentrations on gas permeability	99
Table 4.26: Gas permeability alteration of Bentheimer sandstone	99
Table 4.27 : Gas permeability alteration of Castlegate sandstone	100
Table 4.28 : Gas permeability alteration of Idaho gray sandstone	101
Table 4.29 : Liquid and gas permeability damage due to halite precipitation.	103
Table 4.30 : Porosity and brine permeability of the core samples	104
Table 4.31 : Porosity and gas permeability of the core samples	105
Table 4.32 : Shows comparison between porosity computed by helium gas method (A), liquid saturating method (B) and CT scan method (C)	112

Chapter 1: Introduction

Currently the energy that uses in daily life comes from four major sources:

- i. Fossil fuels (i.e. oil, coal and gas)
- ii. Nuclear power
- iii. Hydropower
- iv. New Regenerative Power (i.e. wind, solar and waste).

Regenerative power sources are probably the cleanest sources of energy but, currently, they cannot support major industries due to the problem of energy storage. Hydropower is also very clean and favourable source of energy, however its availability is quite limited and the major barriers have already been built where possible. Furthermore, the storage of nuclear powers' waste for a couple of thousand years is the main problem of using this type of energy source. Mainly CO₂ is one of the greenhouse gases that are responsible for climate change. The consequences and gravity of a changing climate are currently not well understood, however the price of the worst scenarios to come true is seem to be so high that politicians have agreed on a system of trading CO₂ emission certificates, which will make the emission of CO₂ expensive and hopefully will help to avoid major environmental changes. Figure 1.1 shows CO₂ emissions of industry and power. Saline formations are very deep, porous and permeable rocks holding water that is useless because of its high salt or mineral content. Saline aquifers represent promising way for CO₂ sequestration. Saline aquifers can be sandstones or lime stones, but to be a potential reservoir for CO₂ storage they must have large enough size, sufficiently high porosity and permeability, adequate depth: Usually only aquifers below 800 m below sea level are considered for CO₂ storage. In addition to a reservoir rock, an overlying "cap rock" that is impermeable to the passage of CO₂ is required

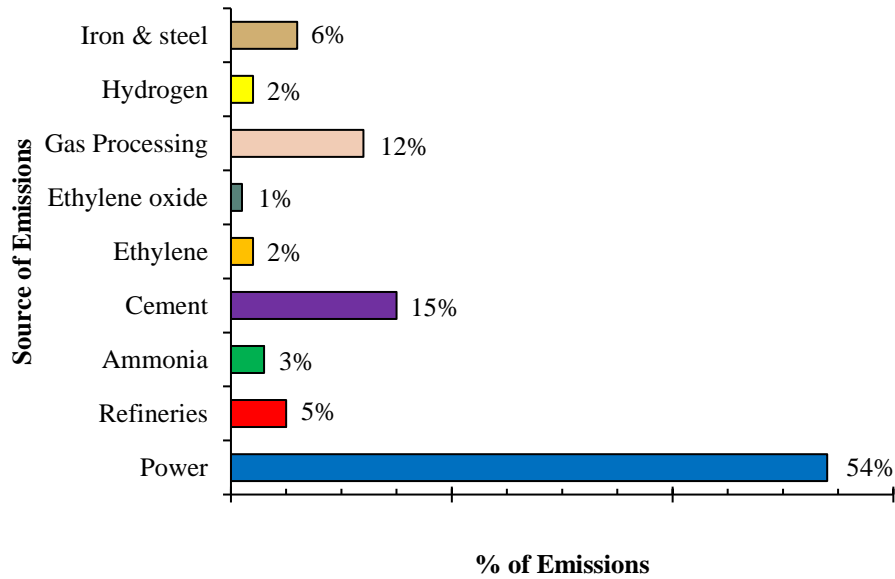


Figure 1.1: CO₂ Emissions of Industry and Power[1]

Most researches have focused on carbon dioxide due to the large quantity; it represents the highest percentage of the total greenhouse gas emissions. A promising method to reduce GHG emissions is geologically store CO₂ in the subsurface. Geological storage is the process where CO₂ is captured and subsequently injected into a geological formation in a supercritical state where it is trapped by one or more trapping mechanisms. This prevents CO₂ from leaking through geological seals. Project monitoring and simulation studies are conducted before, during and after injection to prove that the carbon dioxide can be trapped within a geological time scale (thousands to millions of years) without leaking into overlying groundwater reserves, oceans or into the atmosphere. During this period, a fraction of the CO₂ will ultimately dissolve in the formation water and promote geochemical reactions with the surrounding minerals. These geochemical reactions may alter the cap rock properties and may thus affect the cap rock integrity. Figure 1.2 shows the contribution of different greenhouse gases to global warming

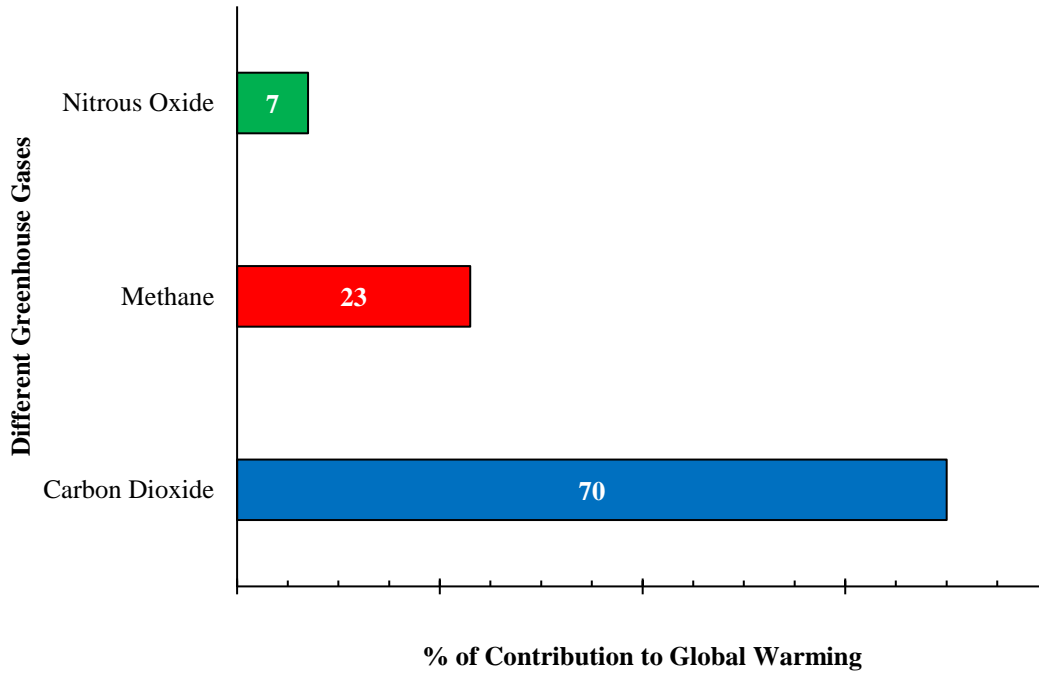


Figure 1.2: The Contribution of Different Greenhouses Gases to Global Warming[2]

1.1. Risks Associated with CO₂ Underground Storage

The risks of CO₂ storage in a geological reservoir can be divided into five categories [3]:

- CO₂ leakage: CO₂ passage out of the reservoir to other formations.
- CH₄ leakage: CO₂ injection might cause CH₄ present in the reservoir to migrate out of the reservoir to other formations and possibly into the atmosphere.
- Ground movement: Subsidence or uplift of the earth surface because of pressure variations
- Displacement of brine: Flow of brine to other formations caused by injection of CO₂ in open aquifers. This may promote the salt precipitation and formation dry out in the near wellbore. This research focusses on the effect of NaCl precipitation on the injectivity.

1.2. Contribution to Knowledge

The contribution to this research is to examine the consequence of the salt precipitation (NaCl) on the injectivity during CO₂ injection into Saline aquifers, utilising the designated Experimental set up and suggest solution to avoid the consequences of salt precipitations.

1.3. Overall Aim

The aim of this work is to examine the effect of Sodium Chloride (NaCl) precipitation on the injectivity and study how the dilution of brine concentrations by low salinity water (i.e. seawater 3.5 wt %) could assist in improving the injectivity and avoid the pressure build up problems.

1.4. Objectives

- To carry out core flooding tests for (Bentheimer, Castlegate and Idaho gray) sandstone core samples, which were saturated with dissimilar brine solutions, and examine the effect of brine concentrations (NaCl wt %) on the injectivity.
- To utilise the apparatus for estimating the porosity, the liquid and gas permeability of the stated core samples.
- To analyse qualitatively the porosities of the stated core samples using CT scan.

1.5. Thesis Structure

The thesis contains the following FIVE Chapters:

Chapter 1: Introduction

Chapter 2: This Chapter presents a survey of literatures. It also covers the definitions, brief history and risk associated with the CO₂ storage

Chapter 3: This Chapter demonstrates the experimental apparatus, method of data processing, which were carried out in this investigation.

Chapter 4: This Chapter discusses the results obtained from the experiment

Chapter 5: This Chapter summarises the presented work in this study. The main contribution is also highlighted with recommendations for future work

Chapter 2: Literature Review

2.1 Overview

Worldwide heating is observed as one of the maximum persistent ecological topics fronting current humanity. This increase in the typical external temperature has been accredited to the greenhouse result, which has been impaired by the overall rise in atmospheric CO₂ is the main greenhouse gas[4]. To struggle these worries, the decrease of carbon dioxide releases with new technologies is needed. One such method comprises the injection of CO₂ into geological formations through a method known as carbon capture and storage (CCS)[5]. This chapter reviews the physical and chemical mechanisms leading the injection of CO₂ into underground systems. Greenhouse gas releases have become a hazard for the earth and current culture by means of universal warming. Among others, a major greenhouse gas, CO₂, has been identified as the major provider in terms of increasing usual surface temperature of the world.

The options to cut CO₂ emissions that can be implemented at the necessary scale using current technology include:

1. Increasing energy efficiency or reducing consumptions.
2. Use of less carbon intensive fuels.
3. Practise of renewable energy bases and / or nuclear energy.
4. Enhancement of natural sinks.
5. Capture the carbon and dispose in engineered sinks.

Geological storage is defined as the procedure of injecting CO₂ into geologic formations for obvious resolution of dodging atmospheric release of CO₂, this possibly the most important near period choice. The charge of attaining bottomless drops in CO₂ emissions over the subsequent few periods is promised to be reduced by geological storage. Figure 2.1 shows the CCS process[6] .

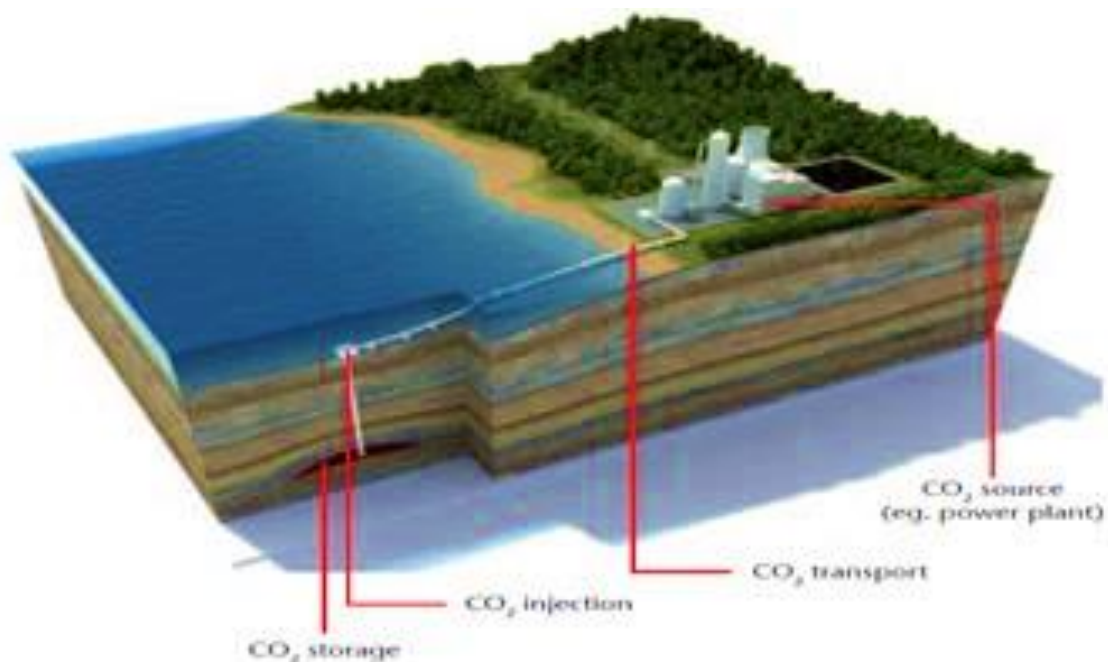


Figure 2.1 : The CCS process

2.2 Sources of CO₂

The chief cause of anthropogenic carbon dioxide (CO₂) release is the burning of fossil fuels. Other causes are burning of biomass-based fuels in certain industrial procedures, such as the manufacture of hydrogen, ammonia, iron and steel, or cement. Studies demonstrate that the power and industry areas joint control present worldwide CO₂ releases, accounting for about 60% of entire CO₂ releases [7].

2.3 Global Warming and CO₂ Emissions

Universal warming is produced by the release of greenhouse gases 72 % of the entirely produced gases are CO₂, 18% Methane, 9 % Nitrous oxide (NOX) [8]. CO₂ releases are the greatest significant reasons of worldwide warming. CO₂ is certainly shaped by boiling oil, natural gas, organic – diesel, petrol, and ethanol. The releases of CO₂ have been dramatically enlarged in the last 50 years and are still rising by almost 0.3% each year. Growing worldwide temperatures are causing a wide choice of variations. Sea levels are increasing due to warm air development of the ocean, in addition to melting of land ice. There are two main effects of worldwide heating :(1) Rise of temperature on the temperature by about (3 – 5 ° C) by the year 2100 (2) Rise of sea level by at least 25 meters (82 ft) by year 2100. It is well known that a rise in atmospheric concentration of CO₂ leads to a rise in the mean

atmospheric temperature, that phenomenon is called global warming. If nothing is done to stabilise CO₂, the concentration will reach about 500 ppm within the next 50 years.

Carbon dioxide (CO₂) is a greenhouse gas, and thus a rise in atmospheric concentration of CO₂ leads to a rise in the mean atmospheric temperature, a phenomenon that is known as global warming. Increasing temperatures have been documented around the world, with the largest anomalies being recorded in the Arctic and Antarctic regions [9] . If nothing is done to stabilise CO₂ levels, the concentration will reach about 500 ppm within the next 50 years. This will lead to an increase in the mean global temperature by 4 to 6 ° C within that same period [9] It is believed that global warming will have dramatic environmental consequences, such as rising sea levels, loss of fragile ecosystems, increased intensity of meteorological phenomena, and increased frequency of extreme droughts and floods [10] . In order to mitigate the effects of global warming, a massive effort must be undertaken to manage carbon emissions and significantly reduce the amount of CO₂ that enters the atmosphere. Figure 2.2 shows the Origin of anthropogenic CO₂ emissions[11] .

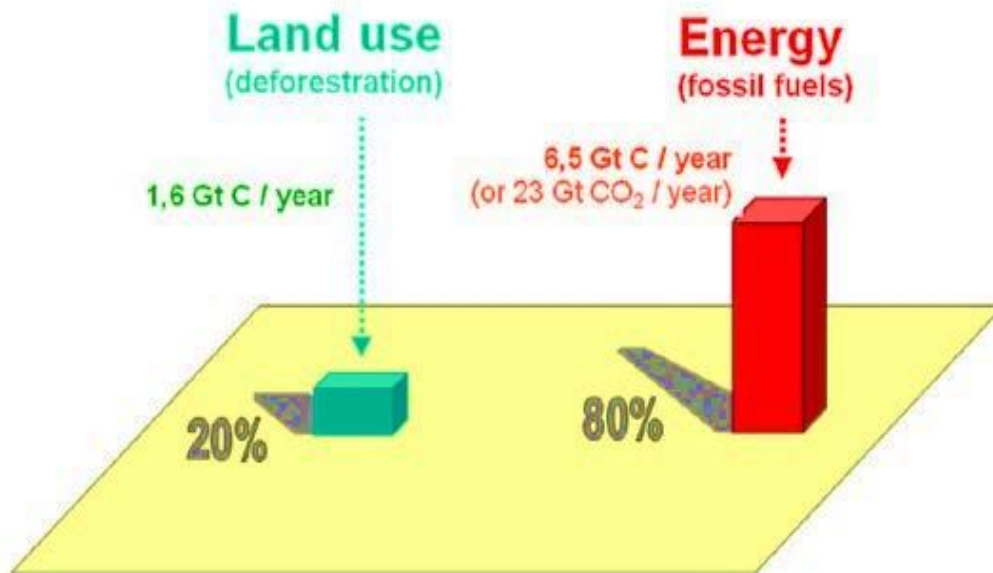


Figure 2.2 : Origin of anthropogenic CO₂ emissions

2.4 CO₂ Storage Options

As a technique of CO₂ justifying and decreasing greenhouse gas emission from the energy area [1], the underground storing or geological sequestration (geo sequestration) of CO₂ is gradually purchase respect throughout the world. The storage of CO₂ in underground formations is an attractive greenhouse mitigation choice for large reduction in atmospheric releases[12].

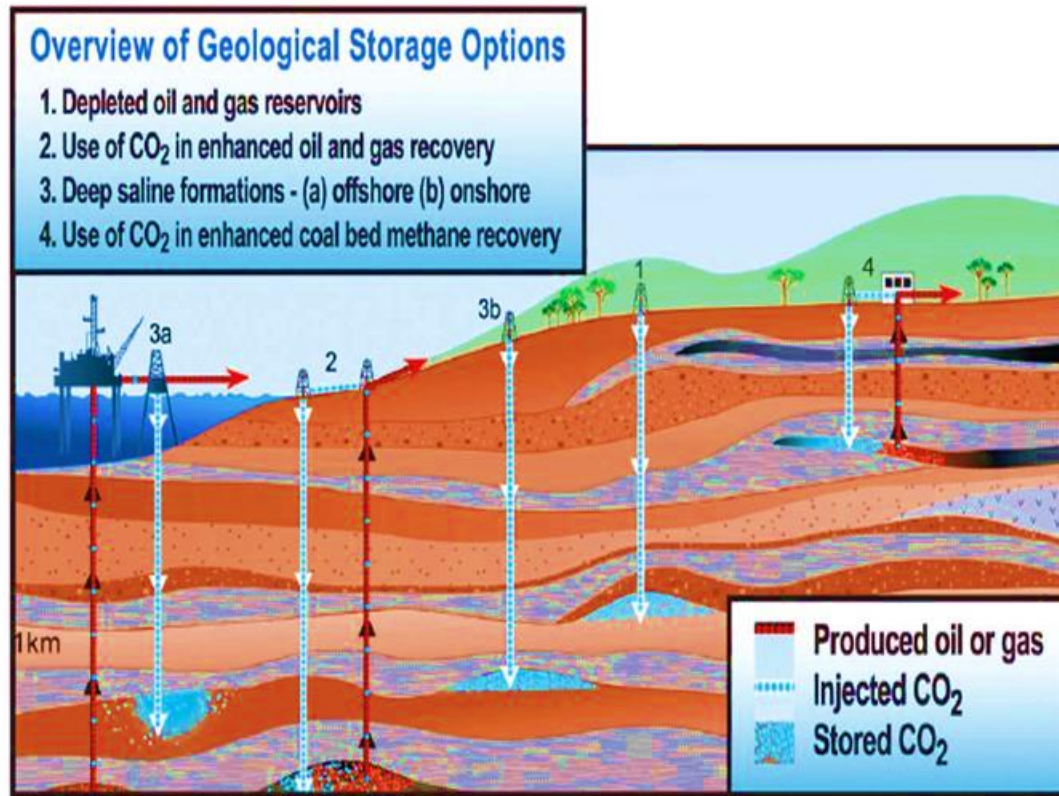


Figure 2.3 : Options for CO₂ storage in deep geological underground formations [1]

2.5 CO₂ Storage into Saline Aquifer

Deep saline formations are defined as those formations holding water with significant salts or other compounds to be measured not drinkable or safe to drink. The deposited rock formations soaked with saline formation waters that are unfitting for social intake or farming use is common. Deep saline formations have been recommended as promising storing places as of their great quantity and theoretically large volume[13] [14]. The IEA – GHG guess potential storage volume in deep formations of 8 x 10¹¹ tonnes CO₂ in northwest Europe. In Europe and North America, deep saline

formations have been used for injection of risky and safe waste and should be measured as providing useful information on sequestration[15] . For deep saline formations, one problem is that the potential efficiency of seals in avoiding pollution of shallower groundwater resources by CO₂ is regularly untested past to CO₂ injection. Additional problem is that there are often partial quantities of data obtainable for site description, needing important calculation charges. Saline aquifers are permeable, geological formations that contain very salty water and are considered a viable option for disposing of CO₂ emissions because of their large potential capacity for CO₂ storing.

The formation of the pore universe that can be employed by injected CO₂ is measured by reservoir heterogeneity, gravity separation and movement and the effectiveness of the injected CO₂ [11]. From industrial opinion, the main concerns of CO₂ disposal in aquifers are connected by:

1. The characterisation of suitable aquifer.
2. The accessible storage volume.
3. The attendance of cap rock of low permeability.
4. The injection flow rate of CO₂ during the injection [11].

2.5.1 Why Saline Aquifers

Deep saline aquifers offer no economic profit for CO₂ injection, but they are common, geographically connected with fossil fuel sources, and, since it is not necessary to identify and inject directly into closed structural traps, are likely to have huge storing volumes and appropriate injection sites in close proximity to power-plant sources of CO₂ [16].

In the United States deep saline aquifers have a greater possible storing volume than any other type of grainy formation, with approximations as high as 500 Gt of CO₂ storage [17]. A drawback with deep saline aquifers is that they are less characterised than petroleum lakes, and a complete characterisation is desired to confirm the fittingness of the aquifer planned as a storing place[18] .

Saline aquifers as storing locations for CO₂ discarding is developing technology, with an increasing figure of field trials for storing. A public problem for CO₂ discarding in aquifers is pressure preservation. taken care of before reservoir pressure reaches critical limits [19]. Deep aquifers

theoretically have CO₂-storage capacities adequate to hold many decades' worth of CO₂ emissions, but estimates of global capacity are poorly controlled, varying from 300 to 10,000 Gigatons CO₂ [20].

2.5.2 Reservoir Properties of Saline Aquifers

Saline aquifers are permeable, geological formations that contain very salty water and are considered a viable option for disposing of CO₂ emissions because of their large potential capacity for CO₂ storage.

About the ability of saline aquifers to contain CO₂ for hundreds of years, they are different from oil and gas reservoirs in that there is often not a well-defined structural trap. Instead, containment of CO₂ will depend on the existence of a confining layer, or cap rock, that extends laterally along the top of the formation. The analysis of the literature makes it clear that CO₂ storage into aquifers is feasible. The main issue with this technique is the characterisation of the aquifer, which is significant part of the entire assessment of the aquifer as a dependable long-term CO₂ storing site. Hence, the current need is to improve technologies and strategies to gather adequate information for aquifer characterisation, as well as to recognize the issues that disturb the volume of aquifers to store CO₂. Numerical simulations can help gain further insight into the CO₂ storage process and thus, the factors, which make the process successful[18]. The Suitable Aquifers should have the following characteristics:

1. Contain saline water (Salinity > 100 g/l) to dodge pampering drinkable water resources.
2. Exceed lowest permeability >500 md, porosity >20%
3. Afford storage depths of 800 m or more (where CO₂ will be in a compressed fluid phase and long way from the ground surface or seabed).
4. Require a least thickness to limit the possible storing areal foot pattern.

Table 2.1 : Main criteria for site selection[21]

High storing volume	Good porosity
High storage volume	Large reservoir
Effective injectivity	High permeability
Safe and secure storage	Low geothermal gradient & high pressure
Safe and secure storage	Adequate sealing
Safe and secure storage	Geological & hydrodynamic stability
Low costs	Good accessibility, infrastructure
Low costs	Source close to storage reservoir

Table 2.2 shows the summary of global storing volume evaluations.

Table 2.2 : the worldwide storing capacities evaluations[22]

Type of formation	Volume Estimate	Source
Depleted oil and gas reservoirs	~ 45 Gt	Stevens et al. 2001 : GHGT 6 pp. 278 - 283
Coal-bed methane reservoirs	60 – 150 Gt	Stevens et al. 1999 : GHGT 6 pp. 175 - 180
Saline aquifers	300 – 10,000 Gt	IEA Greenhouse Gas R&D programme, 1994

2.6 Trapping Mechanism

Depending on the rock formation and reservoir category, CO₂ can be surrounded in the subsurface by a number of dissimilar mechanisms [5], as discussed further in the following sections. Figure 2.4 shows different phases of CO₂ trapping mechanisms[23].

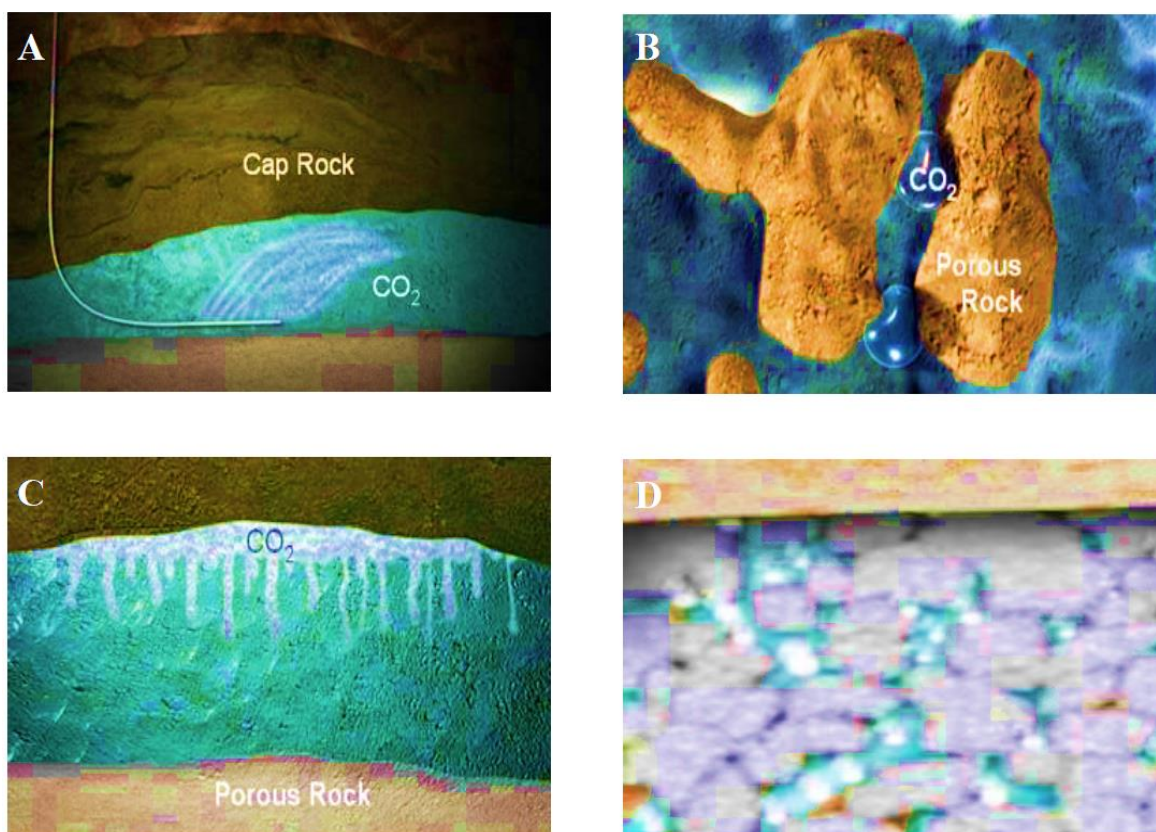


Figure 2.4 : Trapping mechanisms for CO₂ storing in deep saline aquifers A) structural trapping, B) capillary trapping, C) dissolution and D) mineral trapping

2.7 CO₂ Injection Approaches

Studies were carried out on CO₂ stream performance on the process facilities within relevant thermodynamic conditions. Main constituents and environments leading whether large volumes of supercritical CO₂ can be securely, dependably and strongly injected into and stored within a saline aquifer, were examined by modelling many injection methods. The strategies are:

1. Typical CO₂ injection
2. CO₂ – brine surface mixing
3. CO₂ – water surface mixing
4. CO₂ – alternating brine (CAB)

2.8 Present and Scheduled CO₂ Projects

There are four large-scale developments on the planet, which restore anthropogenic CO₂ [24]:

- Sleipner (Norway)
- In Salah (Algeria)
- Weyburn- Midal (Canada)
- Snohvit (Norway)

In terms of cumulative volume injected and knowledge of CO₂ storing, the most important are Sleipner and In Salah. Table 2.3 shows the largest CO₂ storage projects in the world.

Table 2.3 : Storage rates of three industrial-scale CO₂ sequestration projects[2]

Name of the project	Project starting date	Storing rate
Sleipner	Since 1996	1 million tonne CO ₂ /year
Weyburn	Since 2000	500,000 + tonne CO ₂ /year
In Salah	Since 2004	1.2 million tonne CO ₂ /year

2.9 Risks Posed by CO₂ Geological Storage

Similar with any human activity, there are definite hazards related with CO₂ geological storing. Hazard in its engineering explanation is the creation of an event to happen and the consequences of the event-taking place. Henceforward, since consequences are extremely dependent on site and time, the following discussion will address only the various events that may take place and their potential consequences; furthermore, only the risks associated with CO₂ storage will be discussed as the risks

connected with surface and injection/production facilities are well understood[25]. Risks associated with CO₂ geological storing may happen during the injection phase and/or afterwards.

CO₂ escape (leakage) poses different risks because of its possible consequences. Leakage is possible because, besides the pressure force that acts on CO₂ during injection, buoyancy acts on CO₂ at all times, pushing it upwards, and, if a pathway is available, CO₂ will flow along this pathway. Thus, leakage is possible during both injection and afterwards. From the point of view of retention efficacy and safety, CO₂ storage through static and hydrodynamic mechanisms is of most fear because CO₂ is mobile and may escape into overlying formations and perhaps to shallow groundwater. Storage through residual-gas and mineral trapping is of no worry because the CO₂ is immobilised, either in its own chemical form or in a different one. Water saturated with CO₂ is somewhat heavier (by 1-2%) than unsaturated water and its undesirable buoyancy will tend to drive it towards the bottom of the storing aquifer if definite circumstances for the onset of free convection are being met[26] and finally down dip in the aquifer. Carbon dioxide adsorbed onto the coal surface will be immobile as long as the pressure does not drop, which would be the case if the coals were subsequently mined. Only mobile free-phase CO₂ may pose risks due to its buoyancy, which will move it up from its storage unit if a pathway is found, such as open faults and fractures, and defective wells[15]. Local consequences of CO₂ leakage can be short-term or long term, and fall into three categories: health, safety and environmental issues.

2.9.1 Salt Precipitation and Dry out in the near- Wellbore

The most significant physical mechanism of CO₂ injection into deep saline aquifers is the combined dissolution of CO₂ and water, which means that CO₂ can dissolve in formation brine and at the same time, formation brine can evaporate into CO₂. During the injection of dry CO₂, the salt will finally fully saturate the brine producing the salt to start precipitating as a solid phase figure 2.5. This dense precipitation might expressively decrease the porosity and permeability of the porous medium. This problem was first discovered around producing wells in gas reservoirs where high salinity brine is present [27]. This research focuses on the salt precipitation phenomenon in the near wellbore, if salt precipitation takes place, it will effect on the aquifer properties (porosity and permeability) and the well injectivity of the CO₂ injectors will be reduced.

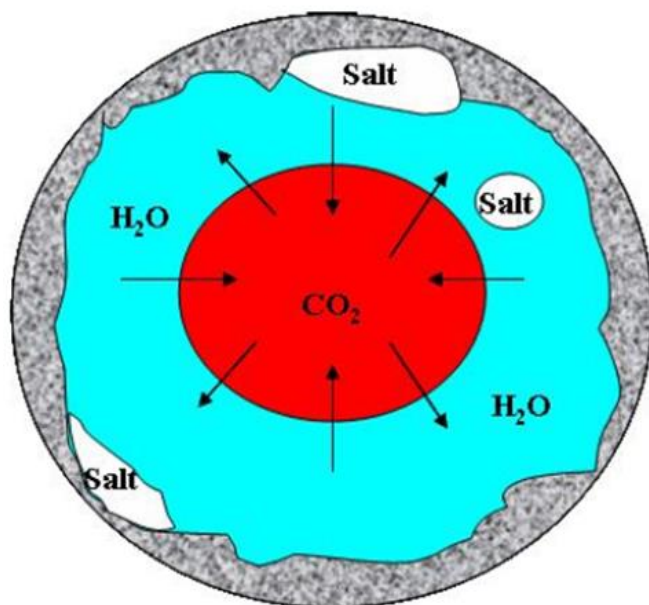


Figure 2.5 : Schematic of CO₂/water mutual dissolution in porous media [39]

The key physical devices touching the dry-out and salt precipitation procedure comprise: (1) the injection of CO₂ will move the brine away from the injection well. (2) The brine will evaporate (3) the Up flow of CO₂ will take place due to the effect of buoyancy. (4) Due to the capillary pressure gradients the Backflow of brine toward the injection well will occur, and (5) Molecular diffusion of dissolved salt.

The impairment of the injectivity has been found to depend on the mobility of the brine phase, with a potentially high impairment at high water saturations. Salt precipitation in the investigated field samples led to a strong decrease of permeability in cases where the brine phase was above residual saturation, i.e. with a mobile brine phase, which means that above residual water saturation there is a potential risk of injectivity loss[23] .

From capacity, point of view deep saline aquifers offer the highest potential for CO₂ storing. Vaporisation of water needs specific consideration, as it is the main source of salt precipitation problems. Research described by Bacci et al aimed to provide variations in porosity and permeability due to salt precipitation (water vaporisation). CO₂ core flooding experiments were conducted on a St.

Bees sandstone core with completely saturated saline water gaining numerous levels of alteration due to halite scaling. Porosity decrease ranged from around 4 to 29 % of the initial value and the permeability damages were from 30 to 86 % [28]. The objective of this work is to examine the effect of brine concentrations on the injectivity and how the dilution by seawater can assist in improving the liquid and gas permeability the injectivity as well.

Permeability change has been measured scientifically for four type of rocks typical of aquifer storing rocks (Vosges Sandstone 1, Vosges Sandstone 2, Lavoux limestone 1 and Lavoux limestone 2). Each sample was completely saturated with a brine of dissimilar salt composition (KCl, NaCl and Keuper brine, a mixture of salt representative of the Paris Basin brine aquifer) and different salinity up to 250 g/l by Peysson et al [29]. The samples were then totally dried in an oven at measured temperature and with vapour removal. A clear linear reduction in permeability was observed. Local study showed that the salt precipitation is localised near the surface of the sample and pores are plugged by solid precipitations, the change of permeability made by drying of brine in porous media.

The investigational work by Müller et al [30] displayed a 60% permeability decrease due to halite precipitation over the whole pore system of the Berea sandstone core after 32 hours of flooding. Non-stop injection of dry supercritical CO₂ into saline aquifers could lead to the development of a dry-out zone in the area of the injection well within which hard salt is precipitated André et al [31]. This salt precipitation results in reduced porosity and permeability, and accordingly, the well injectivity is severely decreased.

2.10 Approaches to Restore the Well Injectivity

While scheduling a CO₂ injection structure the greatest critical factors, apart from containment security and satisfactory storing volume are the injectivity of the potential reservoir unit and storage efficiency. Optimisation of these factors is essential to maximise storage capacity and improve the economics of an injection operation. The injectivity is defined as the ability of a geological formation to accept fluids by injection through a well. The main limiting factor for injectivity is the bottom-hole injection pressure, which should not exceed the formation fracture pressure. It is common for regulators to set a criterion for the maximum injection pressure that is somewhat less than this e.g. 90% of the fracture

pressure. According to the well testing equations, critical restrictions controlling the bottom hole pressures around an injection well are:

- The injection rate of CO₂
- The aquifer permeability
- The relative permeability to CO₂
- The net pay of the completed interval
- Viscosity contrast between brine and CO₂ (mobility) and compressibility.

2.10.1 Fracture managements

It is public to inject water at high wellhead pressures in a well with the purpose of generating definite fractures in the reservoir rock that will rise the general injectivity of the well [19]. Additional choice is to deliberately fracture the reservoir by prop pants. For the shallow reservoir, these two choices were thought unfitting because the cap rock might fracture during this procedure, which would harm the main seal for the injected carbon dioxide and make the reservoir seepage.

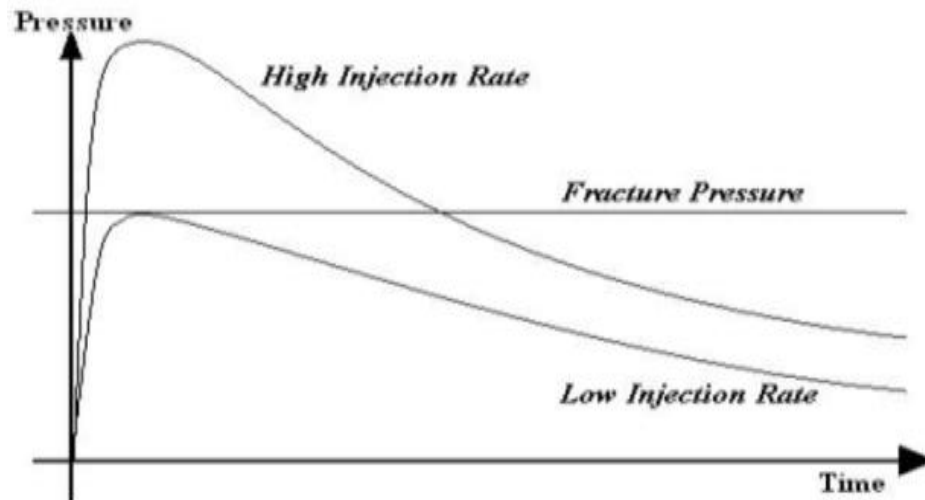


Figure 2.6 : Pressure and time relationship under various CO₂ injection rates

2.10.2 Perforation

Naturally perforating the well is normally reflected a brilliant way to rise the injectivity of a well and is one of the greatest regularly used processes[32] in the oil industry to rise injectivity. Several wells are

even re - perforated to raise injectivity or throughput. However, the high danger of probably harmful watching equipment in the well hindered the application of this choice.

2.10.3 Acid Management

Acid managements are frequently useful to inspire wells. The possible achievement of such managements is normally difficult in the petroleum reservoirs. Additionally, for an ideal treatment, data concerning the environment of the hindering solid would be essential to choose the type, concentration, and shot size of the acid plus the additional chemicals required for the programme. Besides, the intensive care equipment in the well is superficial to definite acids, particularly organic acids. Organic acids are characteristically the preferred acid type for acid treatments for the reason that they are slight, less corrosive to iron and have the possibility to keep iron that was mobilised by the decomposition developments in resolution [33].

2.11 Optimisation of CCS Costs

Figure 2.7 the optimisation of CCS costs.

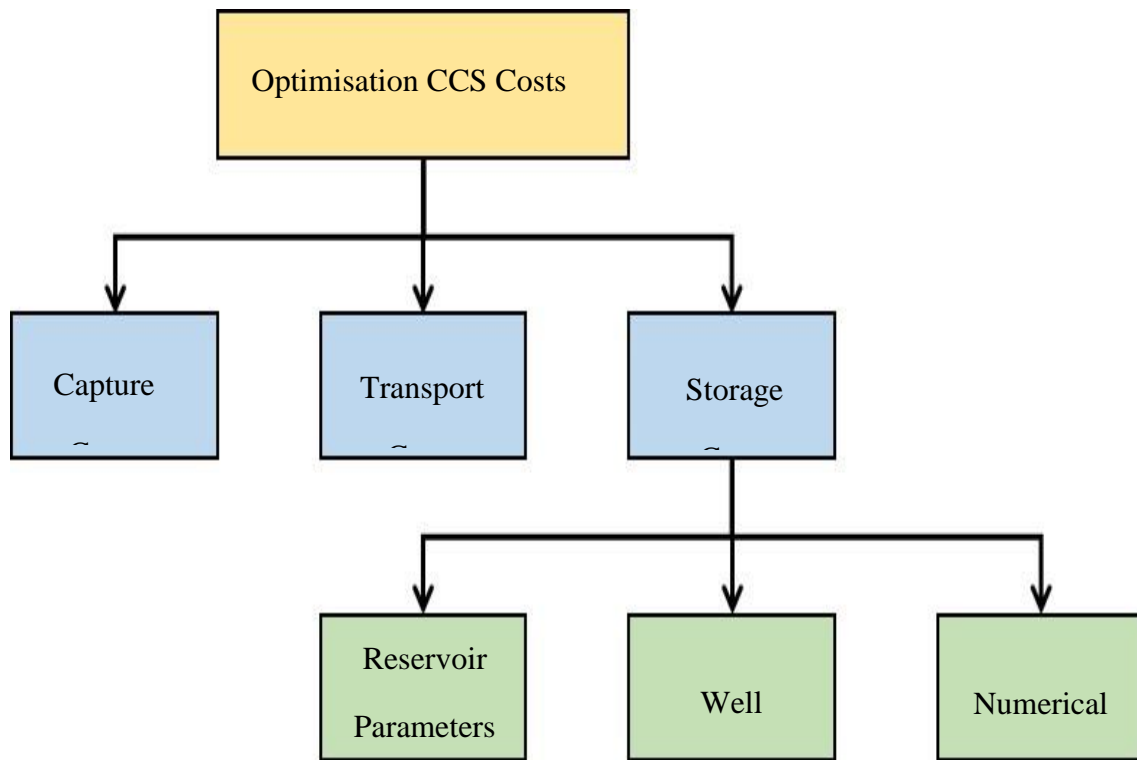


Figure 2.7 : The scheme of cost optimisation of CCS[34]

2.12 Rock Properties

For flow simulation in oil and gas reservoirs, the porosity and permeability are considered the key properties. Porosity is defined as the ratio of the pore volume to the bulk volume. In the oil and gas industry the porosity is classified as absolute and effective porosity, the petroleum engineers are interested in the effective porosity as it represents the interconnected void space. More details about porosity and its measurements are covered in Chapter 3.

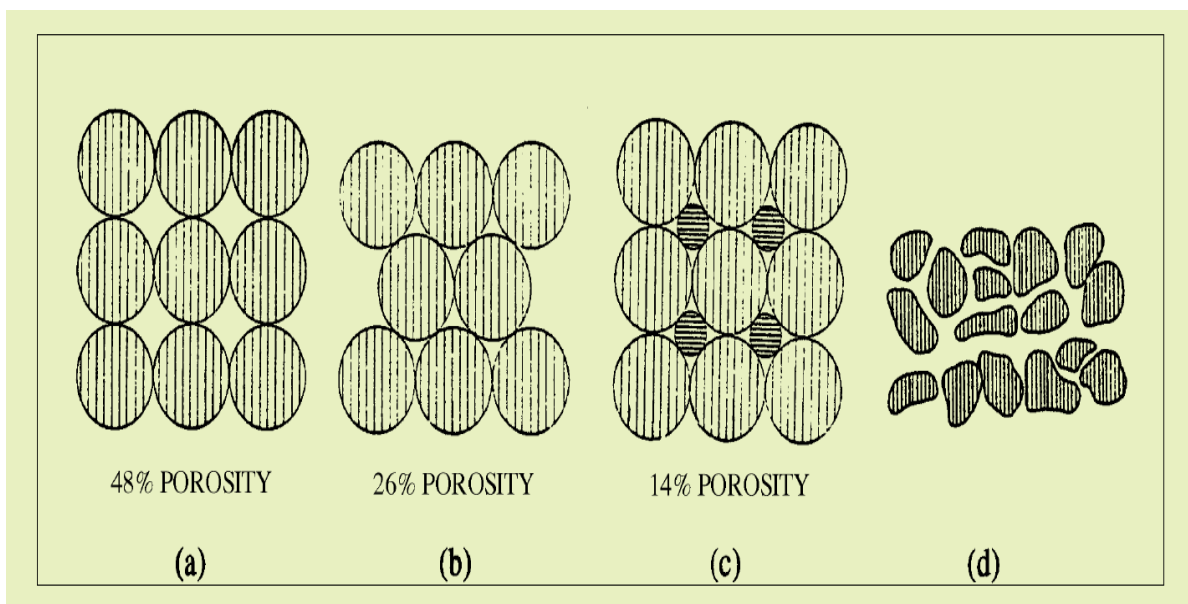


Figure 2.8 : (a) Cubical packing, (b) rhombohedra, (c) cubical packing with two grain sizes, and (d) typical sand with irregular grain shape

2.13 Classification of Porosity

Throughout sedimentation, some of the pore spaces originally developed and became isolated from the other pore spaces by many diagenetic processes such as cementation and the compaction. Therefore, several of the pores will be interconnected, while other will be very isolated. This leads to two dissimilar classes of porosity, namely, total (absolute) and effective, depending upon which pore spaces are measured in defining the volume of that sample; irrespective of whether those void spaces are interconnected or not.

2.13.1 Effective Porosity

The effective porosity (Φ_e), also called the kinematic porosity, of a porous medium is defined as the ratio of the pore volume to the bulk volume. The definition of effective (kinematic) porosity is linked to the concept of pore fluid displacement rather than to the percentage of the volume occupied by the pore spaces. The pore volume employed by the pore fluid that can circulate through the porous medium is less than the total pore space, and, therefore, the effective porosity is always lesser than the total porosity.

2.13.2 Absolute Porosity

It represents the total void space (connected and interconnected pores) to the bulk volume of the core sample and its dimensionless quantity could be reported as fraction or percentage. For the absolute porosity measurement, assuming that the soil system is composed of three phases:

- Solid phase, has volume V_s
- Liquid phase (water) has volume V_l
- Gas phase (air) has volume V_g

Then the pore volume of the sample (V_p) = $V_l + V_g$

The total volume of the sample (V_t) = $V_s + V_l + V_g$, and the sample porosity is determined by:

$$\Phi_t = \frac{V_p}{V_t} = \frac{V_l + V_g}{V_s + V_l + V_g} \quad (2.1)$$

2.14 Permeability

In oil and gas industry, the permeability is defined as ability of the fluid to flow through porous medium, and according to Darcy's law, the permeability is measured in Darcy. The permeability is classified to absolute, effective and relative permeability. The absolute permeability is the measurement of the core sample permeability in the presence of one phase fluid while the effective permeability is the measurement of the permeability in the presence of more than one phase fluid. The relative permeability is the ratio of the effective permeability to the absolute permeability. Normally the permeability depends on the porosity, the higher the porosity the higher the permeability. The connectivity of the pores depends on the size of the grains, the shape of the grains and the grain size distribution. For the permeability of the reservoir rocks, the following points are noticeable:-

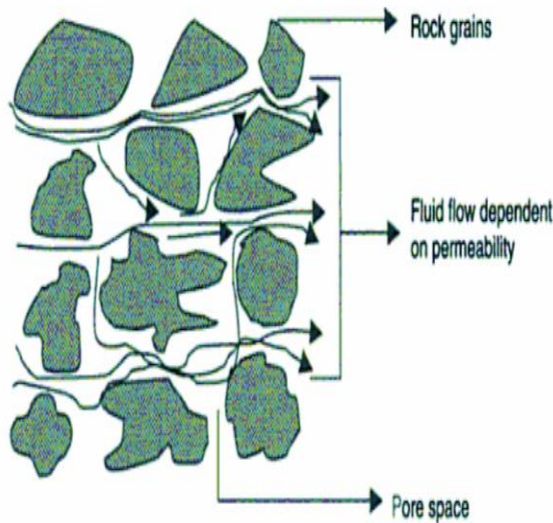
- Higher porosity means high permeability
- Small grains, small pores and small pore throats give low permeability
- High rock compaction gives low porosity and low permeability

Table 2.4 : Classification of reservoir permeability

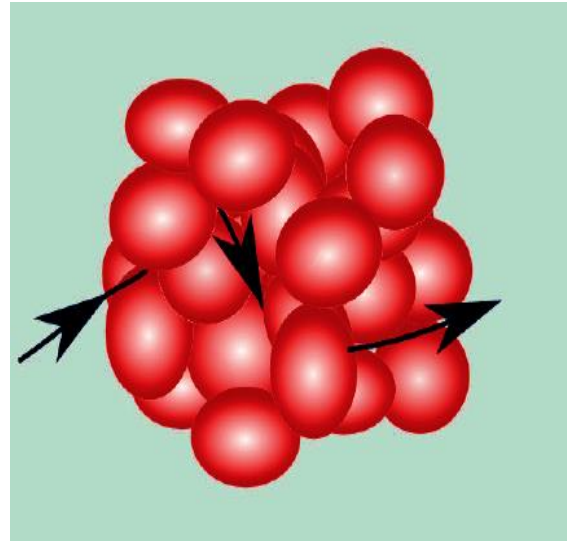
Permeability in (mD)	Permeability Classification
Less than 10	Fair
10 - 100	High
100 - 1000	Very High
Higher than 1000	Exceptional

In general, the permeability depends on

- The rock porosity
- The flow paths connectivity of the rock
- The pore geometry of the rock
- The reservoir heterogeneity. The permeability is calculated by Darcy's equation (3.4)



(a) Pore Space of Rock Grains



(b) Permeability is an indication of how easy is for the fluids to flow through the medium

Figure 2.9 : Permeability is an indication of how easy it is for the fluids to flow through the medium [47]

2.15 Saturation

Saturation is another essential rock property. Saturation is defined as that fraction, or percent of the pore volume occupied by a particular fluid (oil, gas or water). This property is expressed mathematically by the following relationship. Fluid saturation total = (volume of the fluid) / (pore volume). Applying the above mathematical model of saturation to each reservoir liquid provides:

- S_o (oil saturation) = (oil volume)/ (pore volume)
- S_g (gas saturation) = (gas volume)/ (pore volume)
- S_w (water saturation) = (water volume)/ (pore volume)

Where: $S_o + S_g + S_w = 1.0$

2.16 Well Injectivity

The well Injectivity is an essential technical and economic concern for CO₂ geological storing projects, meanwhile very huge volumes of CO₂ must be stored. For long period of storing, water vaporisation has been reported as the chief reason of permeability damages around several gas

producing wells; particularly in high pressure, high temperature reservoirs which are categorised by very high salinity brines[21][35].

The high storing capacity alone is not sufficient for a reservoir to be considered as a suitable storage site. There are two other requirements; high, injectivity and safe containment. The reservoir injectivity measures the ability of a reservoir to accept CO₂ at maximum possible flow rate before losing its mechanical integrity (keep average reservoir pressure less than critical pressure). The well injectivity (or well capacity), on the other hand, measures the ability of a single injection well to accept CO₂ into a formation without reactivating existing faults or creating new fractures[36]. To ensure this, the injection pressure (the well flowing pressure) must not exceed 90% of fracturing pressure considering all others regulatory factors with regard to the injection such as maximum pump pressure [37]. A basin pilot injectivity test is normally required to offer a straight amount of the reservoir injectivity. The following equation can be used for injectivity determination:-

$$\text{Injectivity} = \frac{Q_{\text{CO}_2}}{P_{\text{Injection}} - P_{\text{Reservoir}}} \quad (2.2)$$

Where:

Q CO₂ = the volumetric flow rate of CO₂

P Injection = the injection pressure of CO₂

P reservoir = the reservoir pressure.

2.17 CT Scan

CT scans “Computed tomography” are commonly used for measuring three-dimensional features, but old-style CT scans produce two-dimensional cross-section views of substances. CT scanning offers chance to examine particle and pore connections at any time and location within the sample. A CT scan comprises of two key processes: data collection and image reconstruction. The data collection phase of a CT scan happens after the object is viewed with x-rays from many different directions. Reconstructing a CT scan gives a picture of the internal structures of an object. In this research the CT scanning was used to determine the porosity of (Bentheimer, castlegate and Idaho gray) sandstone core samples using Volume Graphic Software. The pore and grain size distribution of the stated core samples were Visualised. Petroleum engineers utilized CT for fluid-flow experiments and sedimentologists for the analysis of sedimentary structures [38]. CT scanners have been used in petroleum industry as an effective tool for analysing the reservoir rocks for more than 30 years[39] .

An x-ray image is a picture of the x-ray linear attenuation coefficient of an object, which is related to the density of an object [40] .The digital image formed during the x-ray CT process, provides an internal cross-section, in which different materials can be distinguished. Over the last decade, researchers have many experiments using of x-ray CT scanning technologies to quantify physical density, void ratio, and soil collective size distribution [40]. The benefits of x-ray CT scanning comprise time- savings and negligible sample disruption. Nielsen [41] demonstrated that x-ray CT scanning can provide collective size data stable with traditional testing approaches but deprived of the time-consuming sample preparations involved with traditional tests. In specific, CT scan testing offers important savings in time and energy once likened to sample coupon preparation techniques. The non-destructive nature of CT scanning permits the same soil sample to be scanned many different times. Since the sample is not affected by the testing procedure.

2.18 Summary

- After reviewing the options for the geological storage of CO₂ into underground systems and having an overview of the storage sites worldwide, it is noticeable that depleted oil and gas reservoirs and deep aquifers are the most attractive storage sites for CO₂ sequestration.
- CCS is an important process to mitigate emissions of CO₂ into the atmosphere. However, lack of incentives and regulatory regimes are key barriers that need to be overcome.
- It is not evident that all cap-rocks will contain CO₂ safely, since the interfacial tension may be lower and the contact angle higher, implying a lower entry pressure. Furthermore, the CO₂ in solution could react with the cap-rock, eroding escape paths[42].
- CO₂ may also migrate back up through the well after ending the injection process. In case of sealing failure due to fracture that takes place because of pressure build up problem, the CO₂ can escape to the upper formation and might contaminate the water of that formation.
- It is proved by CO₂ – EOR that the CO₂ storage process is feasible and the recent CO₂ storage operations at Sleipner and In Salah are good examples.
- Economics will possibly affect applications, as there is no return value of stored CO₂.
- Confirming adequate injectivity and dodging huge pressure rises at the well and in the underground formation is essential to allow large-scale storing deprived of fracturing the rock or producing intrusion into drinking water.
- CT scan may offer motivating qualitative interpretations of the internal construction of core samples, elements and openings. It can be used for porosity determination using (VG) Volume Graphics Software.

Chapter 3: Experiment Apparatus and Methodology of Data Processing

This Chapter describes the Experimental apparatuses procedures and methodology that carried out throughout these investigations. The experiment was designed to study the effect of salt precipitations in terms of sodium chloride (NaCl) on the liquid and gas permeability of sandstone during the storage of CO₂ in saline aquifers and how the permeability impairment will effect on the injectivity. The relationship between the brine density, viscosity and salinity also considered in this experimental work.

Sea salt was used to dilute different brine salinity concentrations, this demonstrated that the seawater could be utilised and pumped to the CO₂ injectors to avoid the salt precipitation and near wellbore formation dry out and overcome the pressure build up problems. The injected water should be treated properly in order to meet the required technical specifications. All the utilised apparatus are explained in the next sections.

This work of the Chapter is divided into three sections as follows: Phase-I carrying out simple core flooding tests for different sandstone core samples which were saturated with different brine concentrations, the flow tests were carried out to measure the carbon dioxide flow rate in (l/min) through the studied sandstone core samples at different injection pressures in (psi) . Phase - II Utilising the laboratory apparatus to calculate the porosity, liquid and gas permeabilities of the sandstone core samples (Bentheimer, Castlegate and Idaho gray). Phase - III Qualitative analysis of the core samples porosities using the high class CT scanning. Figure 3.1 illustrates the work plan of the thesis.

The core flooding tests carried out to investigate the effect of brine (NaCl) on the stated sandstone core samples. The setup in Figure 3.8 was designed to work under pressure (0 – 60 Psig) and temperature of 25 ° C, the setup is simply composed of Fancher core holder for core samples dimension (1”x1”), compressor system that allows injecting the carbon dioxide gas (CO₂) in (l/min).

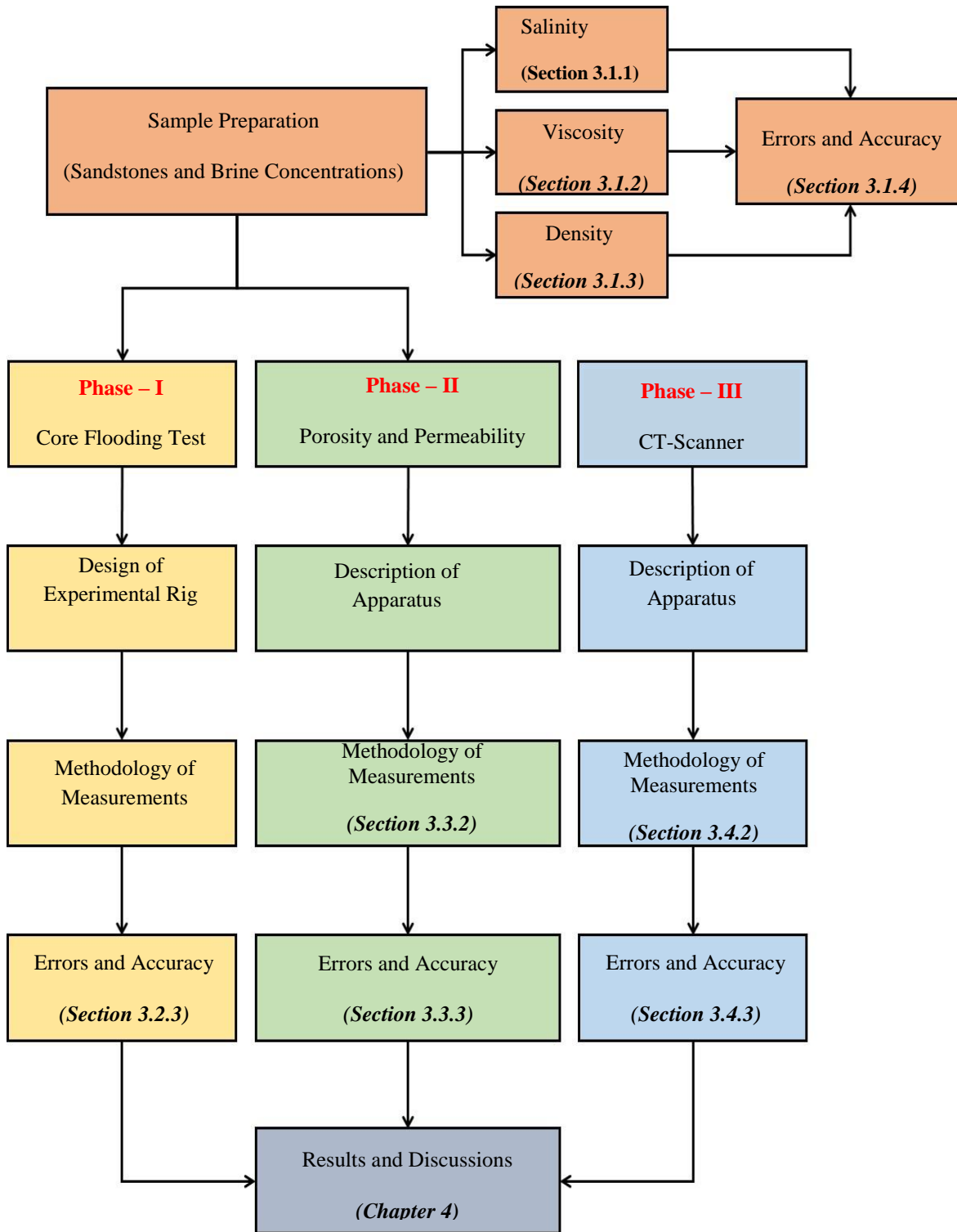


Figure 3.1: Thesis work plan

3.1. Sample Preparation

Samples used for experiments should be clean and dry. Irregularly shaped samples can be used for grain volume determination; however, if porosity is required, the samples must conform to the requirements of the bulk volume apparatus to be used. A serious issue in utilising laboratory measurements is the representativeness of the sample under investigation, i.e., to what degree the results of laboratory data can be extended to characterise large underground rock volumes, or to determine their actual value at a level of certainty needed to make economic decisions leading to reservoir development and production. In dealing with petro physical properties, it is crucial to define the investigation scale, which extends from a small scale a single core, a well or a group of wells to a single reservoir up to a regional geological scale.

Direct core measurements only grant information on a small scale, and can be extended to a larger scale by the aid of properly integrated and calibrated indirect measurements and taking into account the possible heterogeneity and discontinuity of the reservoir by means of geo statistical methods. In general, the most difficult part of any petro physical measurement is to determine the actual values at a level of certainty needed for making economic decisions regarding the possible development or the production management of hydrocarbon reservoir. The core samples that are used for laboratory measurements are usually taken from the subsurface rock using several techniques (i.e. rotary, sidewall and cable-tool coring).

Different Sandstone Core Samples

Three types of sandstone core samples were selected for this study; the selection was based on good porosity and good permeability. The selected sandstone types are (Bentheimer, Castlegate and Idaho gray). These sandstone samples have good porosity and good permeability, and they are very good candidates for CO₂ underground storage. The core samples dimensions (diameter and length) and their weights are recorded. Figure 3.2 illustrates the core samples of the study.

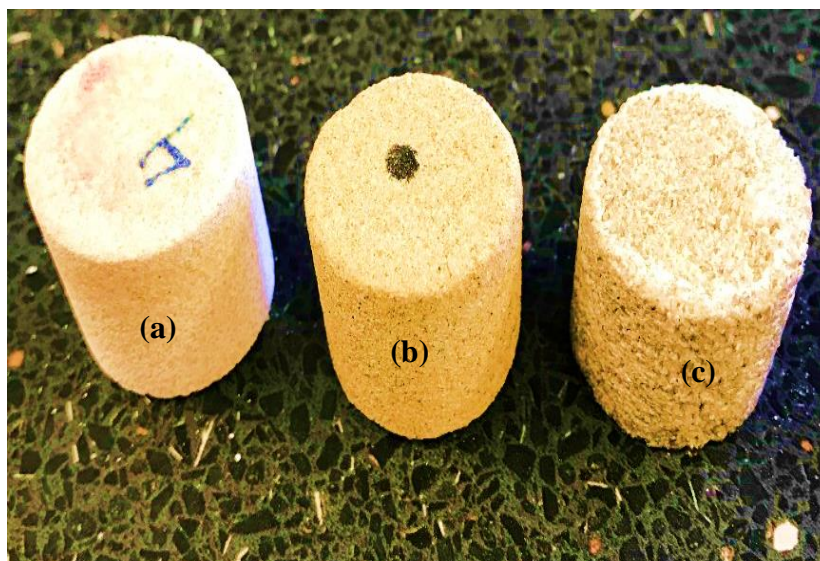


Figure 3.2: Different Types of Sandstones (a) Bentheimer, (b) Castlegate and (c) Idaho Gray

Different Brine Concentrations

In Saline aquifers, the high salinity in PPM or in wt% is expected. Therefore in this study different brine solutions in wt % were prepared (10, 15, 20 and 26.4 wt %), the concentrations were prepared using Sodium chloride (NaCl). For dilution purpose, sea salt was used to prepare 3.5 wt % brine solution. Note that 1.0 wt % equals 10,000 PPM. Concentration is very important property of solutions that must be addressed. In this research, sea salt was used to prepare 3.5 wt % brine solutions to dilute the different brine concentrations. The objective was to investigate the reliability of the dilution to improve the core samples permeability and injectivity. The refractometer was used to measure the different brine concentration in wt %.

One of the important physical mechanisms of CO₂ injection into deep saline aquifers is the mutual dissolution of CO₂ and water, which means that CO₂ can dissolve in formation brine and at the same time, formation brine can evaporate into CO₂. During the injection of dry CO₂, the salt that contains halite mainly will eventually fully saturate the brine causing the salt to start precipitating as a solid phase. This solid deposition could significantly reduce the porosity and permeability of the porous medium. Figure 3.3 shows the brine solutions in % for this study.



Figure 3.3: Brine solutions in (wt %)

3.1.1 Salinity Measurement

The measurement of the total dissolved salts in seawater is called salinity. In this research the refractometer in Figure 3.4 was used for measuring the brine salinity in wt %. It can exactly measure the amount of refraction that is caused by the density. The instrument is temperature compensated. This means that the temperature effects on refraction can be ignored for these measurements, and the salinity can be read directly from the refractometer. The refractometers are low-cost, simple devices that are popular in a multitude of applications. They are popular because they are easy and convenient to use.

Hand-held refractometers work according to the same basic principles and design considerations outlined above. However, The Refractometers are limited in terms of accuracy and applicability because:

- The Refractometers utilise natural (white) light
- There is no way to control temperature
- Light must be transmitted by the sample

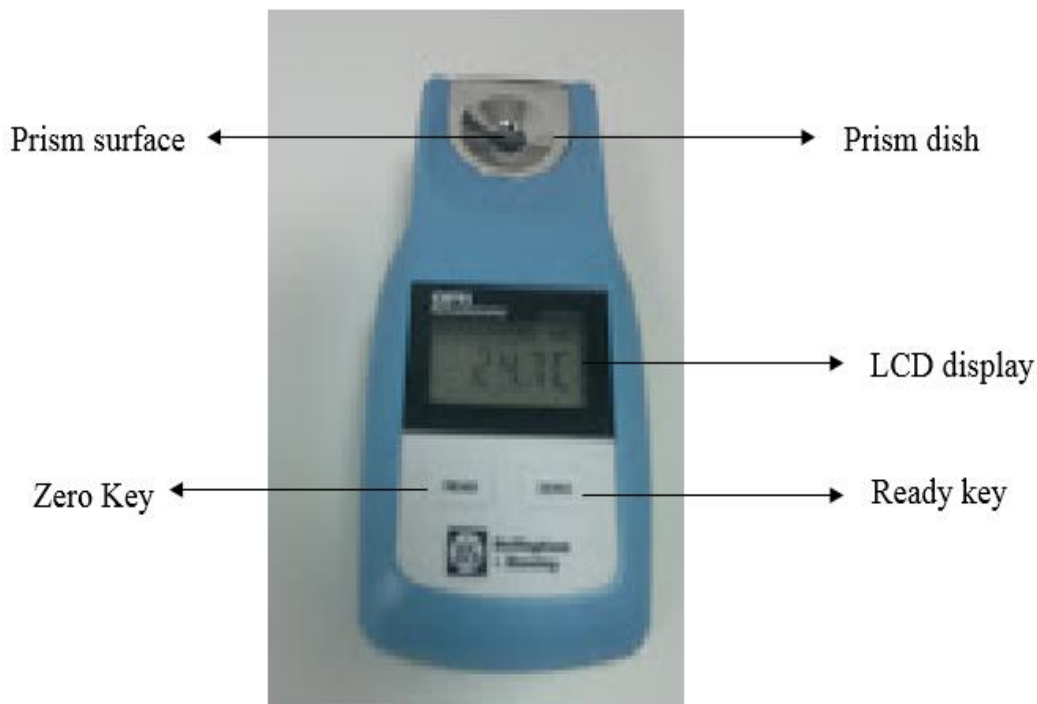


Figure 3.4 : Refractometer gives the salinity in (wt %)

Usually, salinity is expressed in parts per thousand (ppt), regularly written as ‰. The salinity is also expressed percent (%). For example, if 1000 g of seawater contains 35 grams of dissolved salt, the salt solution will be a 3.5% or a salinity of 35 parts per 1000 (35‰).

3.1.2 Viscosity Measurement

The resistance of fluid to flow is called fluid viscosity. In this study, rotational electrical viscometer type was used for dynamic viscosity measurement. Different viscometers are used for viscosity determination

In this, work the viscosities of brine solutions were determined using the OFITE Model 800 8-Speed Electronic Viscometer illustrated in Figure 3.5. In other to determine the viscosities of different brine concentrations in PPM, the viscometer was calibrated in order to get accurate measurements.

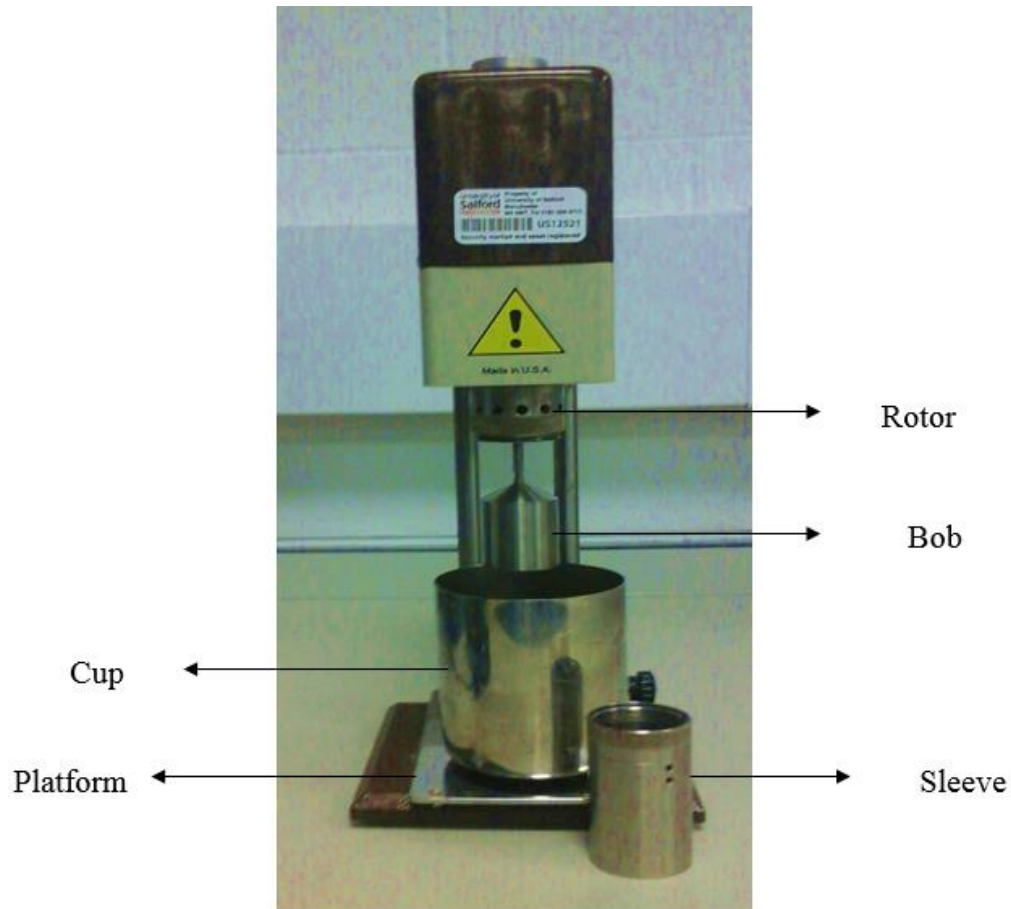


Figure 3.5 : Electronic Rotational Viscometer

Viscosity defines a fluids resistance to flow. Dynamic viscosity (sometimes referred to as Absolute viscosity) is obtained by dividing the Shear stress by the rate of shear strain. The units of dynamic viscosity is Force / area x time. The Pascal unit (Pa) is used to describe pressure or stress = force per

$$\text{Shear stress} = \text{lb}/100 \text{ ft}^2$$

$$\text{Shear rate } \dot{\gamma} = \text{RPM} \times 1.703 \text{ 1/sec}$$

$$\text{Dynamic viscosity} = (\text{lb}/100 \text{ ft}^2) / (1/\text{sec}) = \text{lb} \cdot \text{sec}/100 \text{ ft}^2$$

$$\mu = \text{lb} \cdot \text{sec}/100 \text{ ft}^2, 1.0 \text{ lb} \cdot \text{s}/\text{ft}^2 = 47880.26 \text{ Centipoise.}$$

The viscosity can be calculated by:

$$\mu = KF \frac{\theta}{\text{rpm}} \tag{3.1}$$

Where

μ is the brine viscosity in cP

$K = 300$, F is the spring factor equals 1,

θ is the dial reading (shear stress)

The procedure for viscosity determination is as the following:

- Mixing the sample on the “STIR” setting for 10 seconds until reaches the target temperature
- Rotate the knob at the intended speed setting until stabilisation. When the dial reading stabilises, record the reading and the temperature. Repeat this step for any other speeds that your test requires
- Repeat the above step for any other speeds and record the obtained data.

3.1.3 Density

The density of certain fluid is defined as the mass of that fluid per unit volume. The unit of density is expressed as kilogram per cubic meter. For example, water at a temperature of 20 °C has a density of 998 kg/m³ occasionally the term ‘Relative Density’ is used to define the density of a fluid. Relative density is the fluid density divide by the density of water, which equals 1000 kg/m³. Water at a temperature of 20 °C has a Relative density of 0.998. Brine is a solution of salt (Halite) NaCl in water. In different contexts, brine may refer to salt solutions ranging from about 3.5 wt% (a typical concentration of seawater) up to about 26.4 wt% (a typical saturated solution, depending on temperature). Table 3.1 shows the salinities of different dissolved salts.

Table 3.1 : Water salinity based on dissolved salts

Fresh water	Brackish water	Saline water	Brine
< 0.05 %	0.05 – 3 %	3 – 5 %	>5%

The brine density is measured by mud balance. The mud balance is mud scale device, also known that is used to measure the density of the drilling in ppg (lb/gallon) , cement or any type of liquid. Figure 3.6 illustrates the mud balance for measuring the fluid density. It consists of a graduated beam with a

bubble level and a weight slider along its length and a cup with a lid on one end. The cup is used to hold a fixed amount of fluid so it can be weighed. A slider-weight can be moved along the beam, and a bubble indicates when the beam is level. Density is read at the point where the slider-weight sits on the beam at level.

Sodium chloride (NaCl) is not strictly a scale. The mixing of incompatible waters forms most oilfield scales. Salt, however, is a self-scaling phenomenon requiring only changes in physical conditions to precipitate. It is also, generally, a gas well problem, for reasons that become apparent when looking at the mechanism of salt deposition. There are two mechanisms working to cause precipitation of salt; firstly, evaporation of fresh water from formation brine into the producing gas, which increases, brine salinity, and secondly, changes in pressure and temperature, which can reduce the solubility of the salt in the brine. Either or both can result in the brine becoming salt saturated so that the salt precipitates out. Precipitated salt is generally nearly 100 wt % NaCl.

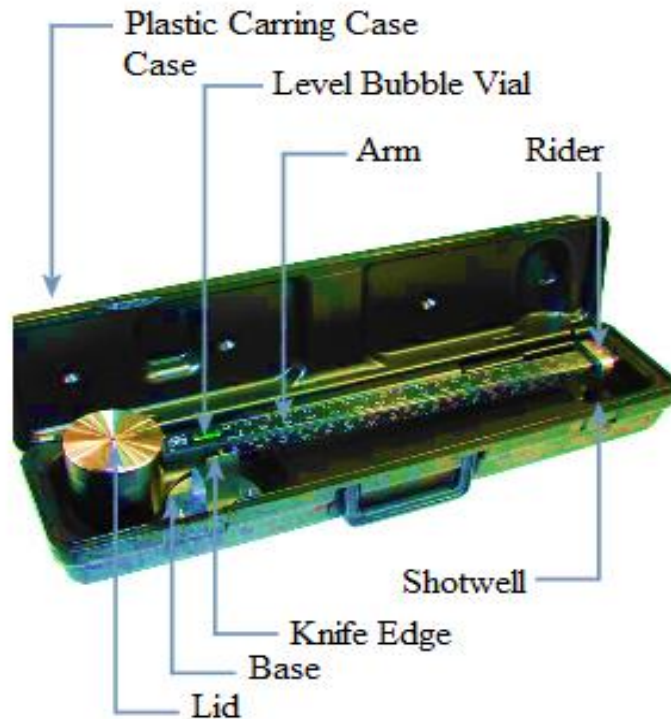


Figure 3.6 : Mud Balance scale device

Figure 3.6 shows the mud balance that is used for fluid density measurement. The arm is graduated and permits accurate measurements to within ± 0.1 pounds per gallon. The measurement procedure summary is as the following:

- i. The mud balance needs to be placed on a flat level surface.
- ii. The temperature of the fluid needs to be measured and recorded.
- iii. The dry and clean cup needs to be filled to the top with the intended mud sample.
- iv. The lid needs to be placed on the cup, and set it with a gentle twisting motion.
- v. The hole in the lid needs to be covered with a finger and wash all mud from the outside of the cup arm.
- vi. The balance needs to be placed Place on the knife-edge and move the rider along the outside of the arm until the cup and arm are balanced as indicated by the bubble.
- vii. At the edge of the rider toward the mud cup, read the mud weight in ppg.
- viii. After each use, the mud balanced needs to be cleaned and dried properly.

3.1.4. Errors and Accuracy

- Salinity
 - The accuracy and precision is limited by the size and optical arrangement. Sample temperature range 5-90 °C. Sample volume 0.30 ml and the temperature sensor accuracy ± 1 °C (5 – 40 °C). The error percent of the reading is ± 0.2 .
- Viscosity
 - Speed accuracy (RPM) = 0.1, Minimum viscosity @600 RPM = 0.5 cP, Maximum viscosity @600 RPM = 33, 000 cP.
- Density
 - The density of the fluid can be measured by mud balance. The arm is graduated and permits accurate measurements to within ± 0.1 pounds per gallon or ± 0.01 specific gravity.

3.2 PHASE-I: Core Flooding Tests

The formation dry-out and precipitation of salt near the injection well is expected to take place during CO₂ in injection in Saline aquifers. The precipitated salts will reduce formation porosity, permeability, and injectivity. One approach to delay the onset of this phenomenon is periodic flush of seawater or

brackish water to the storage formation, if the standard requirements for the pumped water met. The majority of problems associated are the impaired of the saline aquifer formation permeability and the injectivity reduction due to directly problems associated with water quality. A proper understanding of the quality of the pumped water including its composition, contaminants and suspended solids is highly recommended; this will assist in improving the well injection performance, and avoid the pressure build up problems. Mixing different water chemistries to overcome the near wellbore formation dry out during CO₂ storage into saline aquifers can cause scale problems and severe consequences and pore throat plugging can take place if the pumped seawater or brackish water has any associated solid particles such as (iron) if pipe is uncoated. The aquifer salinity dilution by periodically pumping the low salinity water can improve the permeability, reduce the risk of damage if the pumped water is free of suspended particles, and scale deposits. If the pumped water is well treated the well injectivity could improve, the aquifer characteristics (porosity and permeability) could improve, and certainly, the pressure build up problems could be avoided. Table 3.2 shows the seawater specifications for injection.

Table 3.2 : treatment specifications[43]

Parameter	Maximum acceptable
Total suspended solids	0.2 mg/l
pH	7.2
Iron	0.1 mg/l
Sulphate	14 mg/l
Dissolved Oxygen	10 PPb
Particles number > 2 μ	particles per 1/2 ml of water

Figure 3.7 shows that the CO₂ will be injected from the CO₂ cylinder (1), the pressure reading will be controlled by the pressure regulator (psi) (2), the injected CO₂ will flow through the fancher core holder 1"x1" (4) where the core samples of study will be seated up, and CO₂ flow rate can be read from the glass tube gas flow meter (l/ min) (7). Two core-flooding tests were carried out. (i) For the saturated core samples with a NaCl (10, 15, 20 and 26.4 wt %), (ii) for the same samples after re saturating with 3.5 wt % NaCl, all the obtained results were recorded. The main purpose of carrying out the tests is to examine the effect of NaCl on the injectivity. If the brine precipitates in the form of NaCl, it will plug the pore throat of the core sample, then the core sample permeability will damage, the injectivity reduction will take place. During CO₂ storage in saline aquifers if salt precipitation and

formation dry out phenomenon takes place, fracturing of sealing could happen due to pressure build up and CO₂ will migrate to the upper formations and cause contaminations. The dilution of the aquifer salinity by periodic injection of low water salinity like seawater could work as permanent solution to overcome this phenomenon if the injected water is well treat and meet the required technical specifications.

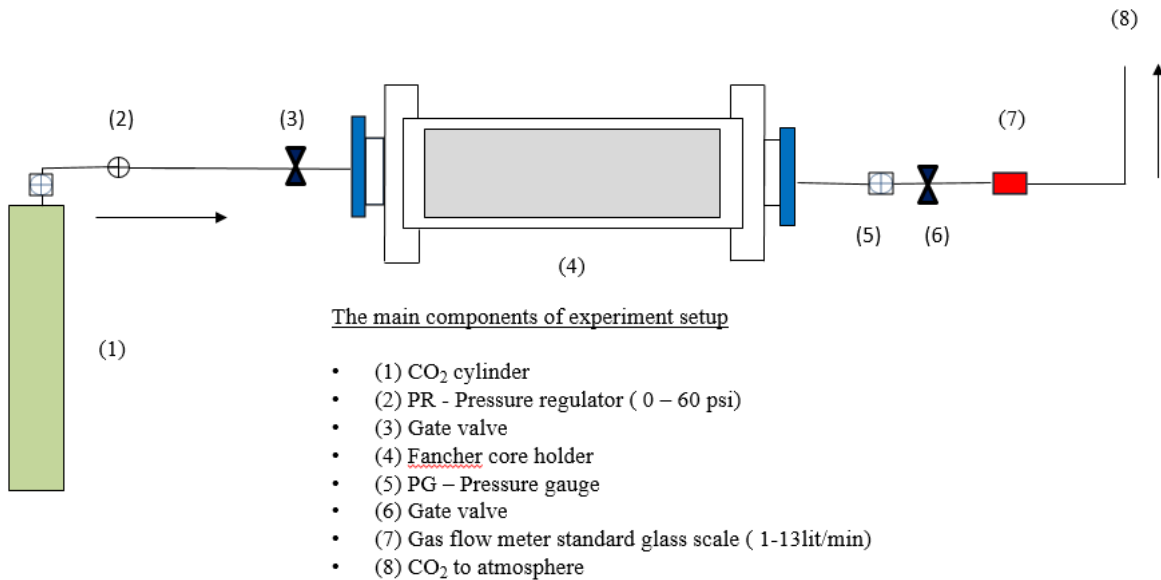


Figure 3.7 : the experimental set up diagram

3.2.1 Experimental Set Up

The Experimental set up in Figure 3.8 consists of (1) CO₂ cylinder, (2) pressure regulator (0 - 60 psi), (3) 1/8” gate valve, (4) fancher core holder, (5) pressure gauge (0- 60 psi), (6) 1/8” gate valve, (7) glass tube gas flow meter (1 - 13 l/min). The main purpose of experimental set up was to carry out linear core-flooding tests through different sandstone core samples, which saturated with different brine solutions using Carbon dioxide (CO₂) gas. The sandstone core samples that were saturated with different brine concentrations were subjected to flow tests (l/min) at different operating pressures in (psi).

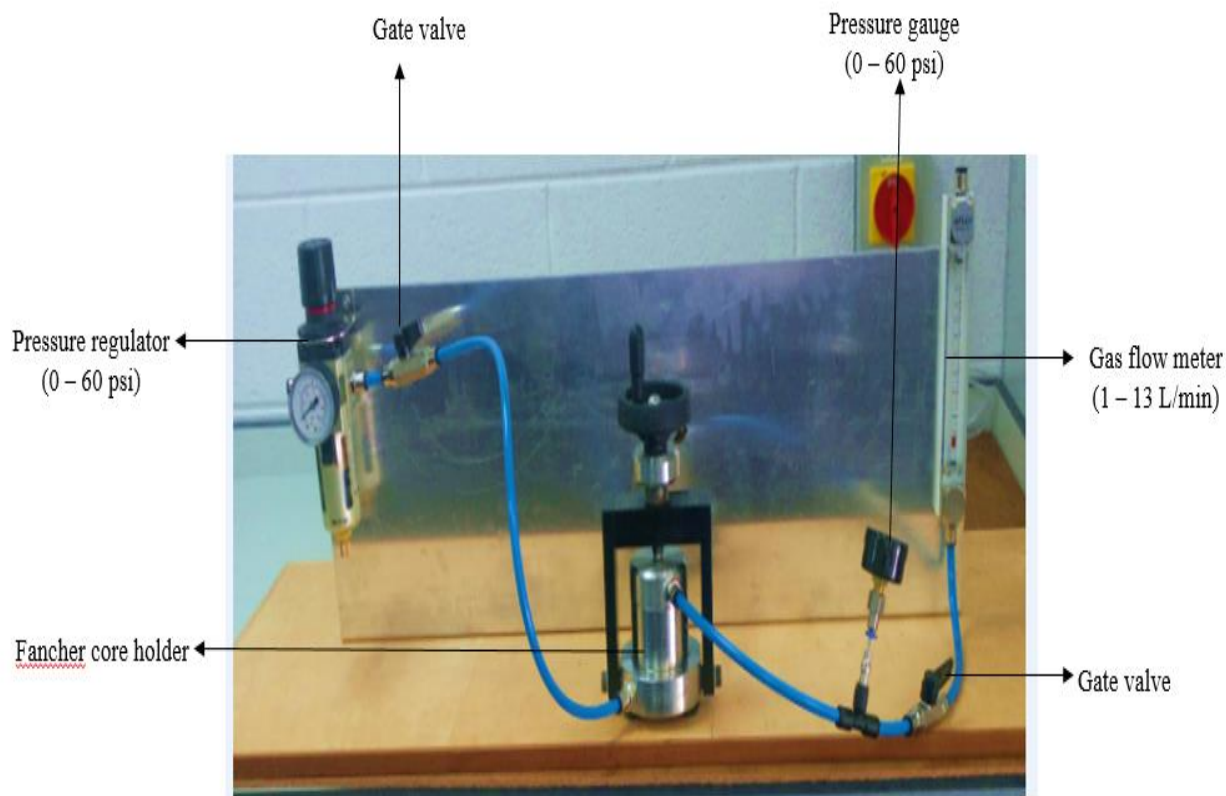


Figure 3.8 : Experimental set up

Figure 3.9 shows the fancher core holder; it consists of a stainless steel cylinder. A stand with an adjustable top plate with an O-ring holds the cup and applies force to seal the cup opening so that helium can be injected into the cup containing the core plug to be evaluated. The Matrix Cup core holder is used with the PORG-200. The apparatus consists of a stainless steel cylinder with several calibration disks of varying known volumes that can be placed inside the cylinder. The disks are used in calibration procedures. The movement of the top plate should be adjusted using the jam nut so that there is enough downward force to affect an O-ring seal when the closing lever meets the stop pin. In this manner, the volume of the closed cup is kept consistent, allowing precise measurements to be made.

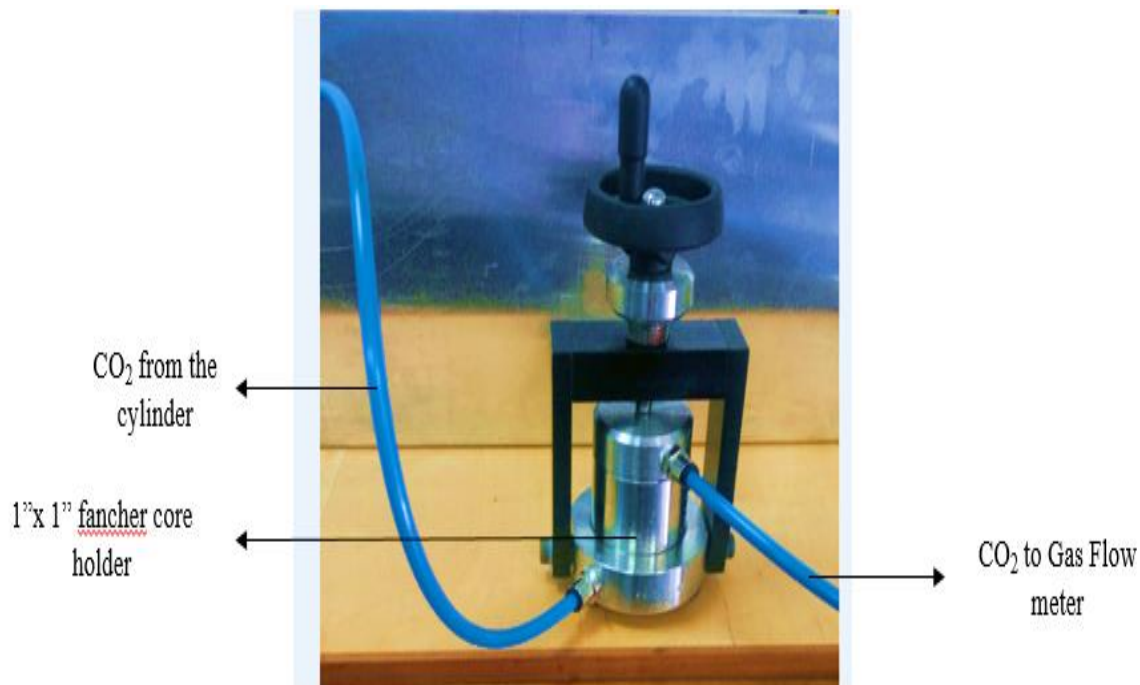


Figure 3.9 : Shows the fancher core holder (1"x1")

3.2.2 Methodology of Measurement

The core flooding tests were carried out to investigate the effect of brine (NaCl) on sandstone core samples (Bentheimer, Castlegate and Idaho gray) liquid and gas permeability. The setup was designed to work under pressure (0 – 60 Psig) and temperature of 22 ° C, the setup is simply composed of Fancher core holder for core samples dimension (1"x1"), compressor system that allows injecting the carbon dioxide gas (CO₂) in (l/ min) Figure 3.8. During the experiment runs the evolution of pressure drop as a function of time showed trend depending on the concentration of NaCl. From engineering point of view, the parameters that affect the injectivity during CO₂ storage include planned rate of CO₂ captured, number of wells and well design (vertical, horizontal, multilateral). In this study, two core-flooding tests were carried out. (i) Scenario 1 for the saturated core samples with a NaCl (10, 15, 20 and 26.4 wt %), (ii) scenario 2 for the same samples after re saturating with 3.5 wt % NaCl.

The experimental setup in Figure 3.8 was designed to carry out flow tests and measure the CO₂ flow rates in (l/min) at different injection pressures (psi). The main purpose of data collection in this experimental work was to determine the brine permeability (md), the gas permeability (md) and the

porosity of the sandstone core samples for (Bentheimer, Castlegate and Idaho gray), and investigate the effect of brine concentration on the liquid and gas permeability of the core samples. To achieve the study objectives, different brine solution concentrations were prepared, and the core samples were saturated with these brine concentrations, and the core flooding tests were carried out at different operating pressures, the obtained results were then plotted and analysed. The collected data sample is shown in Tables 3.3. The objective of the laboratory investigations was to evaluate the effect of brine concentration, as sodium chloride (NaCl) on the permeability and the impairment of this property will negatively effects on the injectivity during CO₂ storage into saline aquifers. The liquid and gas permeability of sandstone core samples (Bentheimer Castlegate, and Idaho gray) was measured at different brine concentrations, core-flooding test using the CO₂ gas were carried out in order to investigate the effect of salt precipitation on the aquifer rock properties. Injection of CO₂ into saline aquifers will induce complex coupled processes on multiple scales.

Formation heterogeneities may play strong role in how dry out and precipitation play out by directing, contain and channelling the injected CO₂. The core flooding flow tests were carried out for the stated core samples at different brine solution concentrations (10, 15, 20 and 26.4 wt %) after drying the core samples in oven at 100 °C for 24 hours utilising the designed rig in Figure 3.8, and Table 3.3 shows a sample of the collected data.

Table 3.3: Sample data of core flooding tests for Bentheimer sandstone

	<i>Bentheimer</i>			
	10% Brine Concentration		Inject Water + 3.5% NaCl	
P-Inlet (P1)	P-Outlet (P2)	Q-Outlet (Q2)	P-Outlet (P3)	Q-Outlet (Q3)
psi	psi	l/min	psi	l/min
10.0	8.0	2.0	7.0	2.5
20.0	16.0	3.0	15.0	3.5
50.0	45.0	6.0	43.0	6.8

3.2.3 Errors and Accuracy

The errors and accuracy of the Experimental rig components summary is shown in Table 3.4.

Table 3.4 : Errors and accuracy of the rig components

Component	Errors and accuracy
Pressure gauge (0 – 60 Psi)	$\pm 1.2 \%$
1/ 8” Gate valve	$\pm 0.002 \%$
Fancher core holder, Max. Pressure (60 psi)	$\pm 0.3 \%$
Gas Flow meter (1 – 13 l / min)	$\pm 0.03 \%$

3.3 Phase-II: Porosity and Permeability

Porosity is one of the main petro physical properties of the reservoir rocks and as stated before it is defined as the ratio of the pore volume to the bulk volume. The Permeability is another significant property of the reservoir rock and it represents the ability of the fluid to flow through porous media, more details about porosity and permeability are explained in the upcoming sections.

3.3.1 Description of Apparatus

This section described the apparatus, which have been used through this study to measure the porosity and permeability of the sandstone core samples (Bentheimer, Castlegate and Idaho gray).

3.3.1.1 Porosity Measurement

Porosity is defined as the ratio of pore volume to bulk volume of the core sample. In laboratory, the porosity can be measured by using gas Porosimeter PORG – 200 or using the liquid saturating method.

Manually Operated Gas Porosimeter PORG – 200: -

It is shown in Figure 3.10; that the apparatus consists of the PORG-200 with a Matrix Cup for core samples 1 inch in diameter and up to 3 inches in length and a set of steel calibration disks. The PORG-200™ uses general gases law to determine grain volume from the expansion of a known volume of helium into a calibrated sample holder (Matrix Cup).Using the supplied Matrix Cup, the PORG-200 can be used to determine grain volume directly. Porosity can be calculated from the equation (3.2).

The Matrix Cup core holder is used with the PORG-200™ to determine the Grain Volume of core plug samples. The apparatus consists of a stainless steel cylinder with several calibration disks of varying known volumes that can be placed inside the cylinder. The disks are used in calibration procedures.

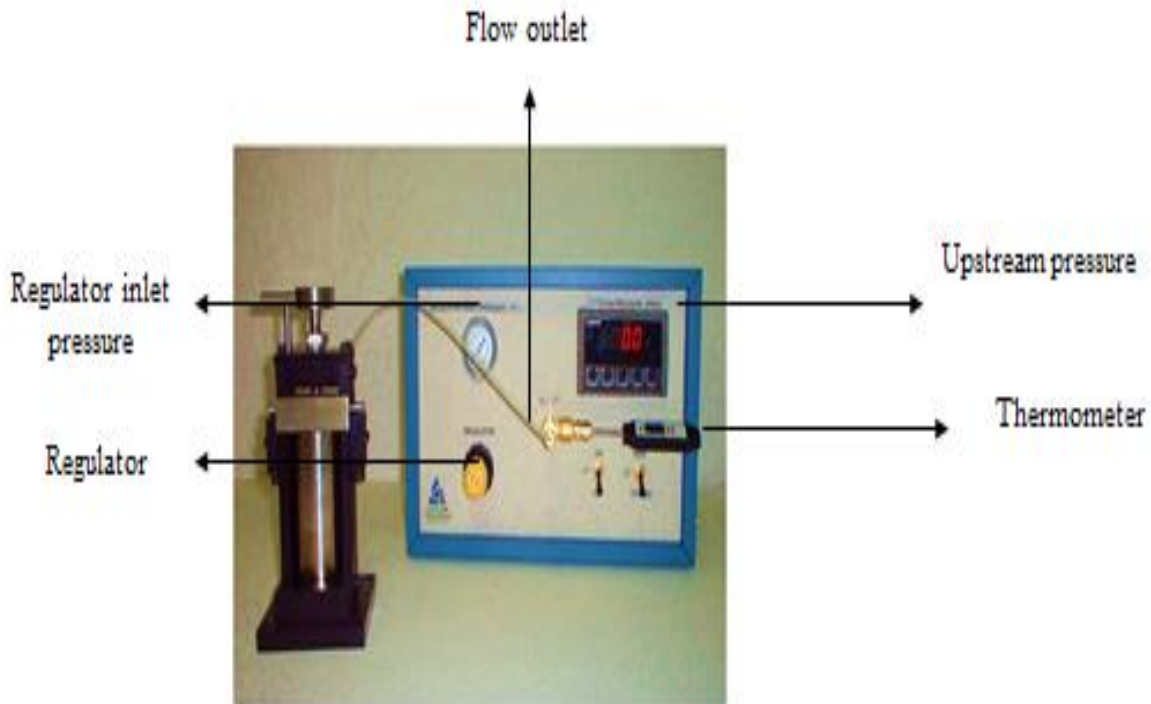


Figure 3.10 : PORG – 200

Liquid Saturating Method for Porosity Determination

The effective porosity of the rock can be measured by this method. The experimental procedure summary of this method is summarised in the following steps:

- The core sample needs to be cleaned and dried.
- The dry weight of the core sample in its state needs to be weighed (W_{dry}).
- Completely, saturate the core sample in a wetting fluid. Now it is more common to saturate the rock with a brine that has been made to mimic that in the reservoir, i.e., contain the same concentrations of major dissolved salts (a synthetic brine).
- Weigh the saturated core sample after (W_{sat}).
- Assuming that the core sample is cylindrical, use the calibre for taking the required measurements and calculate the bulk volume of the rock (V_{bulk}).

- The density of the fluid (ρ_{fluid}) of the saturating fluid can be determined by weighing a known volume of it.

3.3.1.2 Permeability Measurement

Permeability is a measure of the ability of a porous media to conduct fluids. It is an important property in defining the flow capacity of a rock sample. It is measured in Darcy, named after the French scientist who explored the phenomenon in 1856. In the oil and gas industry the accurate determinations for limited range of the reservoir rock samples liquid and gas permeability could be achieved by using the apparatuses PERL – 200 and PERG -200.

PERL – 200: - It is used for core samples Liquid permeability measurement

The apparatus is shown in Figure 3.11; it consists of the PERL-200 permeameter and a newly designed Fancher-type core holder. The permeameter incorporates a digital pressure transducer, and a calibrated visual flow (measurement) cell, along with the valves and flow system to enable the determination of permeability to liquid of one-inch diameter core plugs.

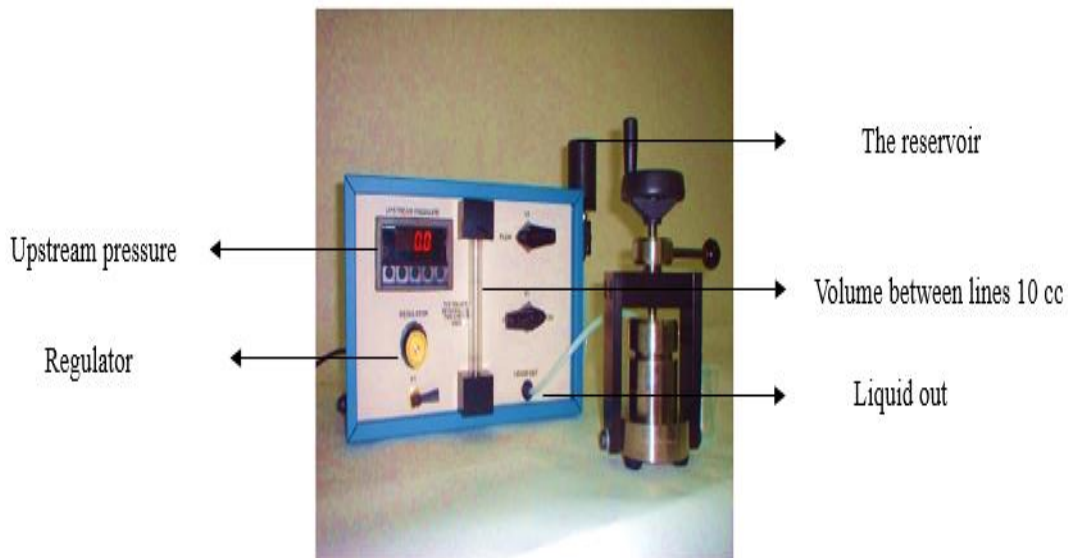


Figure 3.11 : PERL – 200

PERG – 200: - It is used for core samples Gas permeability measurements

The apparatus is shown in Figure 3.12; it consists of the PERG-200 permeameter and a newly designed fancher core holder. The permeameter incorporates a digital pressure transducer, flow-rate meter, and thermometer, along with the valves and flow system to enable the measurement of permeability to air of one-inch diameter core plugs.

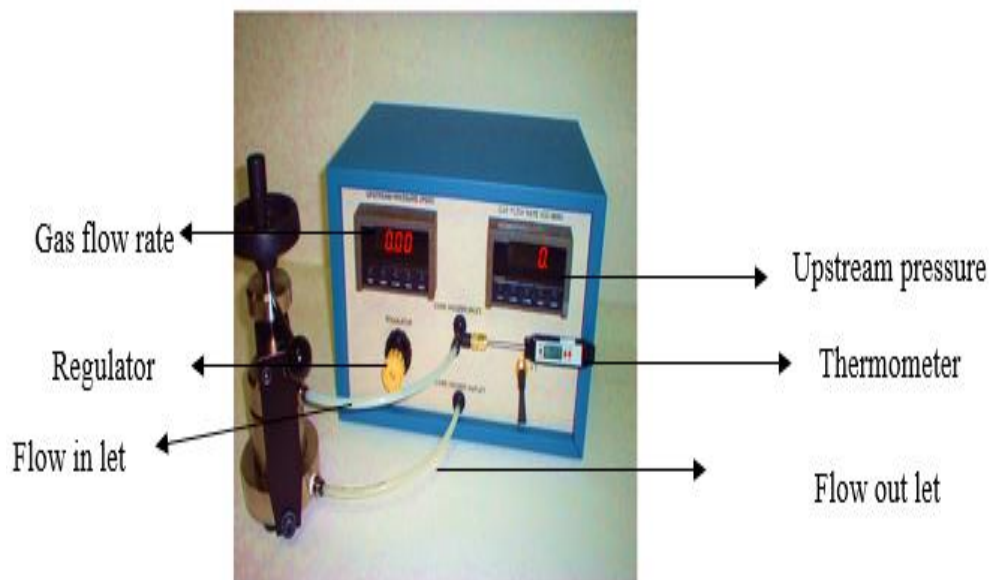


Figure 3.12 : PERG – 200

3.3.2 Methodology of Measurement

In this work, the main objective was to improve the aquifer permeability, maintain the inectivity, and avoid disturbing the operations during CO₂ storage in saline aquifer. To meet this goal the salt precipitation in the near wellbore needs to be eliminated or delayed. The dilution of the formation water, which have high salinity with seawater for of offshore wells or brackish water for onshore wells could assist in keeping steady operations. The Experimental work summary is as follows:

1. The porosity was initially measured for all the sandstone core samples (Bentheimer, Castlegate and Idaho gray), using PORG – 200, the liquid saturating method and the CT scan.

2. The liquid permeability was initially measured for all the sandstone core samples (Bentheimer, Castlegate and Idaho gray), using PERL – 200
3. The Gas permeability was initially measured for all the sandstone core samples (Bentheimer, Castlegate and Idaho gray), using PERG – 200
4. Saturate the sandstone core samples with (10, 15, 20 and 26.4wt %) NaCl.
5. Put the core samples in oven for 24 hours at 100⁰ C, for dry out
6. The liquid permeability for the saturated samples was measured.
7. The gas permeability for the saturated samples was measured.
8. Re saturate the samples with 3.5 wt % NaCl to dilute the concentrations.
9. Repeat steps 6 and 7 and compare the results

The previously stated apparatuses were used for the porosity and permeability determinations and more details are explained in the next sections.

3.3.2.1 Porosity

The porosity is one of the most important petrophysical characteristics from the reservoir-engineering point of view. It is porosity is defined as the ratio of the pore space in a reservoir rock to the bulk volume (total volume), and it is expressed in percentage or fraction. The porosity the rock sample may be measured in laboratory by:

- PERG- 200 for the core sample grain volume determination
- Liquid saturating method, it was explained in section 3.3.1.1

The core analysis determination of porosity has the benefit that no assumption need to be made as to mineral composition, borehole effects, etc. The following equation can be used to calculate the porosity of the core sample:

$$\phi = \frac{VP}{VB} = \frac{VB - VG}{VB} \quad (3.2)$$

Where ϕ is the core sample porosity in percentage (%) or fraction, VP is the core sample pore volume, VB is the bulk volume of the core sample and VG is the grain volume of the core sample.

Porosity may be categorised according to its source as either primary or secondary. Primary or original porosity is developing during the initial deposition of the sediments.

Measurement of Bulk Volume

Even though the bulk volume could be calculated from amounts of the measurements of a homogeneously formed sample, the normal technique utilises the observation of the volume of liquid moved by the sample. The liquid moved by a sample can be observed either volumetrically or gravimetrically. In each technique, it is essential to avoid the liquid diffusion into the pore space of the rock.

Measurement of Pore Volume

The approaches to quantify the pore volume of the rock sample are based on either the removal of a liquid from the rock or the introduction of a fluid into the pore spaces of the rock. One of the most used approaches is the helium method, which engagements the general gases law. The helium gas in the reference cell isothermally enlarges into a sample cell.

Helium has benefits over other gases for the reason that: (1) it has small molecules, which are quickly, entered the small pores. (2) The Helium is an inert gas. (3) It is considered as an ideal gas ($z = 1.0$) for pressures and temperatures, and (4) Helium has a high diffusivity and offers a beneficial means for determining porosity of low permeability rocks. Another method of pore volume measurement is to saturate the sample with a liquid of known density. Then use the weight difference before and after saturation to calculate pore volume.

Measurement of Grain Volume

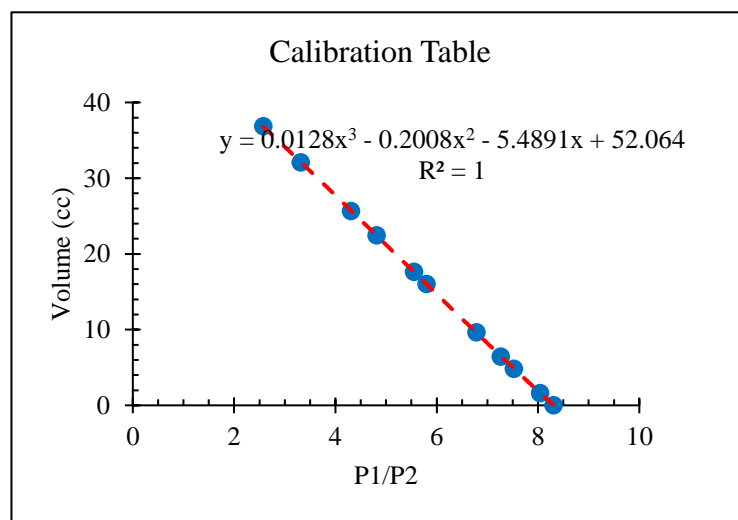
The grain volume of pore samples is normally calculated from sample weight and information of average density. Formations of changing lithology and, hence, grain density limit applicability of this technique. General gases law is often employed with helium as the gas to define grain volume. The method is honestly fast, and is usable on clean and dry core samples sample.

Tables 3.5 and 3.6 show samples of data collected for porosity determination.

Table 3.5 : Spread sheet for grain volume calculation

Disc Volume Table				
Disc No.	Length (in)	Diameter (in)	Disc Area (cm ²)	Volume (cc)
1	0.124	1	5.0671	1.5959
2	0.373	0.999	5.0569	4.7911
3	0.498	1	5.0671	6.4094
4	0.747	1	5.0671	9.6142
5	1.248	0.999	5.0569	16.0301
Total Volume (cc)				38.4407

Calibration Table				
Disc No.	Volume (cc)	Ref. Pressure (psi) P1	Expanded Pressure (psi) P2	P1/P2
empty	0	89.92	10.82	8.3105
1	1.5959	90.09	11.2	8.0438
2	4.7911	90.21	11.99	7.5238
3	6.4094	90.25	12.42	7.2665
4	9.6142	90.28	13.3	6.7880
5	16.0301	90.3	15.57	5.7996
5 + 1	17.6260	90.32	16.26	5.5547
5 + 3	22.4396	90.33	18.77	4.8125
5 + 4	25.6443	90.36	20.96	4.3111
5 + 3 + 4	32.0537	90.41	27.24	3.3190
5 + 4 + 3 + 2	36.8448	90.41	35.09	2.5765



Coefficients Table			
A	B	C	D
0.0128	-0.2008	-5.4891	52.064

Testing Table			
P1	P2	P1/P2	Grain Vol.
90	13.38	6.7265	9.9521
90	13.23	6.8027	9.4603
90	13.35	6.7416	9.8546

Bentheimer
Castlegate
Idaho Gray

Table 3.6 : porosity determination by liquid saturating method (Bentheimer sandstone

	Bentheimer
D (cm)	2.5095
L (cm)	2.7051
A (cm²)	4.9461
VB (cc)	13.3797
W-Before (gr)	25.4
W-After (gr)	28.8
dW (gr)	3.4
Density (g/cc)	1.075
VP (cm³)	3.1628
VG (cm³)	10.2169
Porosity	0.2364
Grain Density (g/cc)	2.4861

Note:

D= diameter of core sample in cm

L = length of core sample in cm

A= Core sample area in cm²

VB = core sample bulk volume in cm³

WR = dry weight of core sample in grams

W_{sat} = weight of saturated core sample in grams

Dw = weight difference in grams (W-After – W-Before) in gm

ρ Brine = brine density in gm/cc

VP = pore volume in cm³

VG = grain volume in cm³

Porosity = (VP / VG), Fraction

Grain density = gm/c

3.3.2.2 Permeability

Permeability is a property of the porous medium and it is a measure of capacity of the medium to transmit fluids. In this work the investigations the main contribution is how to maintain the aquifer permeability during CO₂ storage in Saline aquifer. If salt (NaCl) precipitates around the wellbore, the aquifer permeability will damage with the attendance of reduction in injectivity, due to this circumstances, the pressure will build up and fracturing of sealing could take place CO₂ may migrate out. The dilution of the formation with low salinity water could help and assist to overcome and eliminate these undesirable difficulties.

In analogy to the electric conductance, which is defined by Ohm's law as the ratio of the electric current and the electric potential, we can define the hydraulic conductance as the ratio of the fluid flow and the pressure difference.

Values range considerably from less than 0.01 millidarcy (md) to well over one Darcy. A permeability of 0.1 md is normally considered minimum for oil production. Highly productive reservoirs normally have permeability values in the Darcy range. Darcy's Law expresses permeability:

$$Q = \frac{kA(P_2 - P_1)}{\mu L} \quad (3.3)$$

Where:

Q = Flow rate in cm³/s

μ = Viscosity of the fluid in cP

k = Effective permeability in D

P_2 = Upstream Pressure in atm.

P_1 = Downstream pressure in atm.

L = Length of flow in cm

A = Cross-sectional area of flow in cm

h = Height of the flow length in cm

π = 3.14159.

The unit Darcy results from the choice of cgs system units.

The permeability in SI system has dimension of m^2

$$darcy[D] = \frac{q \left[\frac{cm^3}{s} \right] \mu [cp] L [cm]}{dp[atm] A [cm^2]} \quad (3.4)$$

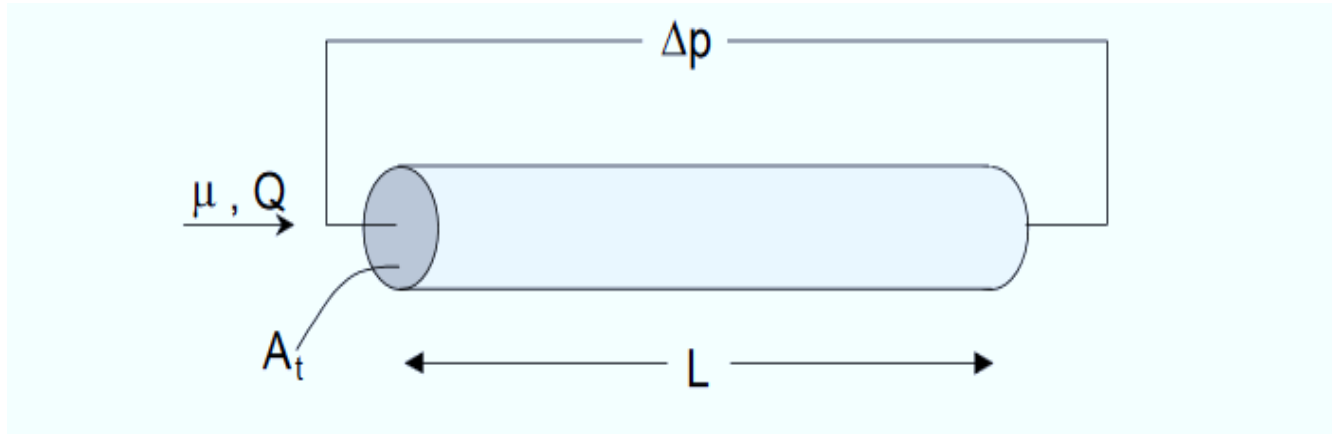


Figure 3.13: Definition of Darcy's law

The apparatus PERL – 200 is shown in Figure 3.11 and it was used to calculate the liquid permeability in (md) and the following equation was applied: -

$$K_{liq} = \frac{1000 * TEF * Q_{pump} * \mu * L}{[\pi D^2 / 4] * dP} \quad (3.5)$$

Where: -

K_L	md	Liquid permeability, millidarcy
TEF	ml/ml	Thermal expansion factor of fluid
Q_{pump}	ml/sec	Injection pump flow rate.
μ	cp	Viscosity of fluid injected
L	cm	Core Length, cm
D	cm	Core Diameter, cm
π		constant PI
dP	atm	Differential pressure across core

Excel sheet was used for core sample Liquid Permeability Calculation as shown in Table 3.7

Table 3.7: Liquid permeability spread sheet for Idaho gray sandstone sample

Length (cm)	2.54	Area (cm ²)	5.07
Diameter (cm)	2.54	Flow Volume (ml)	69.10
Viscosity (cp)	1.01		
Differential Pres (psi)	19.5		
Time (sec)	13		

Permeability (md)

2001.1

The apparatus PERG – 200 is shown in Figure 3.12 and it was used to calculate the gas permeability in (md) and the following equation was applied: -

$$K_g = \frac{2\mu Q_b P_b L T_{act}}{[\pi D^2 / 4][P_1^2 - P_2^2] T_{ref}} * 1000 \quad (3.6)$$

Where: -

k_g	md	Gas Permeability, millidarcy
m	cp	Viscosity of gas injected, cp (at mean flowing core conditions)
Q_b	sccm	Outlet Gas Flow Rate, which is referenced to P _b
	scc/sec	Volumetric Flow Rate, scc/sec (measured by the mass flow meter)
P_b	atm	standard reference pressure for mass flow meter = 1.0 atm
L	cm	Core Length, cm
D	cm	Core Diameter, cm
P₁	atm	Upstream pressure
dP	atm	Differential pressure across core
P₂	atm	Downstream pressure
T_{ref}	F	Reference temperature for mass flow meter = 294 K (21 °C)
T_{act}	F	Actual temperature
π		Constant PI

Excel sheet was used for core sample Gas Permeability Calculation as shown in Table 3.8

Table 3.8: Gas permeability spreadsheet for Idaho gray sandstone sample

Length (cm)	2.54	Area (cm²)	5.07
Diameter (cm)	2.54	Mean Pres (atmos)	1.80
Viscosity (cp)	0.0175	Upstream Pres (atmos)	1.95
Transducer Pres (psig)	14	Downstream Pres (atmos)	1.90
Flow Rate (cc/min)	2700	Flow Rate (cc/sec)	45.00

Permeability (md) 6969.8

Table 3.9: Porosity and permeability sample results


			Results Data Sheet Date: April 2015						
Petro physical properties									
NaCl wt %	Bentheimer core sample			Castlegate core sample			Idaho gray core sample		
	Porosity %	Brine Permeability (md)	Gas permeability (md)	Porosity %	Brine Permeability (md)	Gas permeability (md)	Porosity %	Brine Permeability (md)	Gas permeability (md)
10	21.7	1191	1904	24.7	741	929	23.6	2155	6830
15									
20									
26.4									

Table 3.10 : initial Brine Permeability and Initial Gas permeability

Core sample type	Initial Brine Permeability (md)	Initial Gas Permeability (md)
Bentheimer Sandstone	1200	2000
Castlegate Sandstone	750	1000
Idaho gray	2200	7000

3.3.2.3 Errors and Accuracy

The accuracy of devices and instruments utilised in this this work could be affected by CO₂ flow rates, pressure and temperature measurement. The gas flow meter has accuracy of $\pm 3\%$ and repeatability of $\pm 0.5 \%$ and the accuracy of pressure gauges were $\pm 1.2 \%$. The accuracy of the CO₂ flow rates through the system was $\pm 0.030 \%$. The effect of the operating conditions of the experimental work were highly considered.

3.4 PHASE-III: CT Scan

The CT scan is a powerful non-destructive technique that provides qualitative analysis based on the attenuation of the X-ray beams penetrating the scanned object at different angles. The cross-sectional slices that are taken across the scanned object and the three-dimensional images can be used for studying the structure, pore size and the grain distribution of the core sample. Micro and Nano-CT scanning produce 2D representations of the slice of an object. Segmentation on the image for the scanned sample was done to reduce computational time, enhance image reconstruction resolution. A section of the sample was segmented and used for image extraction and volume analysis. After segmentation, the image is extracted and a 3D visualisation of the extracted geometry of the processed CT scans of the sandstone sample. Porosity of the scanned samples was then determined using Volume Graphics Software. The sandstone core samples (Castlegate, Bentheimer and Idaho gray) were scanned before saturating with brine solutions; the objective was to determine the porosity of each core sample and validate the obtained results with porosity calculation results from Helium pycnometer method and liquid saturating method. In this section, the objective was to perform high-quality CT scans for the stated sandstone core samples and investigate whether the porosity values are consistent with values obtained using standard techniques or not.

3.4.1 Equipment Description and Principles of X-Ray Inspection

CT scanning has been used in medical fields for several decades, and the term “CAT scan” is well known to the public. However, what does a CAT scan, or CT scan, cause? From start to finish, a CT scan consists of two main processes: data collection and image reconstruction.

The desktop micro-CT scanner in the Petroleum laboratory at the Department of Petroleum and Gas Engineering, Salford University (Figure 3.15) was used to scan the studied sandstone core samples (Bentheimer, Castlegate and Idaho gray). Micro-computed tomography (micro-CT) is a powerful tool for characterising, in three dimensions, the internal structure of rock core samples through non-destructive examination. CT is a non-destructive imaging technique that uses X-ray technology and

mathematical reconstruction algorithms to view cross-sectional slices of an object[41]. In petroleum industry, CT scan is used in two main application areas: core description and fluid flow characterisation. The Principles of X-Ray inspection, X-ray are (as light is) electromagnetic waves, and their wavelength is in the range of 0.001 pm to 1 nm.

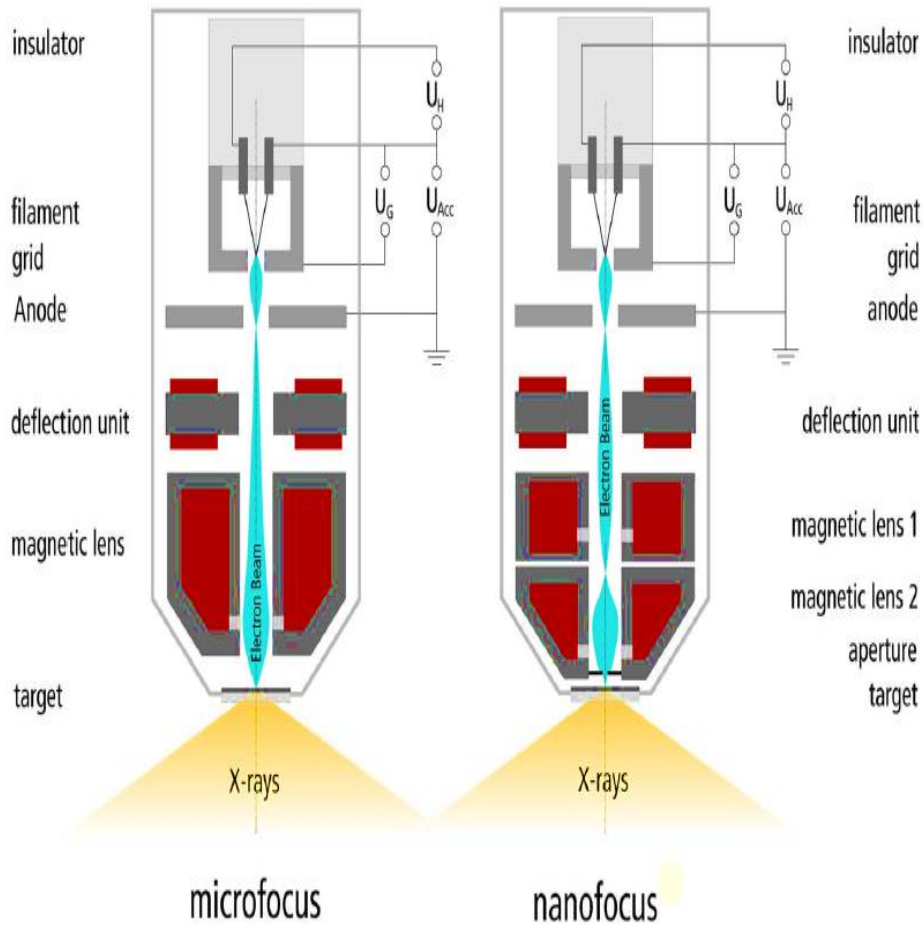


Figure 3.14 : Microfocus – nanofocus

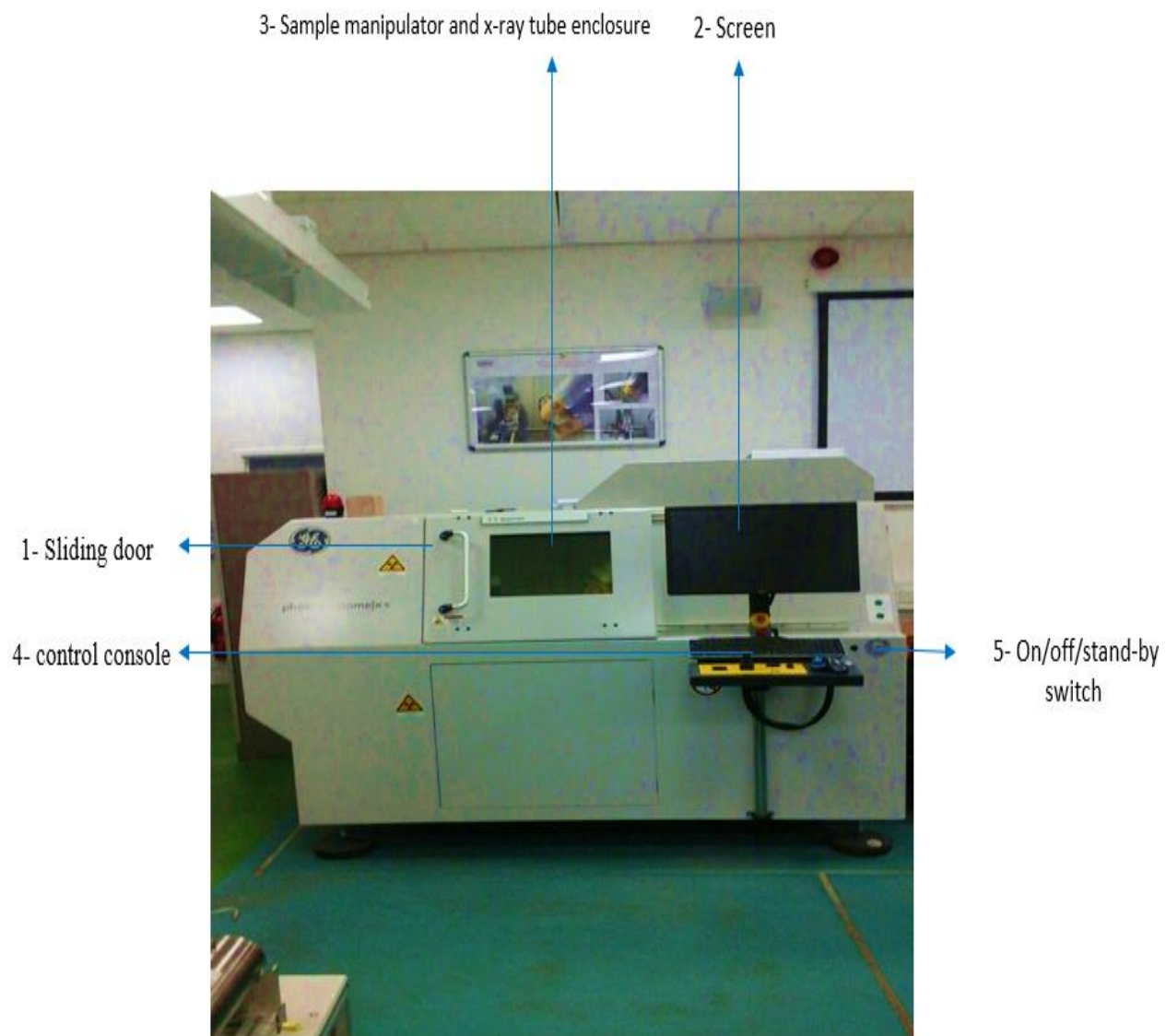


Figure 3.15 : CT scanner at Salford University

3.4.2 Methodology of Measurement

With the CT scanner “Computed tomography” at the University of Salford, the sandstone core samples (Bentheimer, Castlegate and Idaho gray) at a spatial resolution of ca. 2 μm for sample diameters were scanned with the micro focus tube. From scan results, the core sample porosity could be determined using, the module defect analysis of the software Volume Graphics (VG). The obtained results were validated with other tests results for other porosity determination techniques. For the scanned sample the 3D volume, grain structures, layering and fractures could be studied. The acquisition and reconstruction summary is as below:

- 1- Start datos|x acquisition and create a new project
- 2- Mount sample under a tilt to avoid Field Kamp artefacts
- 3- . Switch X-ray ON and press Live-Image
- 4- Set XS = 0 mm (CNC), align sample to centre, select desired sample ROI (Y-, Z- axis)
- 5- Select X-ray parameters (voltage, current, tube filtering) and detector timing and sensitivity to optimise image quality and scanning time
- 6- Create new offset and gain correction, check homogeneity
- 7- Define observation ROI (Region Of Interest).
- 8- (In case of metrology request validate the system using the easy|calib module)
- 9- Select average/skip, no. of projections, enter filter type and thickness
- 10- Select detector shift and auto scan optimiser (if applicable)
- 11- Start CT

CT scan procedure for Bentheimer sandstone core sample (Pore space and grain size distribution):

- Switch on the CT scanner (5) and personal computer for data processing implementation.
- Idaho gray sandstone core sample was inserted in the CT scanner through the sliding door (1).
- The datos|x acquisition software was opened and a new project was created.
- The sample was positioned in the sample manipulator and x-ray tube enclosure (3) for scanning. Using screen (2) and the control console (4). The sample was tilted for effective penetration of the x-ray through the sample.

- The X-ray was then turned on under the X-ray control window and, live image pressed, after ensuring the sliding door was closed properly. The region of interest (ROI) was then selected, and Figure 3.16 shows the Histogram and the scan optimizer for the core sample.

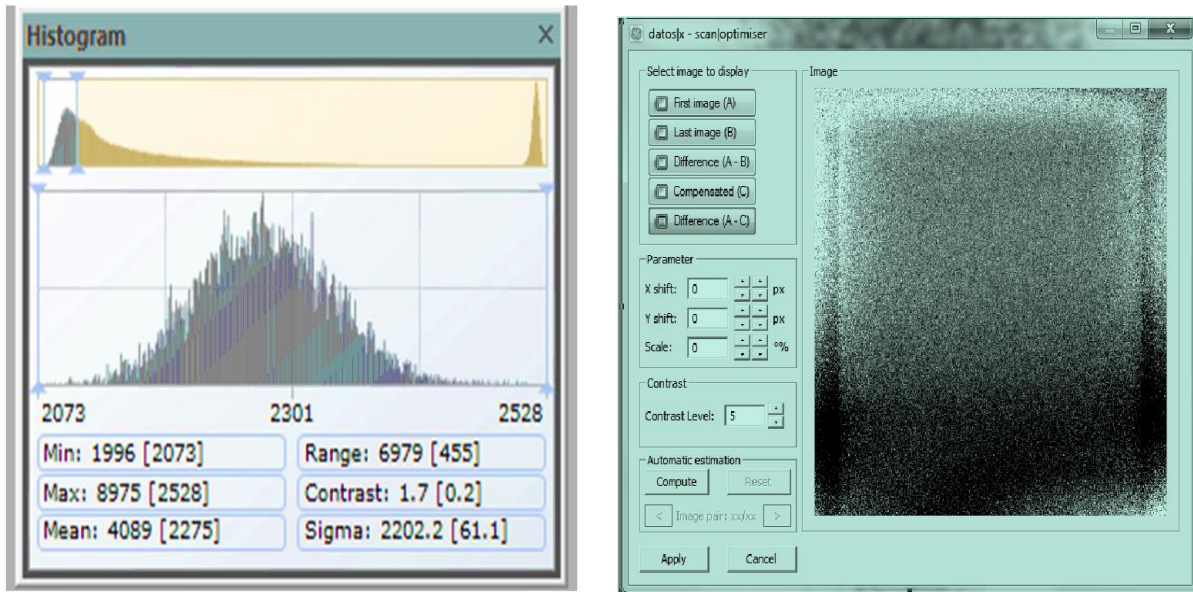


Figure 3.16 : Histogram and scan optimiser for Bentheimer sandstone

- The X-Ray settings need to be adjusted, and scanning can be started: -
 - Power – 10.4 W
 - Voltage – 160 KV
 - Current – 180 μ A
 - Focus – Standard
 - Timing – 333 ms
 - Images – 2000
 - Skip – 1
 - Average – 2
 - V Sensor – 1
 - Binning – 1x1
 - Sensitivity – 2.000

- The duration of CT scan was 1800 seconds. The data reconstruction was opened and the .pca-file loaded. A Free-ray stability check was performed on the grey value in the first and last image. The scan optimiser was used to correct system drifts and then reconstruction was run for volumetric analysis of the scanned sample (Bentheimer sandstone core sample) is shown in Figure 3.17, and grain and pore size distribution can be visualised.

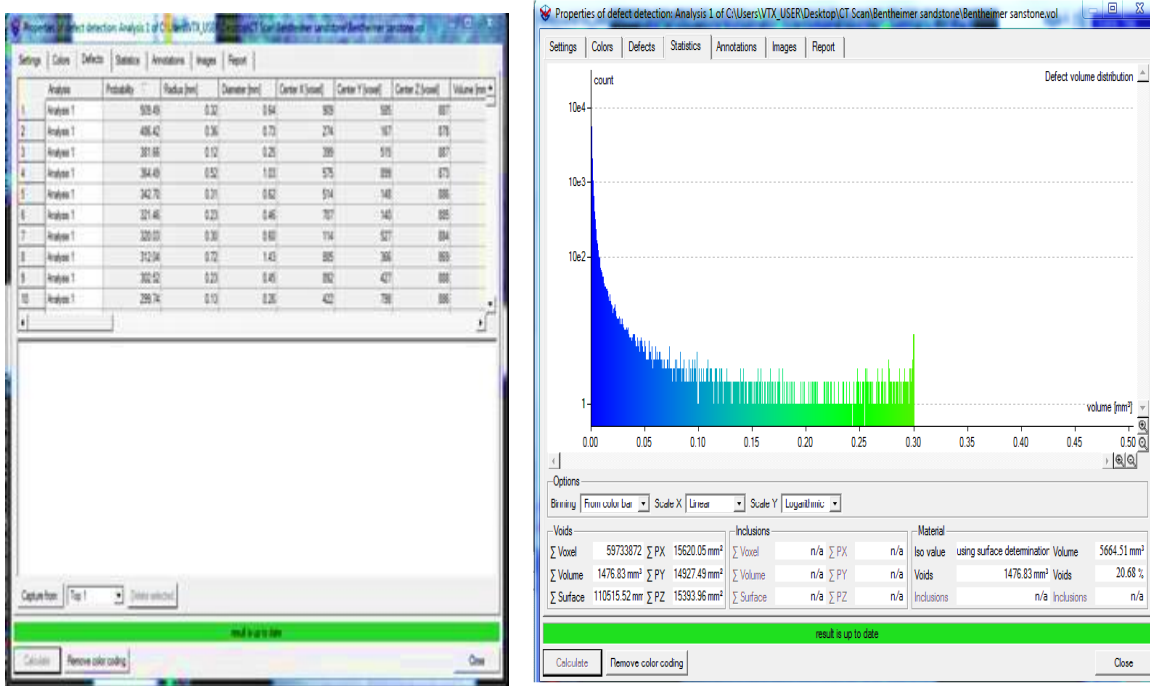


Figure 3.17 : Properties of defect detection analysis for Bentheimer sandstone core sample

3.4.2.1 CT Scan Principles and Applications

In previous decades, X-ray computed tomography (CT) gained wide acceptance as a routine analysis tool in the oil and gas industry due to low the cost of CT scan for rock characterisation in comparison to overall project value, and can improve the probability of reaching the upper-end of an NPV (net present value) range.

CT is non-destructive imaging technique that uses X-ray technology and mathematical reconstruction algorithm to view cross-sectional slices of an object. CT scan testing offers important time and effort

when compared with other techniques. The non-destructive nature of CT scanning permits the same sample to be scanned several different times. CT scanning offers an opportunity to examine particle and pore connections at any time and location.

The three dimensional image can be reconstructed from the cross sectional slices taken a cross the sample. [41] Presented comprehensive list application of CT in oil industry. The investigation grouped the applications and gave examples for each application, following are the suggested categories: core description, desaturation studies, improve recovery, hydrate studies, recovery of viscous oil, formation damage and perforation analysis.

3.4.2.2 Image Segmentation

In geological fields, the common practice employs thresholding techniques to segment the scanned images by applying a visual interpreted threshold or image processing approach. A brief summary of the parameters undertaken to obtain raw X-ray attenuation profiles using Phoenix system provided by the CT scanner at laboratory at Salford University. The detailed procedures are as follows

- **Sample Positioning:** The control panel of the system is used positioning the sample to be scanned. The sample should fills the field of the view as fully as possible. The sample has to be regulated and aligned. This will assist in obtaining the highest possible resolution.
- **Sensor Calibration:** Initially, the energy of X-ray has to be decided by change the voltage. A value of 90 KV is adequate to enter the minerals and makes good contrast between void and solid. The subsequent current is around 100 μ A. Then, the correction images have to be acquired to remove inhomogeneity in the background images i.e. images with only air between source and detector.
- **Operational Parameters:** Limitations such as the number of images to average for one projection image, the sample thickness to reduce the beam toughening effects. One significant factor affecting the image value is the number of projections that should be similar or greater to the width of the object in pixel.
- **Reconstruction:** After finishing a CT scan, the x-ray images are compiled into a quality two-dimensional view of the inner of the scanned sample. This process is known as

reconstruction, and the most significant parameter in the process is called the image centre of rotation. The process of reconstruction is fundamentally an overlaying procedure, where the individual x-ray images are aligned and laid on top of each other to form the final image. Reconstructing a CT scan produces a representation of the inner structures of an object.

- **Pore Space Imaging:** There are two types of method to generate a 3D image of the pore space. The first is direct imaging, which produces 3D images mapping the real interior structure of its original sample, such as the destructive approach of cutting and stacking serial 2D sections, confocal laser scanning microscopy and non-destructive X-ray microtomography (micro-CT). The second category includes various reconstruction methods to construct synthetic 3D rock images from high-resolution 2D thin sections using statistical methods or geological process simulation.
- **Serial Sectioning:** Serial sectioning provides a direct way to visualise 3D microstructures when successive layers of materials are removed and exposed surfaces are imaged at high resolution. The workflow of conventional serial sectioning is illustrated in Figure. 3.18. Salt precipitation in the experimental core samples is analysed using CT scans before and after saturated with sodium chloride (NaCl). CT scan rely on the transmission of X-ray through the studied sandstone core samples. The x-rays attenuation is a function of density and is measured in Hounsfield units, CT scans made of the dry core samples prior to saturate by NaCl solution are compared to CT scans made after the samples were saturated by different brine solutions and dried in oven at 100 ° C.

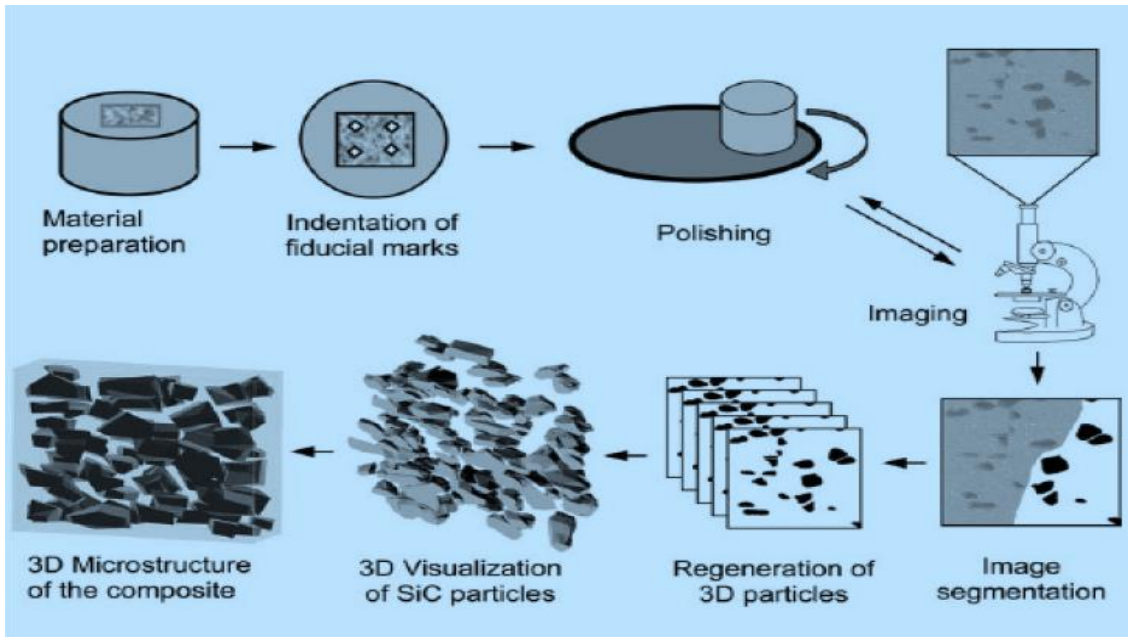


Figure 3.18 : Flow chart of sectioning to obtain 3D images of porous media [54]

- Porosity estimation by CT scan: CT scan is a powerful non-destructive testing tool for characterising and measuring volumetric porosity of rock core samples. The segmentation method based on global thresholding is used to evaluate the CT data and to obtain a measure of porosity with a high level of repeatability. These results show that CT can be used in science and industry as:
 - An alternative method for porosity determination.
 - This method can provide additional information about the internal structure of the object

Some kinds of rocks such as the hydrocarbon reservoir rock contain pores, which can have dimensions varying from microns to centimetres[40]. The porosity is then characterised by the superposition of several sizes of pore. The porosity of rock is the ratio between the volume of empty space and the total volume of the rock usually reported in a percentage between zero and one. There are several ways to estimate porosity, for example: in the petro physics laboratory with a porosimeter by injecting mercury or argon, or in the field by means of geophysical well logs or the build-up of a pressure test.

The core sample porosity can be determined from the CT image with a single scan of a core sample by detecting the pore space by image segmentation techniques. Segmentation is the first treatment applied to CT images before analysing the physical characterisation. From the scan, the core sample porosity can be calculated using the model defect analysis from the software volume graphics (VG) as mentioned before.

3.4.3 Errors and Accuracy

Computed tomography (CT) provides the most accurate images in this study. The accuracy of the scanned samples were high enough. The 3D images visualised for the pore size, grain size distribution and the core samples porosities were determined.

3.5 Chapter Summary

This Chapter is summarised as follows:

- The sandstone core samples used in this work are (Bentheimer, Castlegate and Idaho gray). These sandstone types are very good candidates and promising for CO₂ storing.
- Brine solutions concentrations of the study are (3.5, 10, 15, 20 and 26.4 wt %)
- Salinity, viscosity and density apparatuses were demonstrated.
- **PHASE – I** Core flooding tests results for Bentheimer sandstone core samples demonstrated in that there is direct proportional between the brine solution concentration and the differential pressure across the core simple.
- The solutions of brine (typically sodium chloride) in water, it is called Halite and the prepared solutions for the investigations of this study are (3.5, 10, 15, 20 and 26.4 wt %).
- **PHASE –II** The porosity, permeability, their apparatuses and their measurements were presented in details in this Chapter.
- **PHASE- III** CT scan is powerful non-destructive tool for the porosity determination; the obtained results are reliable for further reservoir studies.

The next Chapter will provide the results and discussions using the apparatus and the procedures that were described in earlier Chapter.

Chapter 4: Results and Discussion

This Chapter presents the results and discussions of the measurements and calculations of different parameters referred to the previous chapters. The results displayed and discussed according to different values obtained. Here the obtained and observed results presented based on the thesis work plan Figure 3.1, brine salinity; brine viscosity and brine density experimentally measured. For phase – I the core flooding tests we carried out for the sandstone core samples (Bentheimer, Castlegate and Idaho gray) using the Experimental set up Figure 3.8, all the obtained results are displayed and plotted in this Chapter. For Phase –II, the effective porosities for the stated core samples were determined using Helium gas porosimeter PORG – 200 in Figure 3.10, liquid saturating method and the CT- Scan method, the liquid and gas permeability were measured using PERL -200 in Figure 3.11 and PERG-200 in Figure 3.12 respectively, all the obtained results are displayed in this Chapter. For phase III the stated core samples were CT scanned and the core samples porosities were determined, pore and grain size distribution were visualised. All the obtained results and plots displayed in the upcoming sections:

4.1 Sample Preparation

The sandstone core samples (Bentheimer, Castlegate and Idaho gray) of the study in Figure 3.2 were selected for the study due to their good porosities and good permeabilities. The stated sandstone core samples are good candidates reservoirs for CO₂ storage, the samples were clean and dry, the core samples dimensions were measured and recorded as shown in Table 4.1

Table 4.1: Dimensions of the core samples used in the study

Core Name	Core Length [cm]	Core Diameter [cm]	Core Bulk volume V_b [cm ³]
Bentheimer	2.51	2.71	13.38
Castlegate	2.54	2.54	12.87
Idaho gray	2.54	2.54	12.87
Average	2.53	2.59	13.04

4.1.1 Salinity

High salinity considers the main driver of the salt precipitation and dry out around the wellbore during CO₂ storing in saline aquifers. It is public for brine to become more saline the deeper it is, but this is not necessarily the case. In this work, the salinity measured by refractometer Figure 3.4. The brine salinities in percent were calculated using equation (3.5), the selected percentage for this work are (3.5, 10, 15, 20 and 26.4 wt %).

Table 4.2 : Brine Salinity (wt %)

Sample	Salinity (wt %)
1	3.5
2	10
3	15
4	20
5	26.4

4.1.2 Viscosity

Viscosity is defined as the ‘fluid’s resistance to flow’. In everyday terms, viscosity typically referred to as ‘internal friction’, in the oil and gas industry the common unit of the viscosity is the cP. In this work the brine viscosity was measured by the electrical viscometer Figure 3.5, different brine solution were prepared and the brine viscosities were measured and the Table below shows the obtained results.

Table 4.3: Brine viscosity

Sample	Salinity (wt %)	Brine viscosity (cP)
1	3.5	2
2	10	2.7
3	15	4
4	20	6
5	26.4	8

4.1.3 Density

The brine density measured by mud balance. A mud balance, also known as a mud scale is a device used to measure the density in ppg of drilling fluid, cement or any type of liquid. The apparatus was

shown in Figure 3.6; the steps in section 3.2.2.3 were followed for the measurements and below the obtained results for different brine solutions.

Table 4.4 : Brine density and specific gravity

Sample	Brine density in kg/m ³	Brine (SG)
1	1025	1
2	1060	1.03
3	1095	1.07
4	1130	1.1
5	1170	1.12

4.1.4 Density, Viscosity and Salinity relationships

This section presents the relationship between (Brine densities as specific gravity vs Brine viscosity in cP), (Brine density in kg/m³ vs Brine salinity in wt %) and (Brine viscosity in cP Brine salinity in wt %). Density, viscosity and salinity are the most important reservoir fluid properties in the oil and gas industry, these properties effect on operations of oil and gas projects. For instance, during CO₂ storage in saline aquifers if the aquifer salinity is high, the salt precipitation phenomenon will take place and will upset the storage process. Therefore, the general understating of these properties comes at the forefront in order to guarantee steady operations for any intended industrial project in oil and gas.

Viscosity and Density of Brine Relationship

Table 4.5: Brine viscosity and density

Brine(SG)	Brine viscosity (CP)
1.03	2
1.07	2.7
1.1	4
1.12	6
1.13	8

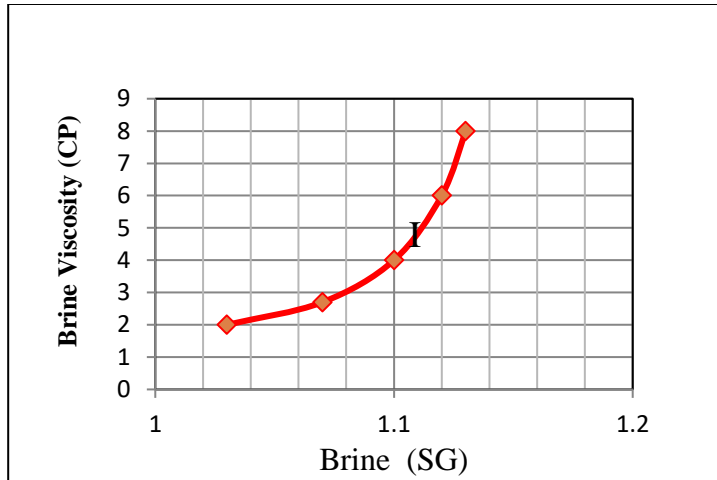


Figure 4.1: Brine density and brine viscosity

The results of brine density as specific gravity and the brine viscosity in cP are shown in Table 4.5 and their relation is shown in Figure 4.1. As the brine density increases the brine viscosity increase, however the plot does not show linear relationship between these parameters.

Brine Salinity and Density Relationship

Table 4.6: Brine salinity and density

Salinity (Wt %)	Density (kg/ m ³)
5	1025
10	1060
15	1095
20	1130
26.4	1170

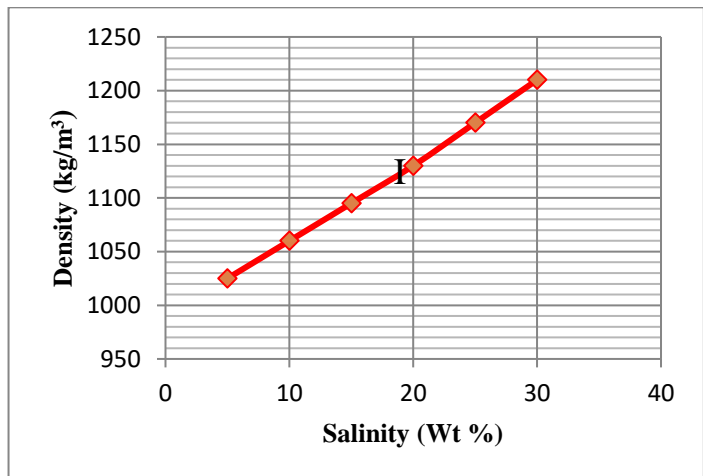


Figure 4.2: Brine salinity and brine density

The results of brine salinity and the brine density in in (kg/m³) are shown in Table 4.6 and their relation is shown in Figure 4.2. As the brine salinity increases the brine density increase, the plot shows linear relationship between these parameters.

Brine Viscosity and Salinity Relationship

Table 4.7: Brine viscosity and salinity

Salinity (Wt %)	Brine viscosity (cp)
5	2
10	2.7
15	4
20	6
26	8

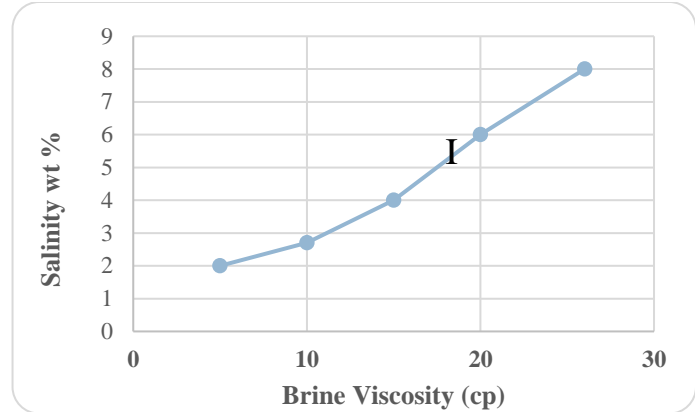


Figure 4.3 :Brine salinity and brine density

The results of brine salinity and the brine viscosity in in (cP) are shown in Table 4.7 and their relation is shown in Figure 4.3. As the brine, salinity increases the brine viscosity increase.

4.2 PHASE – I Core Flooding Tests

These tests were carried out using the Experimental set up in Figure 3.7, the CO₂ was injected at different injection pressure in (psi) to flow in (l/min) through the sandstone core samples, Section 3.3 (Bentheimer, Castlegate and Idaho gray) which were saturated with different brine solutions (10, 15, 20 and 26.4 wt %). The tests were carried after drying the saturated core samples in oven at 100 °C for 24 hours. The purpose was to investigate the effect of the precipitated NaCl on the performance of tests for the stated sandstone core samples. The same samples were re saturated with 3.5 wt % brine solution, the purpose of the dilution was to dissolve any precipitated salts around the core sample and make pores more effective. The sections below show the results for the stated tests:

4.2.1 Core Flooding Tests for Bentheimer Sandstone

Experimental set up in Figure 3.8, the CO₂ was injected at different injection pressure in (psi) to obtain flow in (l/min) through the sandstone core samples (Bentheimer, Castlegate and Idaho gray) which were saturated with different brine solutions (10, 15, 20 and 26.4 wt %). The same core samples were re saturated with 3.5 wt % in order to dilute the brine concentration, and the core flow tests were re – carried out. The sections below show the experimental work results.

Table 4.8 : Core flooding test results for Bentheimer sandstone (10 % NaCl + saturated with 3.5 %)

	Bentheimer			
	10% Brine Concentration		Inject Water + 3.5% NaCl	
	P-Inlet (P1)	P-Outlet (P2)	Q-Outlet (Q2)	Q-Outlet (Q3)
psi	psi	l/min	psi	l/min
10.0	8.0	2.0	7.0	2.5
20.0	16.0	3.0	15.0	3.5
30.0	25.0	4.0	24.0	4.5
40.0	36.0	5.0	34.0	5.5
50.0	45.0	6.0	43.0	6.8

The results in Table 4.8 showed that when the core sample saturated with 3.5 wt % brine solution the flow rate (Q3) in l/min increased, this will lead to an improvement in injectivity. The objective was how the dilution of brine solutions by using seawater or brackish water can assist to dissolve the precipitated salt around the core samples, by the dilution, the core pores become more effective and the core permeability improved. According to Darcy's equation (3.3) the higher the differential pressure across the core sample the lower the permeability obtained. Figure 4.4 illustrated the relations of the operating conditions, and it is obvious that the dilution of the brine solution to 3.5 wt % contributed to improve the CO₂ flow rate in (l/ min). This indicated that the higher salinity would cause damage of the core permeability with the attendance of reduction in injectivity. During CO₂ storage in saline aquifer, the salt precipitation around the wellbore is expected to take place due to high salinity. The salinity considers the main driver of the salt precipitation phenomenon. It is believed that the periodic flush of the aquifer water with lower salinity water (seawater, brackish water) can contribute in eliminating the impact of formation dry out around the wellbore.

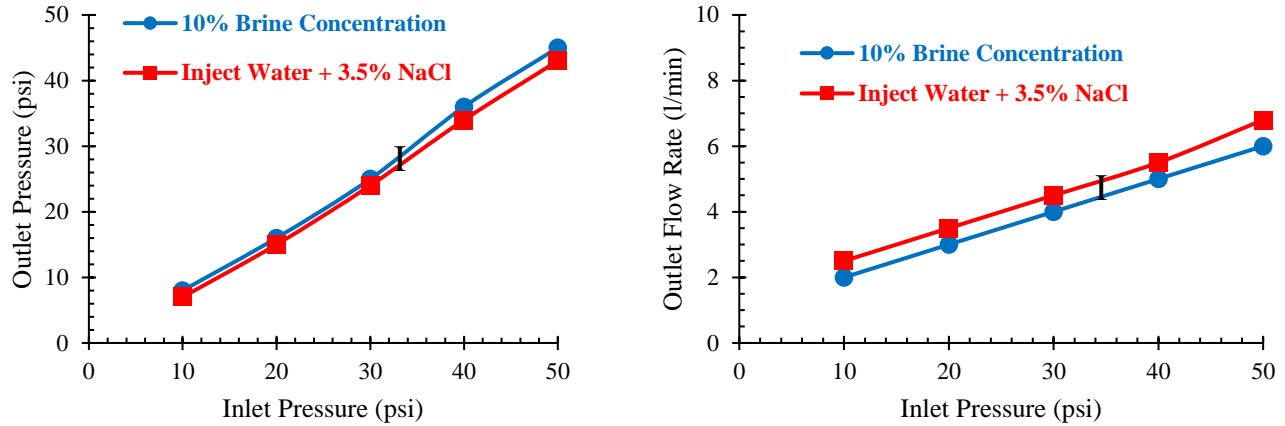


Figure 4.4: Core flow test results for Bentheimer sandstone (10 % NaCl + saturated with 3.5 %)

In the relationship between inlet pressure and outlet pressure, it is obvious that outlet pressure (P3) is greater than the outlet pressure (P2), this means that when the core samples were saturated in 3.5 wt % NaCl, the precipitated salt that were blocking the pores dissolved and the differential pressure across the core samples decreased. In the inlet, pressure and outlet flow rate the value of (Q3) is higher than the value of (Q2); this was due to the effect of the dilution of the brine solution to 3.5 wt %.

Table 4.9: Core flow test results for Bentheimer sandstone (15 % NaCl + saturated with 3.5 %)

	Bentheimer			
	15% Brine Concentration		Inject Water + 3.5% NaCl	
	P-Outlet (P2)	Q-Outlet (Q2)	P-Outlet (P3)	Q-Outlet (Q3)
P-Inlet (P1)				
psi	psi	l/min	psi	l/min
10.0	7.5	1.5	8.0	2.0
20.0	16.0	2.5	17.0	3.0
30.0	26.0	3.5	27.0	4.0
40.0	34.0	4.5	36.0	5.0
50.0	45.0	5.3	43.0	6.0

The results in Table 4.9 shows that when the core samples were saturated with 3.5 wt % brine solution, the CO₂ flow rate (l/min) increased the dilution of the brine concentration to 3.5 wt %. This assisted in dissolving the precipitated salt around the core sample, making the pores in core samples more

effective and increasing core permeability. Figure 4.5 illustrated the relations of the operating parameters, and it is obvious that the dilution of the brine solution to 3.5 wt % contributed to improve the CO₂ flow rate in (l/min). This indicated that the lower salinity could minimise the risk of damage to the core permeability and maintain the injectivity. During CO₂ storage in saline aquifer, the salt precipitation around the wellbore is expected to take place due to high salinity. The salinity considers the main driver of the salt precipitation phenomenon. Minimising the formation salinity by flushing the formation with lower salinity is reliable strategy to overcome the salt precipitation problems.

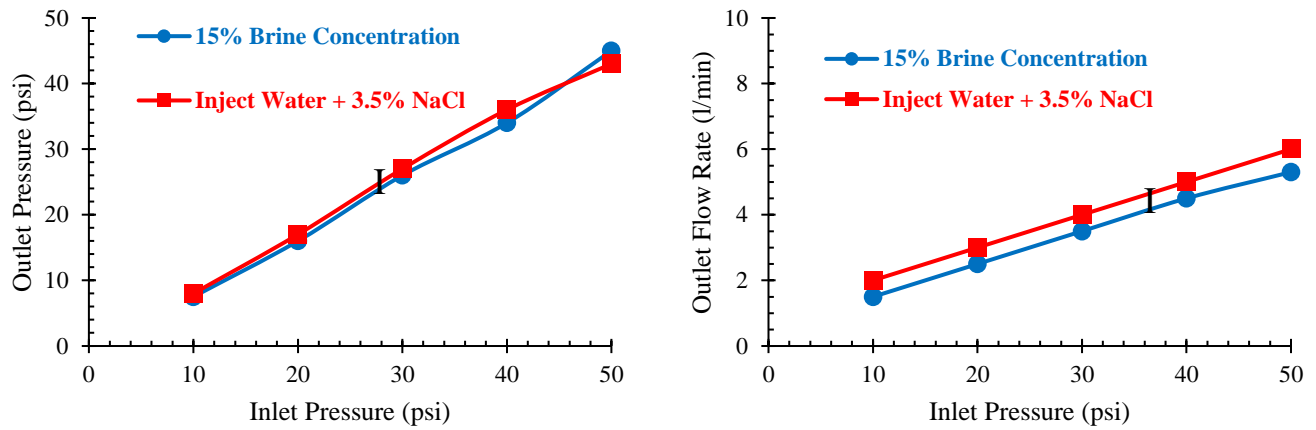


Figure 4.5: Core flow test results for Bentheimer sandstone (15 % NaCl + saturated with 3.5 %)

Table 4.10 : Core flow test results for Bentheimer sandstone (20 % NaCl + saturated with 3.5 %)

	Bentheimer			
	20% Brine Concentration		Inject Water + 3.5% NaCl	
	P-Inlet (P1)	P-Outlet (P2)	Q-Outlet (Q2)	P-Outlet (P3)
psi	psi	l/min	psi	l/min
10.0	6.0	1.0	7.0	1.5
20.0	14.0	2.0	15.0	2.5
30.0	25.0	3.0	26.0	3.5
40.0	34.0	4.0	36.0	4.5
50.0	43.0	4.7	45.0	5.5

Chapter 4: Results and Discussion

The results in Table 4-10 demonstrated that the outlet pressure (P3) increased, this means that the core sample permeability improved and the injectivity will be improved. It is clear that when the core samples were saturated with low brine solution, the CO₂ flow rate in (l/min) increased. The values of (Q3) increased; this indicates that the using seawater can dilute the aquifer water salinity if the injected water meets the technical specification in Table 3.2. Dissolving the salts could be achieved through flushing the storage aquifer with lower salinity water. As stated before the high salinity will cause formation permeability damage. The displayed results in the stated table showed that (Q2) is less than (Q3) due to the precipitated salt around the core samples when they were dried in oven at 100 °C for 24 hours .During CO₂ storage in saline aquifer, the salt precipitation around the wellbore is expected to take place due to high salinity. The salinity considers the main driver of the salt precipitation phenomenon. Figure 4.6 illustrated the relations.

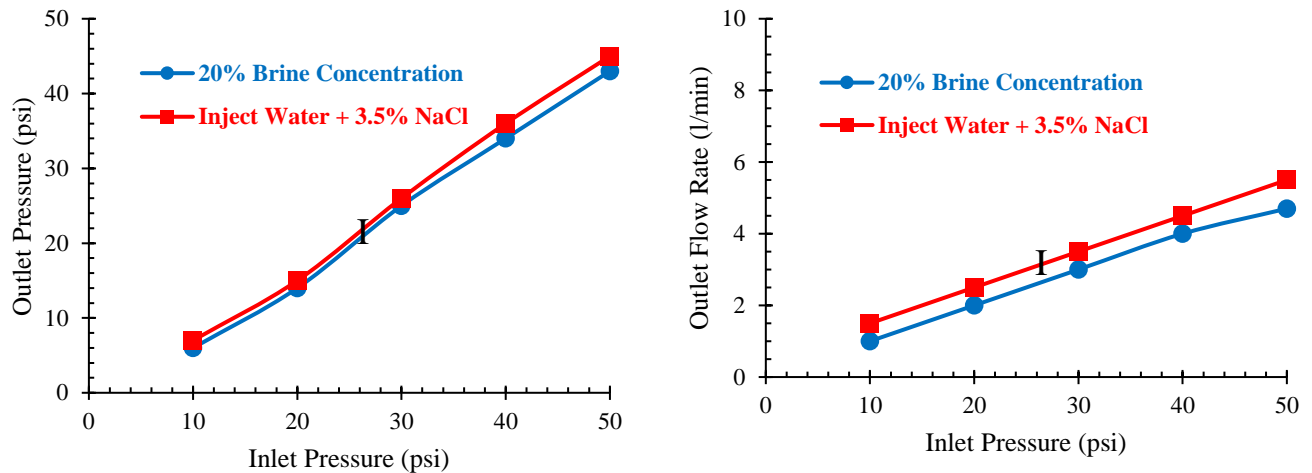


Figure 4.6 : Core flow test results for Bentheimer sandstone (20 % NaCl + saturated with 3.5 %)

Table 4.11: Core flow test results for Bentheimer sandstone (26 % NaCl + saturated with 3.5 %)

	Bentheimer			
	26.4% Brine Concentration		Inject Water + 3.5% NaCl	
P-Inlet (P1)	P-Outlet (P2)	Q-Outlet (Q2)	P-Outlet (P3)	Q-Outlet (Q3)
psi	psi	l/min	psi	l/min
10.0	5.0	0.4	6.0	0.6
20.0	13.0	1.0	15.0	1.4
30.0	23.0	1.8	25.0	2.8
40.0	31.0	2.5	36.0	3.7
50.0	41.0	3.2	45.0	4.8

The results in Table 4.11 showed that there was high differential pressure across the core sample, the outlet pressure (P2) at the injection pressure of 50 psi was 41 psi when the core sample was saturated with 26 wt. % i.e. the differential pressure was 9 psi. In this case, the outlet flow rate (Q2) was 3.2 l/min; the flow rate was low because the precipitated salt around the core sample effected the core sample permeability. This was the first scenario. In the second scenario when the sample was saturated in lower brine solution 3.5 wt%, and the objective was to remove the precipitated salt around the core sample, the outlet pressure (P2) was 45 psi and the flow rate was 4.8 l/min, and the differential pressure across the core sample was 5 psi. The reduction in the differential pressure indicates that that there was an improvement in the core sample permeability and injectivity. Figure 4.7 illustrated the relations of the operating conditions, and it is obvious that the dilution of the brine solution to 3.5 wt % contributed to improve the CO₂ flow rate in (l/min), i.e. the periodic flush of the aquifer with low salinity water is good strategy to be adopted during CO₂ storage in saline aquifers.

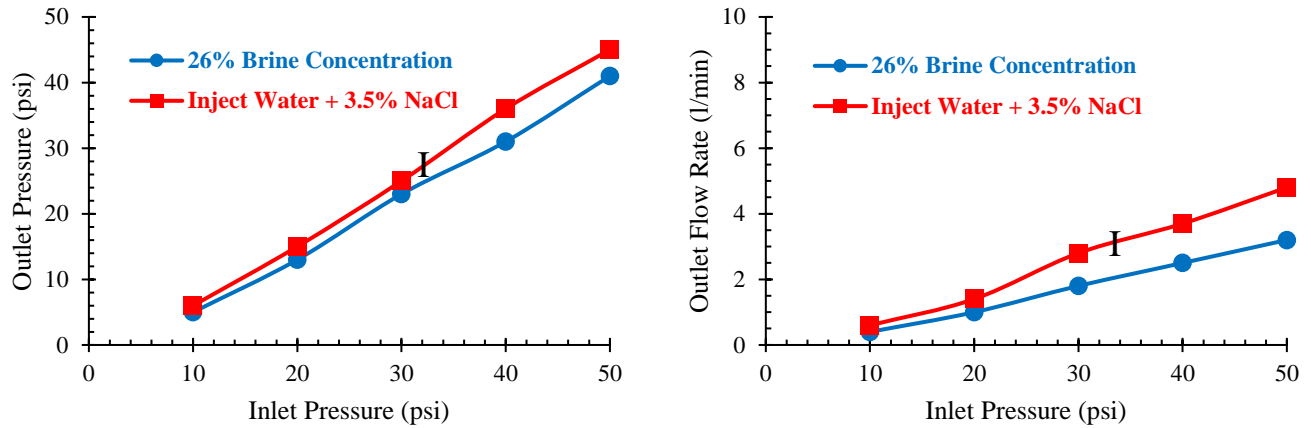


Figure 4.7: Core flow test results for Bentheimer sandstone (10 % NaCl + saturated with 3.5 %)

The results of the core flow tests for the Bentheimer, sandstone core samples in Tables 4.8 – 4.11 demonstrated that the differential pressure across all the tested core samples decreases when the cores were saturated with 3.5 wt % brine solution, i.e the dilution of the brine solution assists in dissolving the salt around the core sample and reduces the pores blocking. When the salt precipitates the pores of the core sample becomes less effective, this will affect the permeability and the injectivity. If this takes place during CO₂ storage in saline aquifer the pressure will build up, the seal may fracture, and the CO₂ will migrate to the upper formation.

4.2.2 Core Flooding Tests for Castlegate Sandstone

In the Experimental set up Figure 3.8, the CO₂ was injected at different injection pressure in (psi) to flow in (l/min) through the sandstone core samples (Bentheimer, Castlegate and Idaho gray) which were saturated with different brine solutions (10, 15, 20 and 26 wt %). The same core samples were re saturated with 3.5 wt % in order to dilute the brine concentration, and the core flow tests were re – carried out. The sections below show the experimental work results.

Table 4.12: Core flow test results for Castlegate sandstone (10 % NaCl + saturated with 3.5 %)

	Castlegate			
	10% Brine Concentration		Inject Water + 3.5% NaCl	
P-Inlet (P1)	P-Outlet (P2)	Q-Outlet (Q2)	P-Outlet (P3)	Q-Outlet (Q3)
psi	psi	l/min	psi	l/min
10.0	7.0	2.0	8.0	2.5
20.0	15.0	3.0	17.0	3.5
30.0	26.0	4.0	26.0	4.5
40.0	33.0	5.0	34.0	5.5
50.0	43.0	5.5	44.0	6.5

The results in Table 4.12 are similar to previous ones that obtained from carrying out the tests on Bentheimer sandstone core samples. The dilution of the brine salinity to 3.5 wt % contributed in lowering the differential pressure across the core samples. For example, when (P2) was 15 psi (P3) was 17 psi, i.e at (P1) the differential pressure across the core sample was 5 psi and at (P3) the differential pressure across the core sample was 3 psi. This is good indication that the dilution of the solution assisted to dissolve the precipitated salt, the core pores become more effective and the core permeability improved. Figure 4.8 illustrated the relations of the operating parameters, and it is very clear that when the differential pressure decreases across the core samples the flow rate (Q3) in l/min increases.

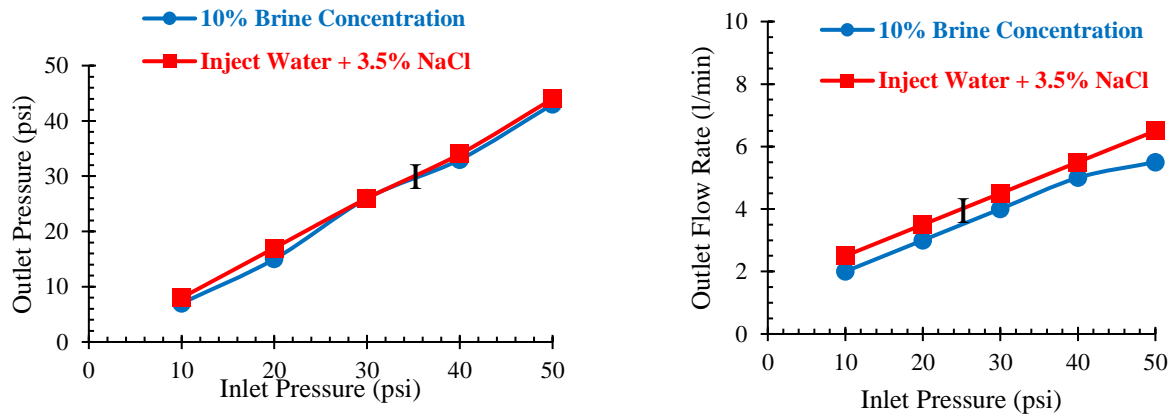


Figure 4.8 : Core flow test results for Castlegate sandstone (10 % NaCl + saturated with 3.5 %)

Table 4.13: Core flow test results for Castlegate sandstone (15 % NaCl + saturated with 3.5 %)

	Castlegate			
	15% Brine Concentration		Inject Water + 3.5% NaCl	
P-Inlet (P1)	P-Outlet (P2)	Q-Outlet (Q2)	P-Outlet (P3)	Q-Outlet (Q3)
psi	psi	l/min	psi	l/min
10.0	6.5	2.0	7.0	2.5
20.0	16.0	3.0	17.0	3.5
30.0	25.0	4.0	26.0	4.5
40.0	32.0	4.5	35.0	5.0
50.0	40.0	5.0	42.0	6.0

The results in Table 4.13 showed that there is an improvement in the flow rate (Q3) in l/min; this was due to the effect of the dilution of the brine solution concentration to 3.5 wt %. For example at brine concentration of 15 wt % when the injection pressure (P1) was 30 psi, the outlet pressure (P2) was 25 psi and the outlet flow rate (Q2) was 4 l/min. When the brine solution diluted to 3.5 wt % the outlet pressure (P3) was 26 psi, flow rate (Q3) was 4.5 l/min at the same injection pressure (P1) was 30 psi. Therefore, the dilution of the solution assisted to dissolve the precipitated salt, the core pores become more effective and the core permeability improved. Figure 4.9 illustrated the relations of the operating parameters, and it is obvious that the dilution of the brine solution to 3.5 wt % contributed to improve the CO₂ flow rate in (l/ min). This indicated that as the salinity increases the core permeability decreases and this would affect the injectivity performance. Consequently, the dilution of the salinity of the formation water during CO₂ storage in saline aquifer considers a reliable option to avoid the impact with the salt precipitation problems.

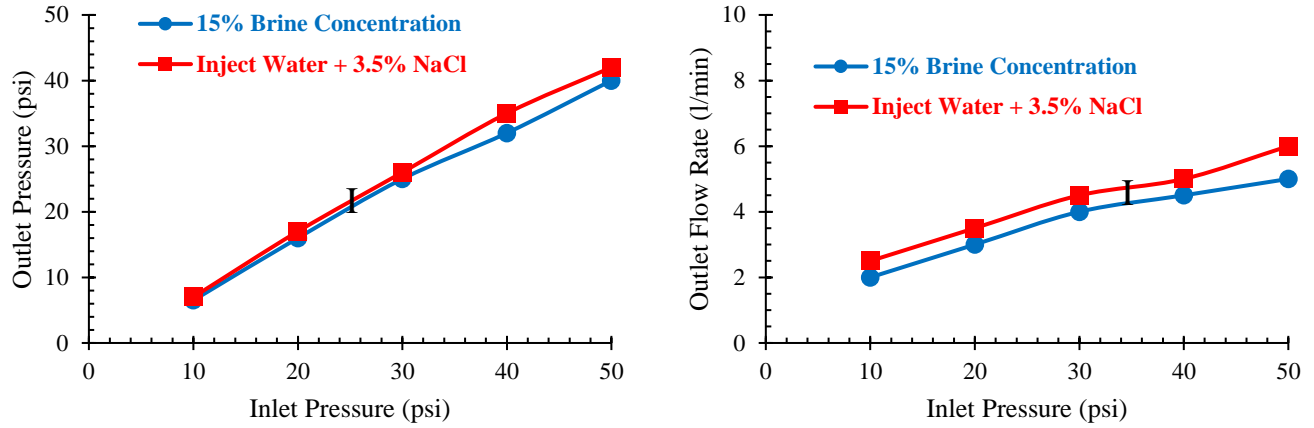


Figure 4.9 : Core flow test results for Castlegate sandstone (15 % NaCl + saturated with 3.5 %)

Table 4.14: Core flow test results for Castlegate sandstone (20 % NaCl + saturated with 3.5 %)

	Castlegate			
	20% Brine Concentration		Inject Water + 3.5% NaCl	
P-Inlet (P1)	P-Outlet (P2)	Q-Outlet (Q2)	P-Outlet (P3)	Q-Outlet (Q3)
psi	psi	l/min	psi	l/min
10.0	6.0	1.0	7.0	1.3
20.0	15.0	2.0	16.0	2.5
30.0	22.0	3.0	24.0	3.5
40.0	30.0	4.0	32.0	4.5
50.0	40.0	5.0	43.0	5.5

The results in Table 4.14 showed that there is improvement in the flow rate (Q3). This was due to the effect of the saturation of the core sample in the diluted brine solution 3.5 wt % . , the dilution of the solution assisted to dissolve the precipitated salt, the core pores become more effective and the core permeability improved. Figure 4.10 illustrated the relations of the operating parameters, and it is obvious that the dilution of the brine solution to 3.5 wt % contributed to improve the CO₂ flow rate in (l/ min). This indicated that the higher salinity the higher the deferential pressure across the core sample. As result, the core sample permeability will damage due to the precipitation of salt around the core sample. During CO₂ storage in saline aquifer, the salt precipitation around the wellbore is

expected to take place due to high salinity. The salinity considers the main driver of the salt precipitation phenomenon.

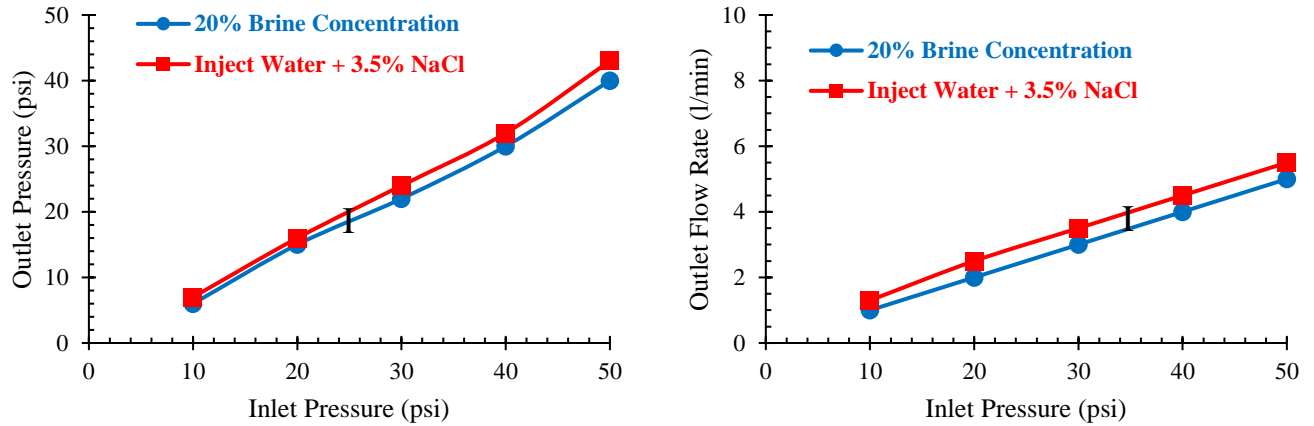


Figure 4.10 : Core flow test results for Castlegate sandstone (20 % NaCl + saturated with 3.5 %)

Table 4.15 : Core flow test results for Castlegate sandstone (26 % NaCl + saturated with 3.5 %)

	Castlegate			
	26.4% Brine Concentration		Inject Water + 3.5% NaCl	
P-Inlet (P1)	P-Outlet (P2)	Q-Outlet (Q2)	P-Outlet (P3)	Q-Outlet (Q3)
psi	psi	l/min	psi	l/min
10.0	4.0	0.4	7.0	0.6
20.0	10.0	1.0	14.0	1.4
30.0	12.0	2.0	22.0	3.0
40.0	18.0	3.0	31.0	4.5
50.0	25.0	4.0	39.0	6.0

The results in Table 4.15 showed the data that was collected at the worst scenario of this study when the brine concentrating was 26.4 wt %, the outlet pressure (P2) was 25 psi at the injection pressure 50 psi. When the core sample was saturated in the diluted brine solution 3.5, the outlet pressure was 39 psi at the same injection pressure (P1) 50 psi. When the sample was saturated in the diluted brine solution 3.5 wt % the pores of the core sample become more efficient, the core sample permeability improved and the injectivity will increase. It is clear that the dilution of the brine solution to 3.5 wt % contributed to improve the CO₂ flow rate in (l/ min). This indicated that the higher salinity will cause damage of

the core permeability and certainly, the injectivity will be reduced. During CO₂ storage in saline aquifer, the salt precipitation around the wellbore is expected to take place due to high salinity. The salinity considers the main driver of the salt precipitation phenomenon. Figure 4.11 illustrated the relations of the obtained results.

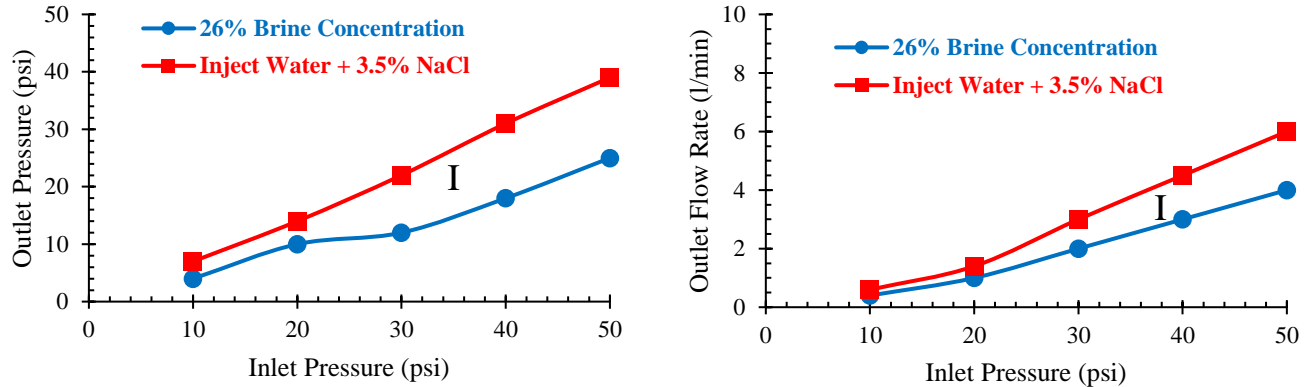


Figure 4.11 : Core flow test results for Castlegate sandstone (26 % NaCl + saturated with 3.5 %)

The results of the core flow tests for the Castlegate sandstone core samples in Tables 4.12 – 4.15 demonstrated that the differential pressure across the entire tested core samples decreases when the cores were saturated with 3.5 wt % brine solution. The dilution of the brine solution assists in dissolving the salt around the core sample and reduces the pores blocking. To avoid the impact with salt precipitation consequences during CO₂ storage in Saline aquifers it is believed that flushing the aquifer with low salinity water (i.e. seawater) can eliminate this problem and assist in keeping steady operations.

4.2.3 Core Flooding Tests for Idaho gray Sandstone

Experimental set up in Figure 3.8, the CO₂ was injected at different injection pressure in (psi) to flow in (l/min) through the sandstone core samples (Bentheimer, Castlegate and Idaho gray) which were saturated with different brine solutions (10, 15, 20 and 26.4 wt %). The same core samples were re-saturated with 3.5 wt % in order to dilute the brine concentration, and the core flow tests were re-carried out. The sections below show the experimental work results.

Table 4.16: Core flow test results Idaho gray sandstone (10 % NaCl + saturated with 3.5 %)

	Idaho Gray			
	10% Brine Concentration		Inject Water + 3.5% NaCl	
P-Inlet (P1)	P-Outlet (P2)	Q-Outlet (Q2)	P-Outlet (P3)	Q-Outlet (Q3)
psi	psi	l/min	psi	l/min
10.0	8.0	2.5	8.5	3.0
20.0	17.0	3.5	17.0	4.0
30.0	24.0	4.5	26.0	5.0
40.0	34.0	5.0	36.0	6.0
50.0	43.0	6.0	45.0	7.0

The results in Table 4.16 showed similar results to the obtained for Bentheimer sandstone core samples and Castlegate sandstone core samples. It is very clear that the salt precipitation in the form of NaCl has considerable effect on the core sample permeability. The main objective of this work was to search for remedial work that can eliminate the impact of salt precipitation phenomenon during CO₂ storage in Saline aquifer. It is believed that the dilution of the formation salinity with lower water salinity can assist to delay the onset of salt precipitation problems. As stated before if the differential pressure across the core sample decreases, the core sample permeability increases. Figure 4.12 illustrated the relations of the operating conditions, and it is obvious that the dilution of the brine solution to 3.5 wt % contributed to improve the CO₂ flow rate in (l/ min). At (P1) 50 psi the (P2) was 43 psi when the core sample was saturated with 10 wt % brine solution. When the core sample was saturated in 3.5 wt % the outlet pressure (P3) was 45 psi and the outlet flow rate (Q3) was 7.0 l/min.

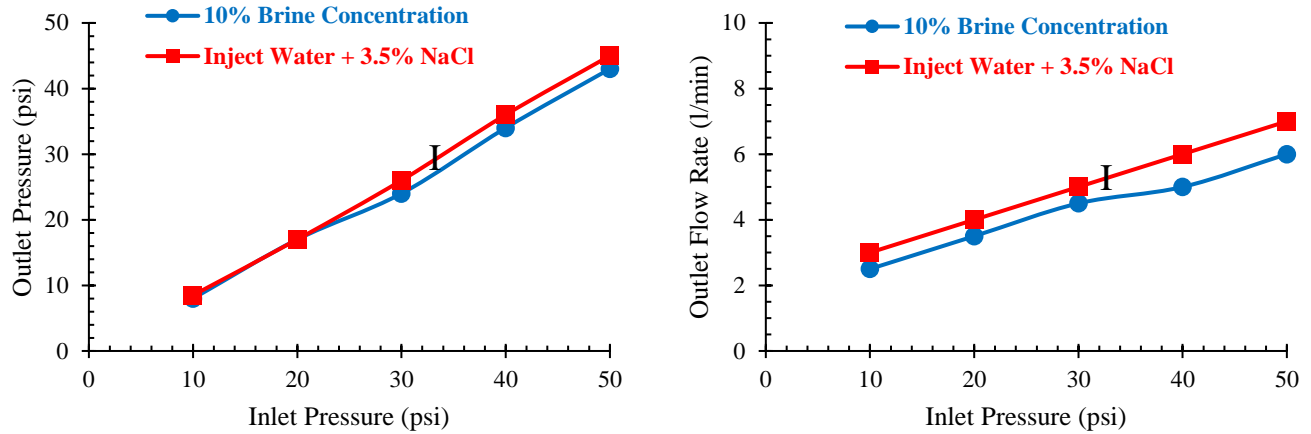


Figure 4.12 : Core flow test results for Idaho gray sandstone (10 % NaCl + saturated with 3.5 %)

Table 4.17: Core flow test results Idaho gray sandstone (15 % NaCl + saturated with 3.5 %)

	Idaho Gray			
	15% Brine Concentration		Inject Water + 3.5% NaCl	
P-Inlet (P1)	P-Outlet (P2)	Q-Outlet (Q2)	P-Outlet (P3)	Q-Outlet (Q3)
psi	psi	l/min	psi	l/min
10.0	7.0	2.0	8.0	2.5
20.0	16.0	3.0	17.0	3.5
30.0	24.0	4.0	26.0	4.5
40.0	34.0	5.0	36.0	5.5
50.0	43.0	5.5	45.0	6.5

The results in Table 4.17 demonstrated that the differential pressure across the sample decreased. When the core sample was saturated with 3.5 wt% at injection pressure 40 psi, the outlet pressure (P3) was 36 psi and the flow rate was 5.5 l/min while at 15 wt % the outlet pressure was 34 psi and the flow rate was 5.0 l/min. As explained before the reduction in the differential pressure across the core sample indicates that the core sample pores are interconnected, and the sample permeability is good. Figure 4.13 illustrated the relations of the collected data, and it is obvious that the dilution of the brine solution to 3.5 wt % contributed to improve the CO₂ flow rate in (l/ min).

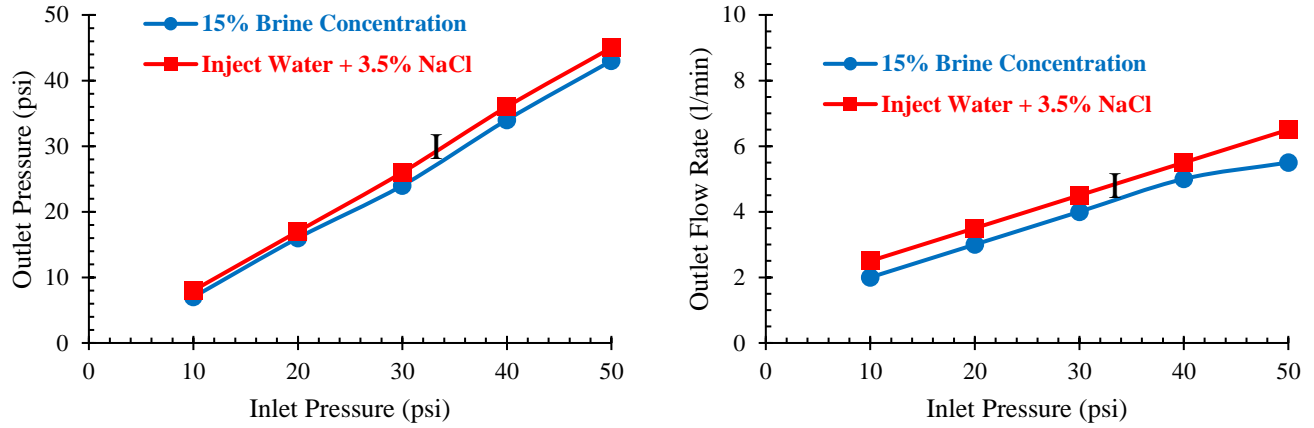


Figure 4.13: Core flow test results for Idaho gray sandstone (15 % NaCl + saturated with 3.5 %

Table 4.18 : Core flow test results Idaho gray sandstone (20 % NaCl + saturated with 3.5 %)

	Idaho Gray			
	20% Brine Concentration		Inject Water + 3.5% NaCl	
P-Inlet (P1)	P-Outlet (P2)	Q-Outlet (Q2)	P-Outlet (P3)	Q-Outlet (Q3)
psi	psi	l/min	psi	l/min
10.0	6.0	1.5	7.0	1.8
20.0	15.0	2.5	17.0	3.0
30.0	24.0	3.5	26.0	4.0
40.0	34.0	4.5	36.0	5.0
50.0	42.0	5.5	45.0	6.4

The results in Table 4.18 showed that there is an improvement in the flow rate. In this case at the brine solution concentration 15 wt % the outlet pressure (P2) was 42 psi and the flow rate was 5.5 l/min at the injection pressure (P1) 50 psi. When the core sample was saturated with 3.5 wt % brine solution the outlet pressure (P3) was 45 psi and the flow rate (Q3) was 6.4 l/min. Figure 4.14 illustrated the relations of the obtained results, and it is obvious that the dilution of the brine solution to 3.5 wt % contributed to improve the CO₂ flow rate in (l/ min). During CO₂ storage in saline aquifer, the salt precipitation around the wellbore is expected to take place due to high salinity as the salinity considers the main driver of the salt precipitation phenomenon.

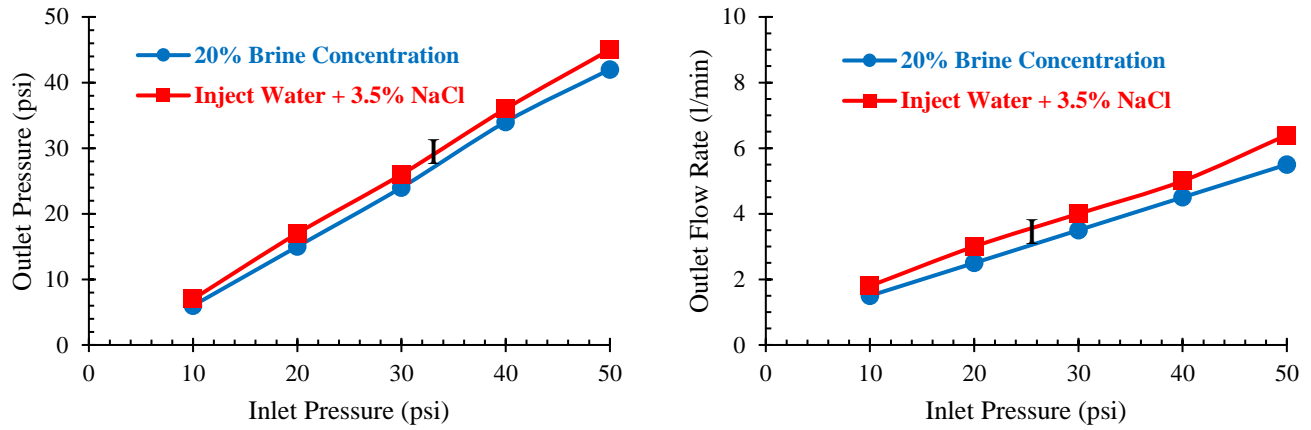


Figure 4.14 : Core flow test results for Idaho gray sandstone (20 % NaCl + saturated with 3.5 %)

Table 4.19 : Core flow test results Idaho gray sandstone (26 % NaCl + saturated with 3.5 %)

	Idaho Gray			
	26.4% Brine Concentration		Inject Water + 3.5% NaCl	
P-Inlet (P1)	P-Outlet (P2)	Q-Outlet (Q2)	P-Outlet (P3)	Q-Outlet (Q3)
psi	psi	l/min	psi	l/min
10.0	6.0	0.5	7.0	0.7
20.0	12.0	1.5	15.0	2.1
30.0	20.0	2.5	24.0	3.5
40.0	31.0	3.5	36.0	5.0
50.0	39.0	4.2	43.0	5.6

The results in Table 4.19 showed the data that was collected for the worst scenario in this study. The brine solution concentration was 26.4 wt % , at this concentration when the inlet pressure (P1) was 50 psi the outlet pressure (P2) was 39 psi and the outlet flow rate (Q2) was 4.2 l/min. At brine concentration of 3.5 wt % when the inlet pressure (P1) was 50 psi the outlet pressure (P2) was 43 psi and the flow rate (Q3) was 5.6 l/min. This indicates that due to the dilution of brine concentration to 3.5 wt% the core sample pore throats become more effective and the core sample permeability improved. Figure 4.15 illustrated the relations of the collected data.

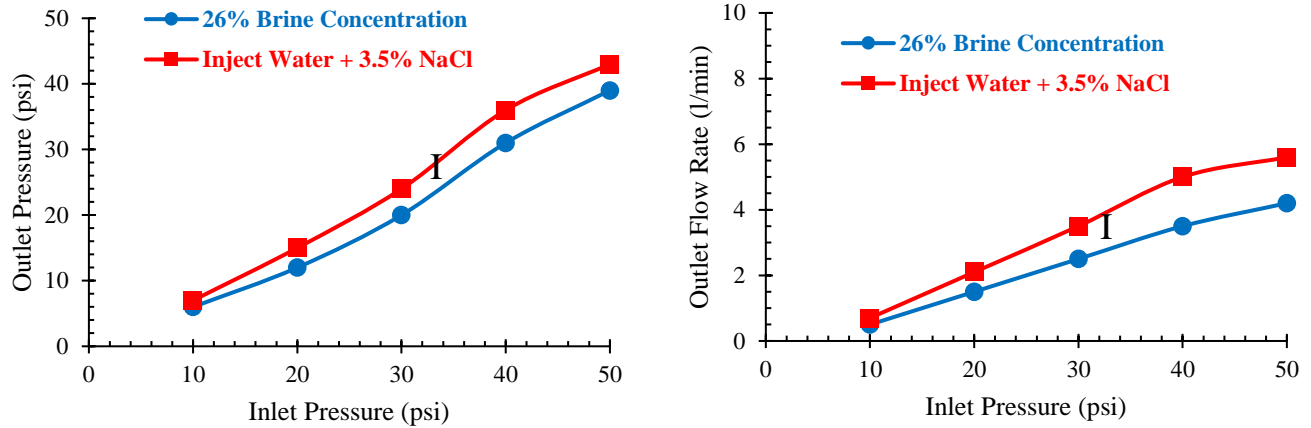


Figure 4.15 : Core flow test results for Idaho gray sandstone (20 % NaCl + saturated with 3.5 %)

The results of the core flow tests for the Idaho gray sandstone core samples in Tables 4.16 – 4.19 demonstrated that the differential pressure across all the tested core samples decreases when the cores were saturated with 3.5 wt % brine solution. This means that the dilution of the brine solution assists in dissolving the salt around the core sample and reduces the pores blocking. The experiment results of this research demonstrated that as the salinity increases the differential pressure across the core samples increases. This will have negative impact on the core sample permeability and injectivity as well. Using seawater is considered reliable option if the technical specification of the used water are met. Weakening the brine concentration in the near well bore area by satisfying it with low salinity will hinder and decompose the salt precipitation.

In the next section the core samples porosities, the core samples liquid, gas permeabilities, and their methods of determination are covered.

4.3 PHASE-II Porosity & Permeability

This section deals with the porosity determination by two methods, the helium gas porosimeter PORG-200 in Figure 3.10, and the liquid saturating method, the procedures to calculate the porosity for both methods covered in section 3.4.1.1. The experiments carried out for the sandstone core samples (Bentheimer, Castlegate and Idaho gray). In addition to porosity, the liquid and gas permeability measurement were covered as well. More details are explained as follows:

4.3.1 Porosity

This section deals with one of the important reservoir properties, which is the reservoir porosity. Porosity defines as the ratio of the void space in a rock to the bulk volume (BV) of that rock, multiplied by 100 to express in percent. Porosity is a scalar quantity because it is a function of the bulk volume used to define the sample size. In oil and gas industry this property could be measured by several methods, the most common ones are (i) using the Helium gas porosimeter Figure 3.10 to determine the pore grain volume, then the porosity can be calculated directly using equation (3.2) . (ii) porosity determination by liquid saturating method in which the core sample should be saturated with brine solution for certain period of time and then porosity calculation steps should be followed as shown in the below section.

PORG -200 for Porosity Determination

This apparatus in Figure 3.10 explained in section 3.4.1.1. It is used to determine the grain volume of the sandstone core samples (Bentheimer, Castlegate and Idaho gray). From core samples dimensions in Table 4.1, the bulk volume of each sample is calculated. The effective porosity can be directly from equation (3.2). The obtained porosities results for the stated sand stone core samples are below

Table 4.20 : core samples porosities by Helium gas porosimeter

	Bentheimer	Castlegate	Idaho Gray
D (cm)	2.52	2.53	2.54
L (cm)	2.52	2.53	2.54
A (cm ²)	4.9876	5.0273	5.0671
VB (cc)	12.5687	12.7190	12.8704
P1 (psi)	90	90	90
P2 (psi)	13.38	13.23	13.35
VG (cc)	9.9521	9.4603	9.8546
VP (cc)	2.6166	3.2586	3.0158
Porosity	0.2082	0.2562	0.2343

Where: VB is the bulk volume (core cross-sectional area x core length) in cm³

VG is the grain volume in cm³

Vp is the pore volume in cm³

ϕ (%) is the core sample porosity, fraction

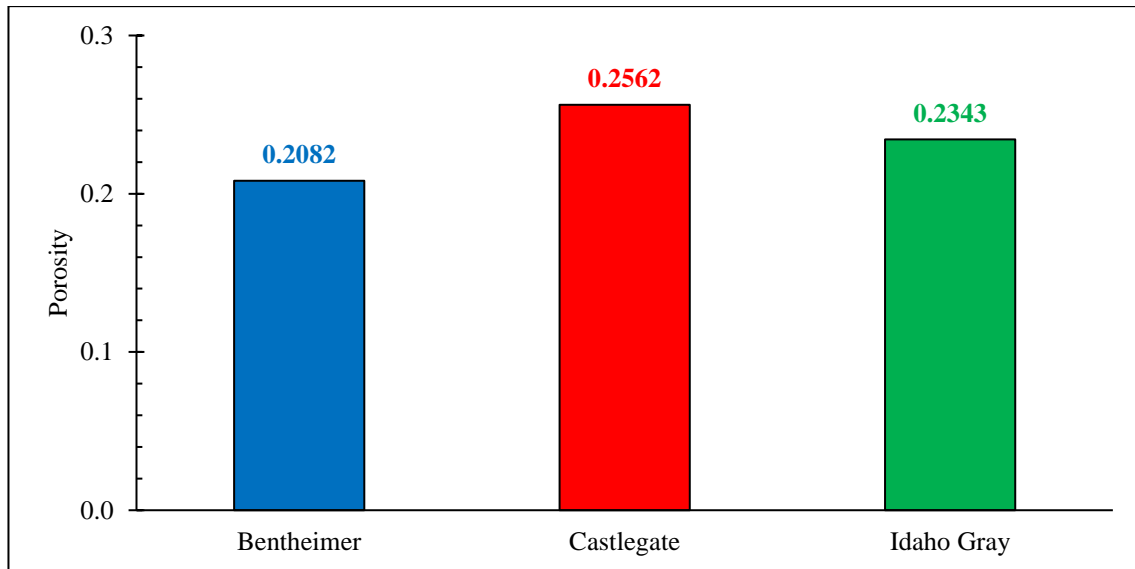


Figure 4.16: Porosity Measurement using PORG- 200

In Figure 4.16 the castlegate sandstone core sample gave the highest porosity (0.2562) comparing with the Bentheimer and Idaho gray core samples .This means that the core pores of this core sample are

well interconnected. On the other, hand all the above-mentioned types of sandstone are very good candidate to be utilised for CO₂ storage.

In summary, the Helium gas porosimeter method and the liquid saturating method for porosity measurement are common methods in the oil and gas industry. Both of them provide accurate and reliable results that can be used in the evaluation of reservoirs study.

Porosity Determination By Liquid Saturating Method

The porosity of a rock is a measure of the storage capacity (void space) that is capable of holding fluids. Quantitatively this important rock property is determined mathematically. The calculation is upon the weight difference between dry and wet core 100 % saturated with diluted core samples with known density. The porosity was then determined from equation (3.2). This method explained in section 3.4.1.1, the effective porosity determination carried out (interconnected void space of the core sample / core sample bulk volume). In this study spread excel sheet was prepared Table 3.6, and the porosity was calculated for the sandstone core samples (Bentheimer, Castlegate and Idaho gray). The obtained results are shown in Table 4.21

Table 4.21 : porosity determination spread sheet by liquid saturating method

	Bentheimer	Castlegate	Idaho Gray
D (cm)	2.5095	2.54	2.54
L (cm)	2.7051	2.54	2.54
A (cm²)	4.9461	5.0671	5.0671
VB (cc)	13.3797	12.8704	12.8704
W-Before (gm)	25.4	22.4	20.5
W-After (gm)	28.8	25.9	23.6
dW (gm)	3.4	3.5	3.1
Density (gm/cc)	1.075	1.114	1.073
VP (cm³)	3.1628	3.1418	2.8891
VG (cm³)	10.2169	9.7285	9.9813
Porosity	0.2364	0.2441	0.2245
Grain Density (g/cc)	2.4861	2.3025	2.0538
ρ Brine	1.075	1.114	1.073

Note:

D= diameter of core sample in cm

L = length of core sample in cm

A= Core sample area in cm²

VB = core sample bulk volume in cm³

W-Before (gm) = weight of the sample before saturating with brine solution

W-After (gm) weight of the sample after saturating with brine solution

dw = weight difference in grams (W-After – W-Before) in gm

ρ Brine = brine density in gm/cc

VP = pore volume in cm³

VG = grain volume in cm³

Porosity = (VP / VG), Fraction

Grain density = gm/cm³

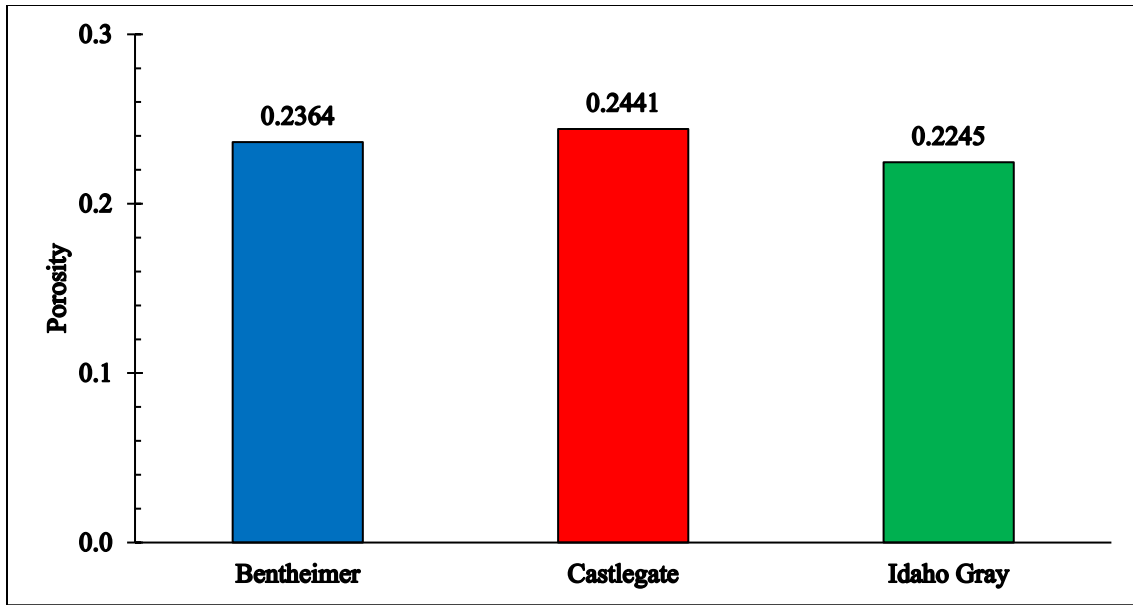


Figure 4.17 : Porosity Measurement using Liquid Saturating Method

In Figure 4.17 the Castlegate sandstone core sample gave the highest porosity (0.2441) comparing with the Bentheimer and Idaho gray core samples .this means that the core pores of this core sample are well interconnected. On the other hand, all the above-mentioned types of sandstone are very good candidate to be utilised for CO₂ storage.

4.3.2 Permeability

The permeability defines as measure of the fluid conductivity of the particular material. In 1856, Darcy investigated the flow of water through sand filters for water purification. Darcy used experimental apparatus; his observations interpreted and produced his equation named as Darcy's equation, which was explained in section 3.3.4. In this research the objective was to investigate the effect of brine solutions (10, 15, 20, 26.4 wt %) of (NaCl) on the liquid and gas permeability if the sandstone core samples (Bentheimer, Castlegate and Idaho gray) dried out in oven at 100⁰ C. The liquid permeability measured by PERL – 200, Figure 3.11 and spread excel sheet in Table 3.7 used to calculate the liquid permeability in (md). The gas permeability measured by PERG – 200, Figure 3.12 and spread excel sheet in Table 3.8 used to calculate the gas permeability in (md).The sections below show the effect of salinity on liquid permeability of the stated sandstone core samples.

4.3.3 Effect of Salinity on Liquid Permeability

Generally, only sandstone and carbonate rocks have the porosity needed to provide storage capacity and the permeability required for injectivity, while confining low-permeability shales and evaporates known as cap rock in the petroleum industry. All the above requirements are essential for achieving efficient storage of CO₂ in Saline aquifers and in depleted oil and gas reservoirs. Continuous dissolution of reactant minerals alters the concentration of aquifer fluid, therefore in later times leading to precipitation of product phases and Precipitation process may alter permeability and porosity significantly [44].

For maintaining the aquifer permeability, the diluting the brine in the near wellbore area or filling it with low salinity (seawater, brackish water or Fresh water) fluid before and during CO₂ injection can help in increasing the storage efficiency and avoid the pressure build up problems.

The most important property affecting injectivity is the absolute permeability of the rock. Regardless of porosity, the injected amount of CO₂ increases nearly with the reservoir permeability. In this study the Sandstone core samples (Bentheimer, Castlegate and Idaho gray) showed significant damage; between 2.0 % and 47 % loss in liquid core permeability after saturating samples with brine solutions (10, 15, 20, 26.4 wt %). The damage of the permeability took place due to assumed dry out phenomenon, the sandstone core samples dried in oven at 100⁰ C for 24 hours. An experimental work carried out in order to investigate the effect NaCl concentration on brine permeability. The apparatus PERL -200 Figure 3.11 was used to measure the brine permeability (K) in (md), and below the summary of the obtained results. The effect of salt precipitation in terms of NaCl on sand stone core samples (Bentheimer, Castlegate and Idaho gray) was investigated and, the obtained results and plots are shown below

Table 4.22 :Bentheimer sandstone core samples bine permeability

Bentheimer sandstone			
NaCl wt%	K(md) initial	K (md) final	Damage %
10	1200	1191	0.75
15	1200	1039	13.5
20	1200	924	23
26.4	1200	714	40.5

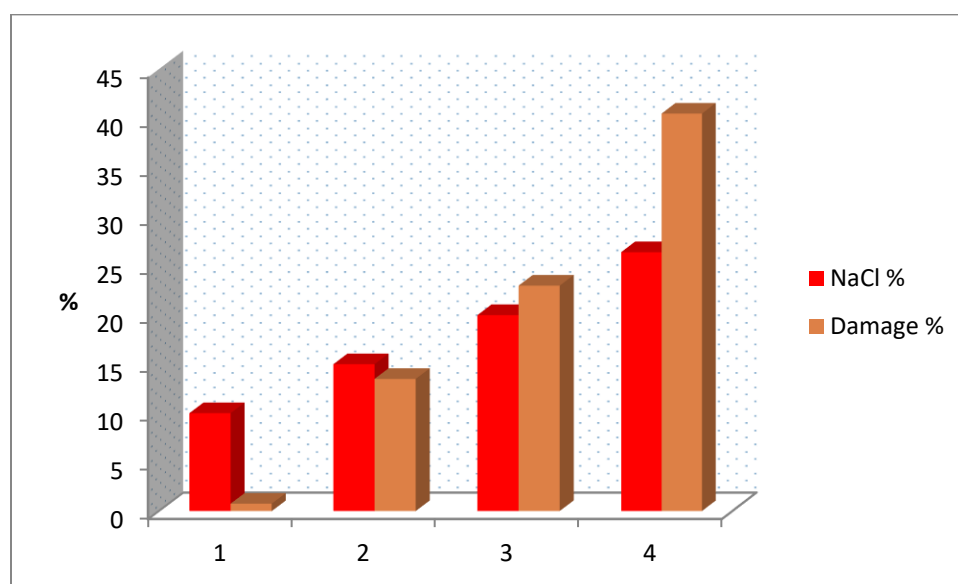


Figure 4.18: NaCl concentration % and permeability Damage % (Bentheimer sandstone)

Table 4.23 : Castlegate sandstone core samples brine permeability

Castlegate sandstone			
NaCl wt %	K (md) initial	K(md) final	Damage %
10	750	741	1.2
15	750	666	11.2
20	750	509	32
26.4	750	432	42

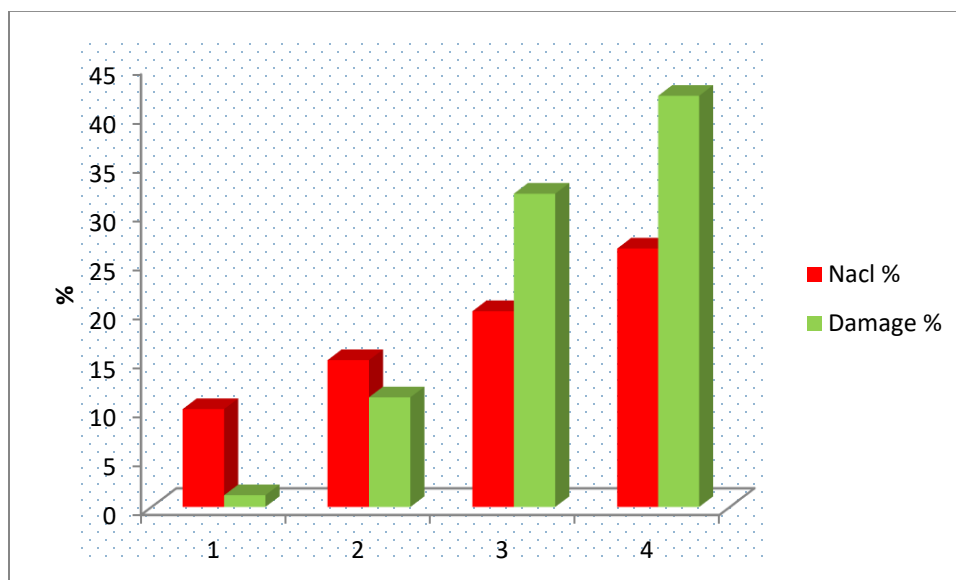


Figure 4.19: NaCl concentration % and permeability Damage % (Castlegate sandstone)

Table 4.24 : Idaho gray core samples brine permeability

Idaho gray sandstone			
NaCl wt %	K(md) initial	K(md) final	Damage %
10	2200	2155	2
15	2200	1986	9.7
20	2200	1814	17.5
26.4	2200	1178	47

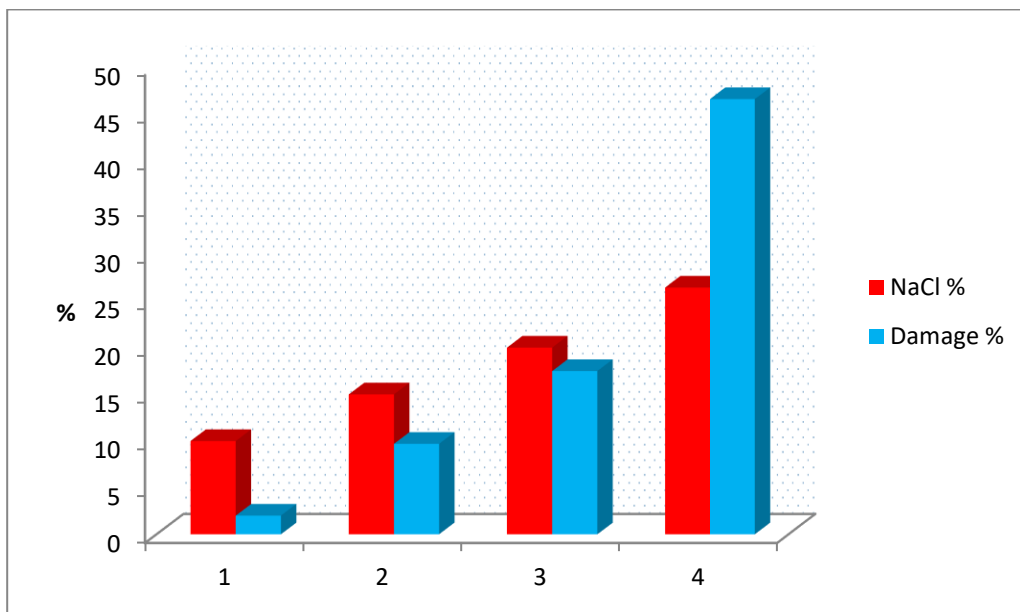


Figure 4.20: NaCl concentration % and permeability Damage % (Idaho gray sandstone)

In Figures 4.18 – 4.20 for all the studied sandstone core samples (Bentheimer, Castlegate and Idaho gray) it is clear that as the brine solution increases (NaCl %) the damage of the permeability increases, this takes place due the salt precipitation around the core samples, the precipitated salt blocked the pore throats of the core samples . All the stated sandstone core samples were dried in oven at 100 °C, this was done to meet the impact of salt precipitation and the dry out .The dry out has alteration on the core samples permeabilities and their injectivity performance. Therefore, it is believed that the dilution of formation water of the aquifers with low salinity (i.e. seawater, brackish water or fresh water) can assist to overcome these undesirable circumstances.

4.3.4 Effect of Salinity on Gas Permeability

Injection of huge quantities of CO₂ for underground geological storing in shallow or deep saline aquifers will lead to a strong water desaturation of the near wellbore because of drying mechanisms. In this context, drying mechanisms can precipitate the salt present in the aquifer and then lead to injectivity alteration. Saline aquifers contain water in the form of formation water. Formation water can contain considerable amounts of dissolved salts. Normally evaporation takes place due to high temperature in the aquifer, this will effect on the injection rate of CO₂ and will increase the bottom hole pressure and this disturbs the life time of CO₂ storage project.

If the salt precipitation phenomenon takes place, the rock permeability will damage and this leads to injectivity impairment. Sand stone core samples (Bentheimer, Castlegate and Idaho gray) Idaho gray, were subjected to be saturated with different brine salinity concentrations (10, 15, 20 and 26.4 wt%). The core samples dried in oven at 100 ° C for 24 hours, the objective was to investigate the permeability alteration Permeability (K_f/K_i), K_f is the final gas permeability of the core sample in (md) due the assumed dry out, and K_i is the initial gas permeability of the core sample in (md). The PERG - 200 in figure 3.12 used for the experimental work. Spread excel sheet in Table 3.8 used for the gas permeability calculation in (md), and the Table 4.17 shows the permeability variations and the experimental results. Figures 4.21 – 4.23 illustrate the gas permeability reduction of the studied sandstone core samples due to the effect of different brine concentrations in the form of NaCl wt %. The alteration of gas permeability investigated for the above-mentioned sandstone core samples and the details of the obtained results are shown below

Table 4.25 : effect of NaCl concentrations on gas permeability

Sample Name	NaCl	Final gas permeability K_{gf} (md) after vaporization
Bentheimer sandstone core sample, k_{gi} (initial gas permeability) = 2000 md	10	1904
	15	1750
	20	1311
	26.4	750
Castlegate sandstone core sample, k_{gi} (initial gas permeability) = 1000 md	10	929
	15	785
	20	580
	26.4	288
Idaho gray sandstone core sample, k_{gi} (initial gas permeability) = 7000 md	10	6830
	15	5894
	20	3483
	26.4	1438

4.3.4.1 The Gas permeability Alteration of Bentheimer Sandstone Core Samples

The Table 4.26 shows the obtained experimental results of gas permeability reduction due to the effect of salt precipitation (NaCl) on Bentheimer sandstone core samples. The core samples dried in oven at 100 °C for 24 hours to investigate the effect of dry out and salt precipitation on gas permeability.

Table 4.26: Gas permeability alteration of Bentheimer sandstone

NaCl %	Initial permeability K_i (md)	Final permeability k_f (md)	Permeability alteration (K_f/K_i)	Permeability damage %
10	2000	1904	0.95	4.8
15	2000	1750	0.88	12.5
20	2000	1311	0.66	34.5
26.4	2000	750	0.38	62.5

The Table 4.26 shows that for the Bentheimer sandstone core sample as the brine salinity increases in wt %, the gas permeability decreases , this was due to the effect of the precipitated salt around the core sample resulting from the assumed dry out problem (the core sample was dried in oven at 100 °C for 24 hours). Therefore, the decomposition of the precipitated salt by low salinity water could improve the aquifer permeability. Figure 4.21 shows the relation between the permeability alteration and the brine salinity, NaCl wt %.

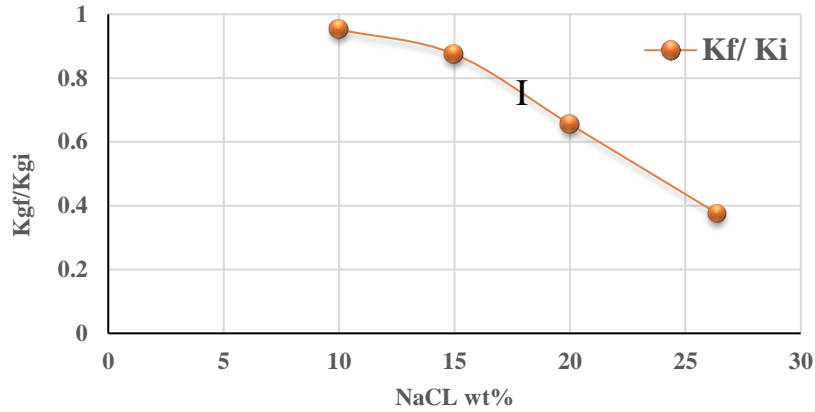


Figure 4.21: the permeability alteration and NaCl % for Bentheimer sandstone

4.3.4.2 The Gas permeability Alteration of Castlegate Sandstone Core Samples

The Table 4.27 shows the obtained experimental results of gas permeability reduction due to the effect of salt precipitation (NaCl) on Castlegate sandstone core samples. The core samples dried in oven at 100 °C for 24 hours to investigate the effect of dry out and salt precipitation on gas permeability.

Table 4.27 : Gas permeability alteration of Castlegate sandstone

NaCl %	Initial permeability K _i (md)	Final permeability k _f (md)	Permeability alteration (K _f /K _i)	Permeability Damage %
10	1000	929	0.93	7.1
15	1000	785	0.79	21.5
20	1000	580	0.58	42
26.4	1000	288	0.29	71.2

The Table 4.27 showed that for the Castlegate sandstone core sample as the brine salinity increases in wt %, the gas permeability decreases , this was due to the effect of the precipitated salt around the core sample resulting from the assumed dry out problem (the core sample was dried in oven at 100 °C for 24 hours). Therefore, the decomposition of the precipitated salt by low salinity water could improve the aquifer permeability. Figure 4.22 shows the relation between the permeability alteration and the brine salinity, NaCl wt %.

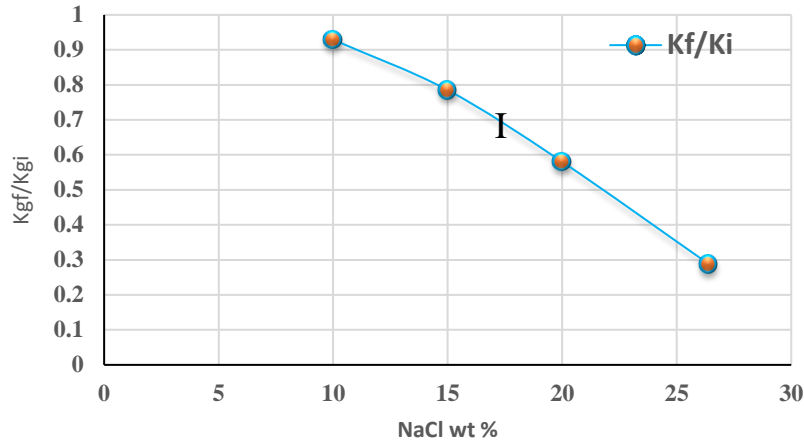


Figure 4.22: the permeability alteration and NaCl % for Castlegate sandstone

4.3.4.3 The Gas permeability Alteration of Idaho gray Sandstone Core Samples

The Table 4.28 shows the obtained experimental results of gas permeability reduction due to the effect of salt precipitation (NaCl) on Idaho gray sandstone core samples. The core samples dried in oven at 100 °C for 24 hours to investigate the effect of dry out and salt precipitation on gas permeability.

Table 4.28 : Gas permeability alteration of Idaho gray sandstone

NaCl %	Initial permeability K _i (md)	Final permeability k _f (md)	Permeability alteration (K _f /K _i)	Permeability Damage %
10	7000	6830	0.97	2.4
15	7000	5895	0.84	15.8
20	7000	3483	0.49	50.2
26.4	7000	1438	0.20	79.5

The Table 4.28 showed that for the Idaho gray sandstone core sample as the brine salinity increases in wt %, the gas permeability decreases , this was due to the effect of the precipitated salt around the core sample resulting from the assumed dry out problem (the core sample was dried in oven at 100 °C for 24 hours). Therefore, the decomposition of the precipitated salt by low salinity water could improve the aquifer permeability. Figure 4.23 shows the relation between the permeability alteration and the brine salinity, NaCl wt %.

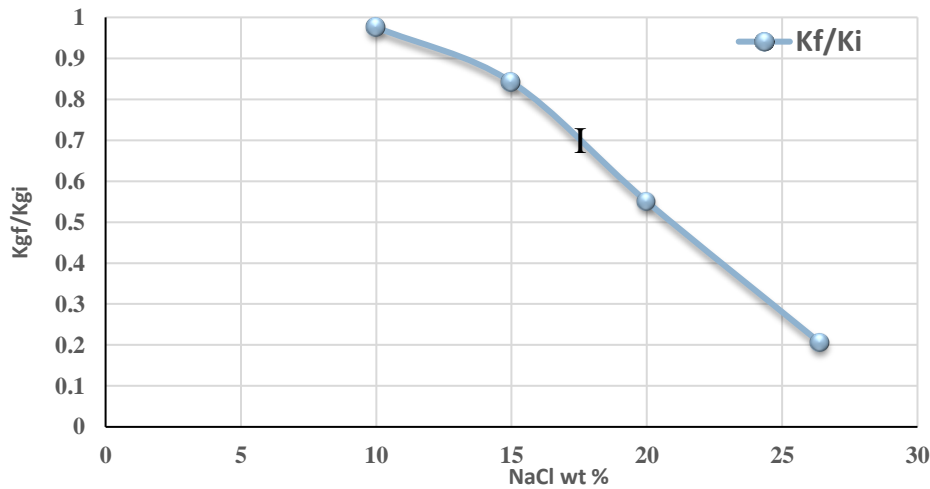


Figure 4.23 : the permeability alteration and NaCl % for Idaho gray sandstone

In Figures 4.21 – 4.23 for all the studied sandstone core samples (Bentheimer, Castlegate and Idaho gray) It is clear that as the brine solution increases (NaCl %) the damage of the gas permeability increases, this takes place due to the effect of salt precipitation around the core samples. All the stated sandstone core samples were dried in oven at 100 °C, this was done to meet the impact of salt precipitation and the dry out .The dry out has alteration on the core samples permeabilities and their injectivity performance. Therefore, it is believed that the dilution of formation water of the aquifers with low salinity (seawater, brackish water or fresh water) is perfect option that can assist to overcome these undesirable circumstances, if the used water for the dilution purpose meets the required technical specifications to avoid the impact of water incompatibility problems.

4.3.4.4 Liquid and Gas Permeability Damage Summary

In CO₂ standard storage strategy when CO₂ is injected as supercritical fluid, the salt precipitation is expected to take place in the near wellbore of the CO₂ injector, When this phenomenon occurs the aquifer petro physical properties will be effected. Bacci et al [28] measured porosity changes and the resulting permeability variations during supercritical CO₂ core flooding experiments. The experimental results showed that porosity decreased from an initial value of 22.6 to 16.0% after the fourth vaporisation test, while permeability decreased by 86% of the original value, dropping from 7.78 to

1.07 md. In this study, the investigation showed that the reduction in liquid and gas permeabilities due to the dry out were as the following:

Table 4.29 : Liquid and gas permeability damage due to halite precipitation.

Core sample	Initial liquid permeability in (md)	Initial gas permeability in (md)	Liquid Permeability damage %	Gas Permeability damage %
Bentheimer	1200	2000	0.75 – 40.5	4.8 – 62.5
Castlegate	750	1000	1.2 - 42	7.1 – 71.2
Idaho gray	2200	7000	2 - 47	2.4 – 79.5

It is believed that dilution of the aquifer salinity with low water salinity (Seawater) could assist to eliminate or delay the onset of salt precipitation problems, if the injected water is well treated. The core flooding tests results for the studied sandstone core samples (Bentheimer, Castlegate and Idaho gray) demonstrated that the brine concentration dilution has effectively improved the flow rate of CO₂ in l/min across the core samples. This means the periodical injection of low salinity water to the aquifer is reliable solution and it could be adopted as permanent strategy for improving the well injectivity during CO₂ storage in Saline aquifers.

Well injectivity is controlled by several factors, including formation permeability, thickness, relative permeability, and porosity reduction resulting from the precipitation of various minerals and salts. Of these factors, salt precipitation caused by brine vaporisation into the dry supercritical CO₂ stream is regarded as one of the most influential factors that decrease injectivity. Mitigation and control of borehole pressure at the bottom of an injection well is directly related to the effective management of well injectivity during geologic carbon sequestration activity. The bottom-hole pressure resulting from salt precipitation is one of the most important factors governing the efficiency and effectiveness of injection well as well as its life period.

4.4 The Porosity and the Permeability Relationship

A classic method of estimating permeability in the absence of permeability measurements is the so-called k-Phi method. Specifically, for unconsolidated sandstones it is often difficult to measure permeability because of irregularly shaped core plugs, which do not fit in the Ruska permeameter.

However, porosity can reliably measure on irregular samples using the buoyancy method and the permeability then estimated using the k-Phi method. The k-Phi method is based on an assumed logarithmic dependence of permeability on porosity.

4.4.1 The Porosity and the Brine Permeability Relationship

The Table 4.30 shows the sandstone core samples porosities and permeabilities that studied in this research.

Table 4.30 : Porosity and brine permeability of the core samples

Core Name	Porosity (%)	Brine Permeability (md)
Bentheimer	24	1200
castlegate	27	750
Idaho gray	29	2200
Average	26.7	1383

Figure 4.24 shows the relationship between the porosity and brine permeability.

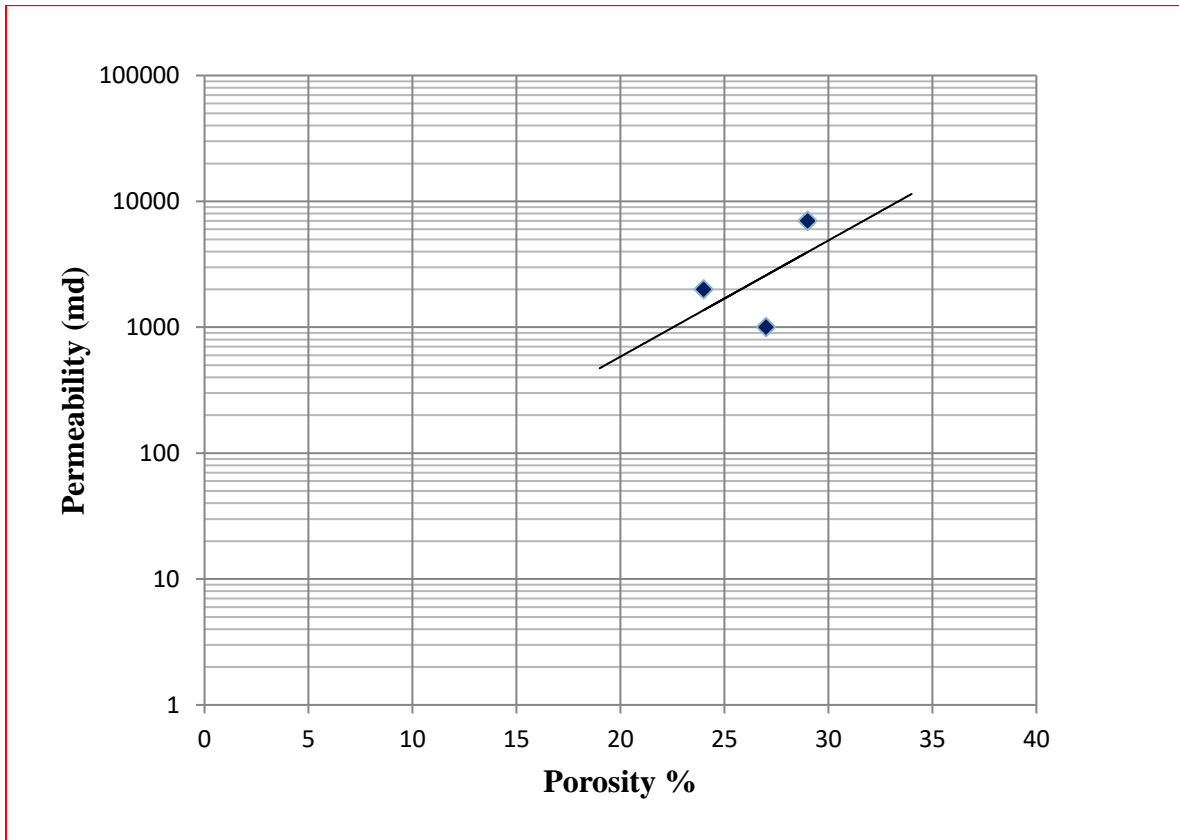


Figure 4.24: the relationship between the porosity and brine permeability

4.4.2 The Porosity and the gas Permeability Relationship

Three types of sandstone core samples were used for the investigations (Bentheimer, Castlegate and Idaho gray). The initial average properties of the samples that obtained from the core samples supplier Kocurek Industries, Inc. are given in Table 4.30 and Figure 4.25 shows the relationship between the porosity and gas permeability of the studied rocks.

Table 4.31 : Porosity and gas permeability of the core samples

Core Name	Porosity (%)	Gas Permeability (md)
Bentheimer	24	2000
castlegate	27	1000
Idaho gray	29	7000
Average	26.67	3333.33

Figure 4.25, illustrates the permeability vs. porosity of the employed core samples.

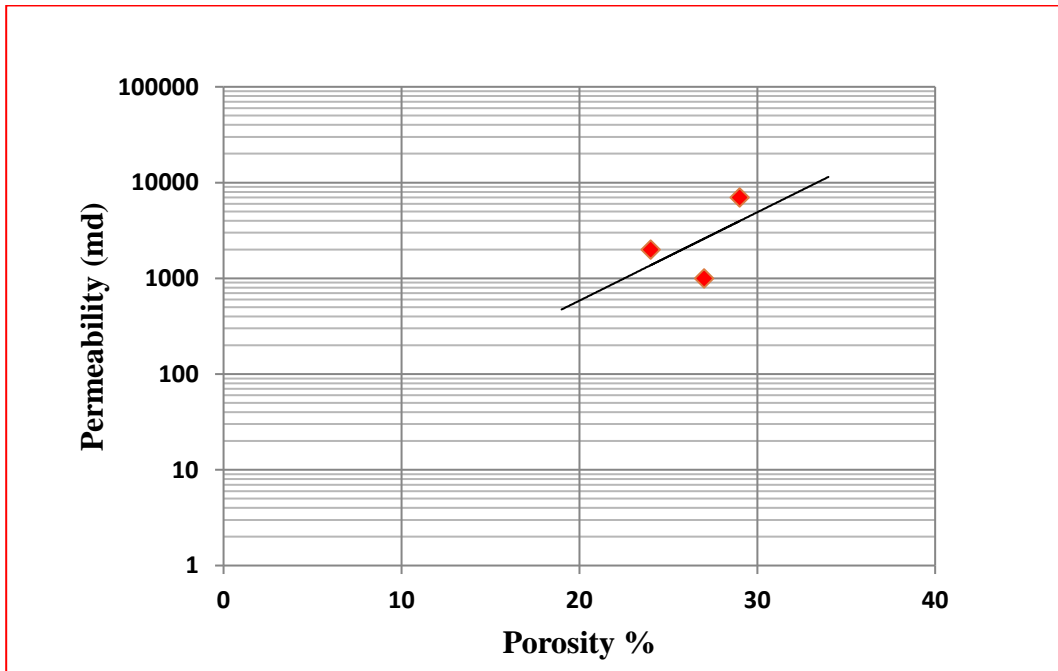


Figure 4.25: the relationship between the porosity and gas permeability of the studied rocks

The next section displays the CT scan. In this work the CT scan was used for porosity determination of the sandstone core samples (Bentheimer, Castlegate and Idaho gray), the objective was to validate the obtained results by this method with other techniques for porosity measurements. The stated core samples pore sizes and grain distributions were visualised.

4.5 PHASE III: CT Scanning

In this, work the sandstone core samples (Bentheimer, Castlegate and Idaho gray) CT scanned using CT scanner in Figure 3.15. The objective was for Visualisation (grain size and distribution), and porosity determination of the stated sandstone core samples in Figures 3.2. For quantification of the salt precipitation around the core sample, the Castlegate sand core sample that saturated with 26.4 wt% and dried in oven at 100 °C was CT scanned, the scan images displayed and analysed in next section. The main purpose of this phase is to validate the porosities results of CT scan for the stated core samples with the porosities that were calculated by Helium gas porosimeter and liquid saturating method.

4.5.1 CT Scan of Bentheimer Sandstone

The scan procedure of this sandstone core sample was explained in section 3.5.2. The Histogram, scan optimizer and the properties of defect detection analysis are shown in Figures 3.16 and 3.17.

4.5.2 CT Scan of Castlegate Sandstone

This section deals with the CT scan methodology of measurement presented in section 3.5.2. Carry out CT scan for the sand stone core sample of Castlegate. From scan results, the core sample porosity could be determined using, the module defect analysis from the Software Volume Graphics (VG).The obtained result was validated with other tests results for porosity determination. In the 3D volume, visualise grain structures, layering and fractures. For scanning the stated sandstone core sample, the scan procedure in the above-mentioned section (steps 1-7) were applied. Figure 4.26 shows the Histogram, scan optimizer and Figure 4.27 shows the properties and defect detection the sandstone core sample (Castlegate)

Chapter 4: Results and Discussion

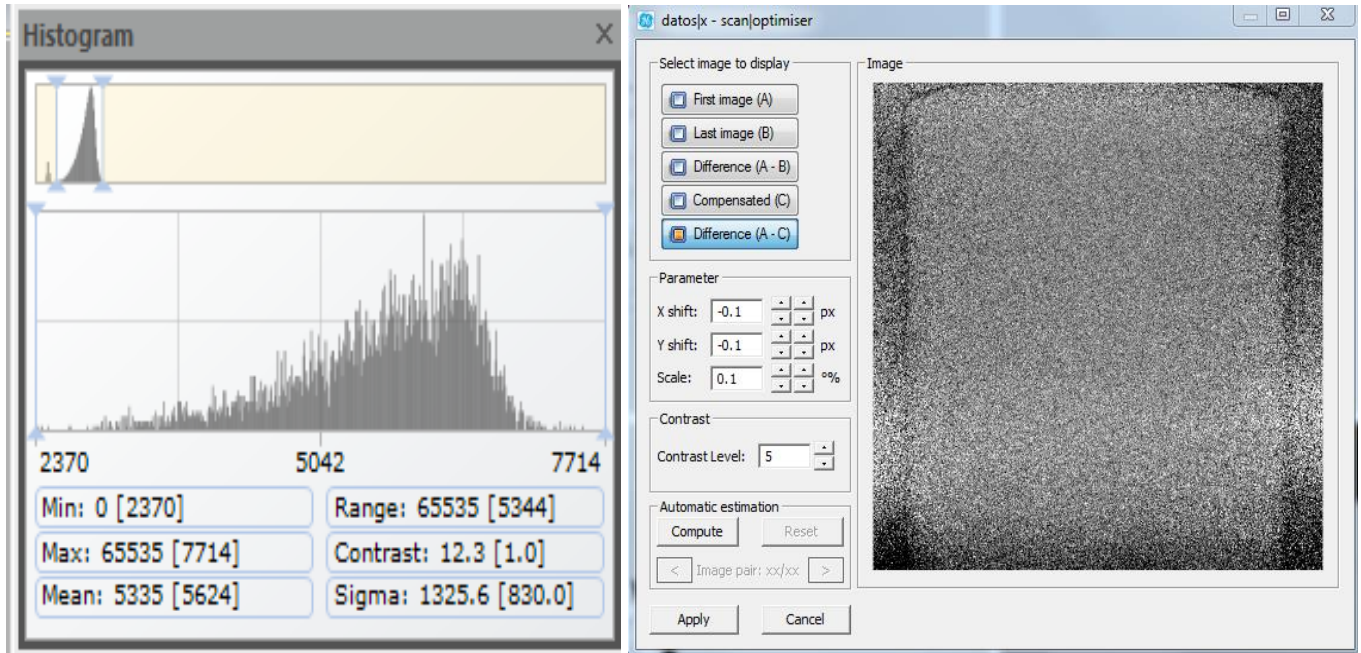


Figure 4.26: Histogram and scan optimiser for Castlegate sandstone.

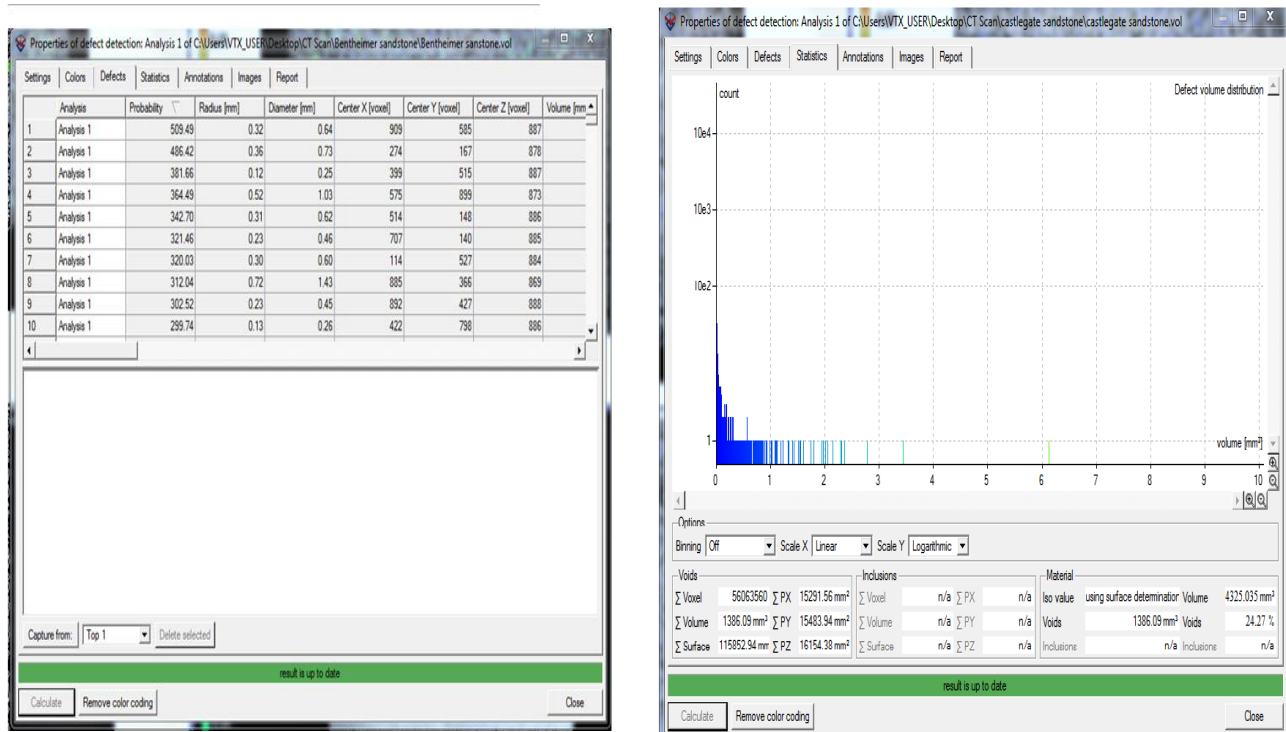


Figure 4.27: Properties of defect detection analysis for Castlegate sandstone core sample.

4.5.3 CT Scan of Idaho gray Sandstone

This section deals with the CT scan methodology of measurement presented in section 3.5.2. Carry out CT scan for the sand stone core sample of Idaho gray. From scan results, the core sample porosity could be determined using, the module defect analysis from the software volume Graphics (VG).The obtained result validated with other tests results for porosity determination. In the 3D volume, visualise grain structures, layering and fractures. For scanning the stated sandstone core sample, the scan procedure in in the above-mentioned section (steps 1-7) were applied. Figure 4.28 below represents the scan Histogram, scan optimizer and Figure 4.29 shows the properties and defect detection the sandstone core sample (Idaho gray)

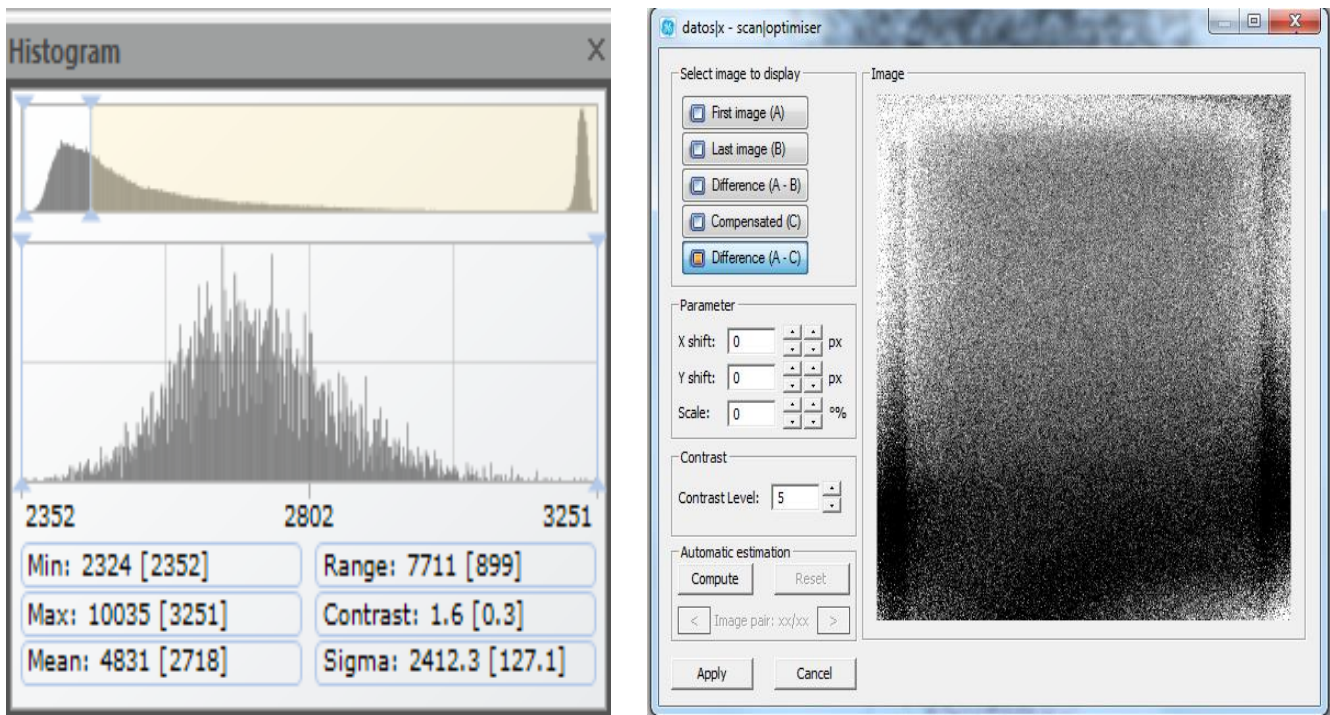


Figure 4.28: Histogram and scan optimizer for Idaho gray sandstone.

Chapter 4: Results and Discussion

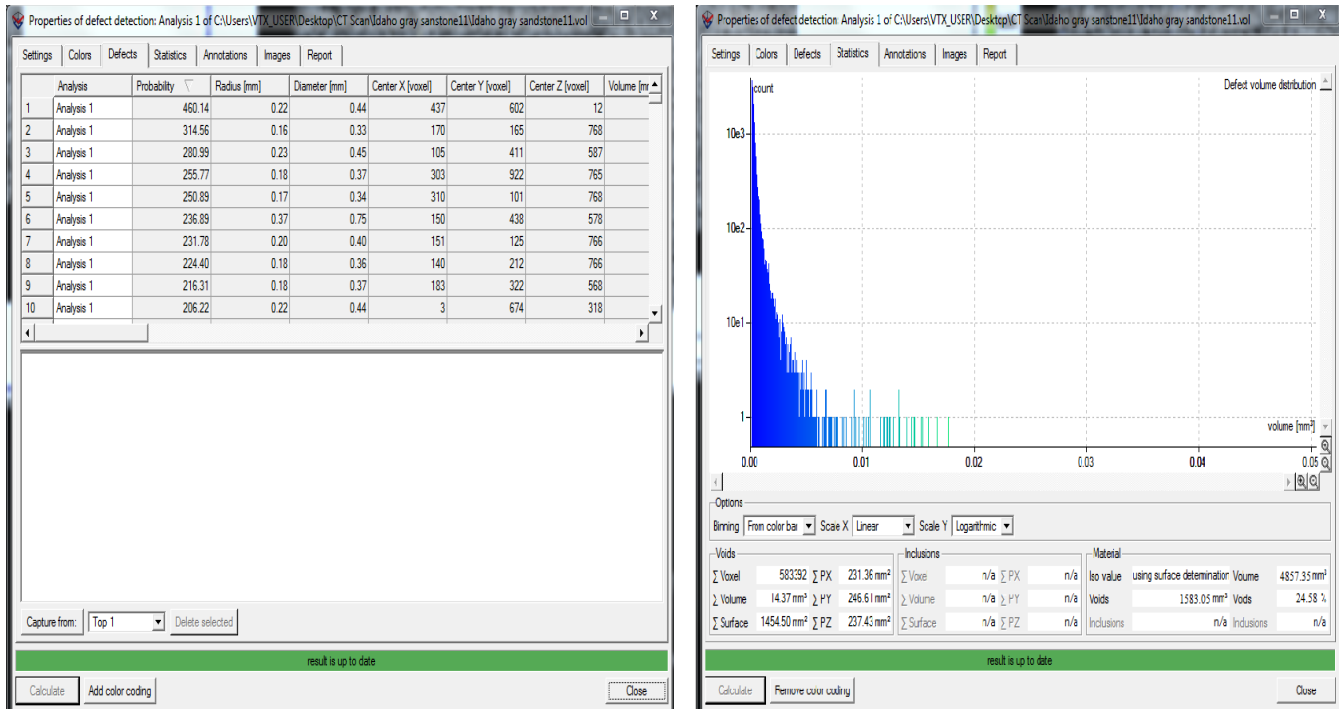


Figure 4.29: Properties of defect detection analysis for Idaho gray sandstone core sample.

4.5.4 Images and Visualisation of the Scanned Core Sample

Figures 4.30 – 4.32 show representative image for the scanned core samples (Bentheimer, Castlegate and Idaho gray). Visually all the scanned core samples show the grain size distribution and the pore size distribution. The pore distribution demonstrates that the stated core samples have good porosity. The Volume Graphics Software was used for the porosity determination of the scanned core samples. The porosity results are shown in the above-mentioned Figures.

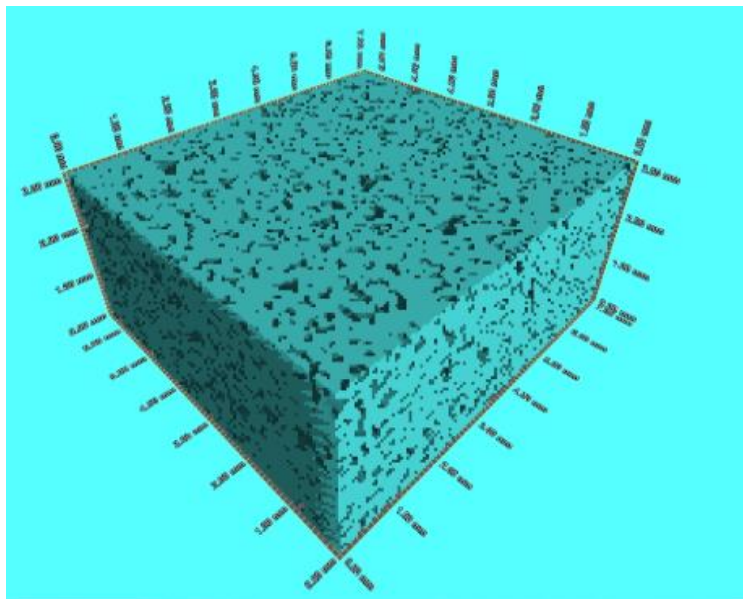


Figure 4.30: Visualisation of the pore spaces for porosity calculation (Bentheimer sandstone), Porosity = 20.7 %

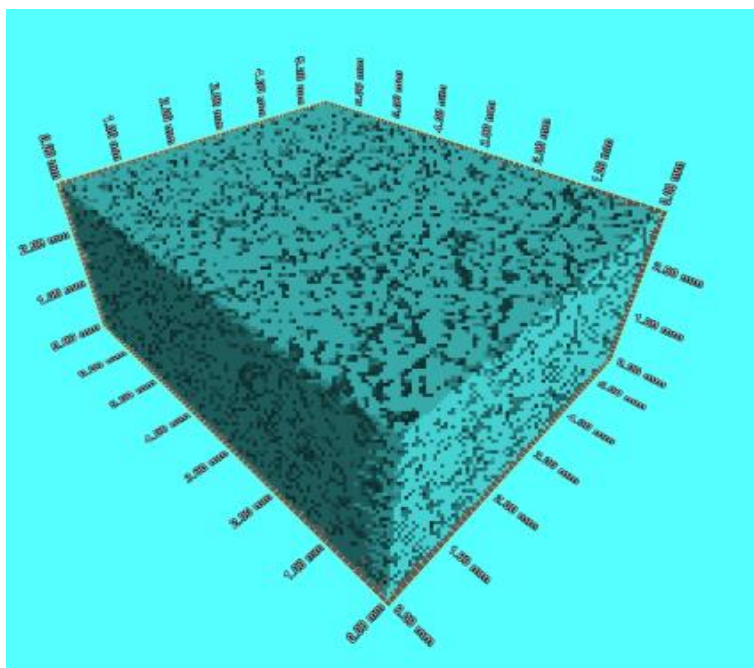


Figure 4.31: Visualisation of the pore spaces for porosity calculation (Castlegate sandstone), Porosity = 24.3 %

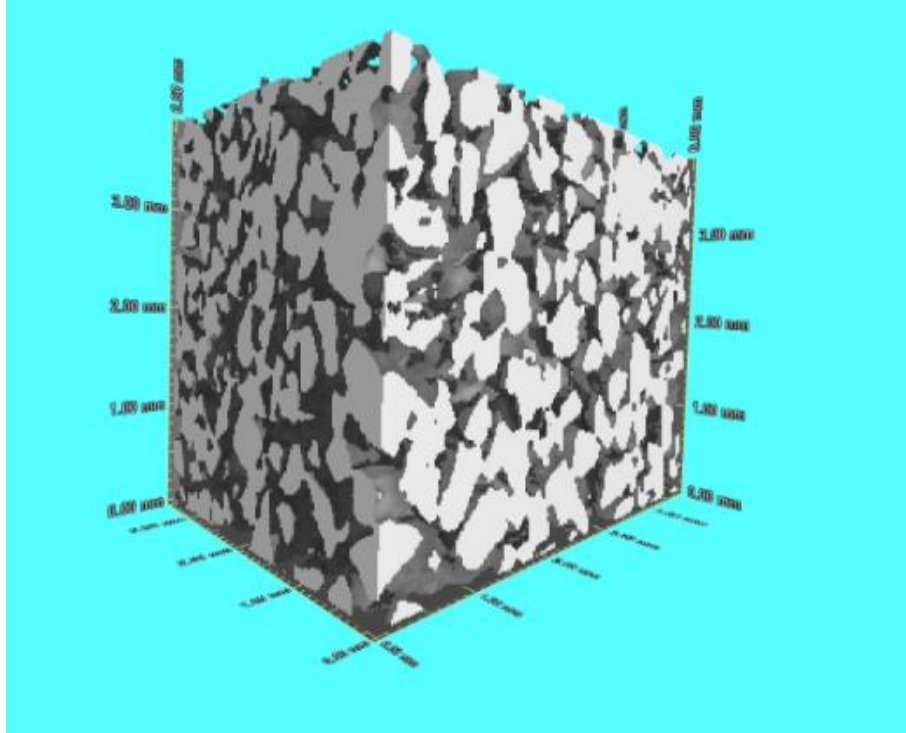


Figure 4.32: Visualisation of the pore spaces for porosity calculation (Idaho gray) sandstone), Porosity = 24.6 %

4.5.5 CT Scan Visualisation and Quantification of Salt Precipitation

Figure 4.33 shows 3D image obtained by μ -CT scanning for Idaho gray core sample after the dry-out experiment, the scan was carried out for the sample that was saturated with 26.4 wt % brine concentration. The image quality allows for a clear distinction between gas, solid matrix and precipitated salt. Precipitated salt is clearly visible as bright spots in the pore space compared to the initially dry rock. Approximately 1000 slices reconstructed along the core length resulting in a 3D image in Figure 4.33. On the left-hand side, the wall thickness, while the initial rock is shown on the right side. The location of formation of salt crystals is crucial to the connectivity of the flow path. The salt formation can be observed in small, well as large pores and a uniform distribution throughout the core. Solid salt could not quantify directly from the CT scans, but the results indicate that salt precipitation takes place throughout the upper part in case of the Idaho gray core sample. The precipitated salts had higher density compared to the others and were recorded as brighter solids on CT image.

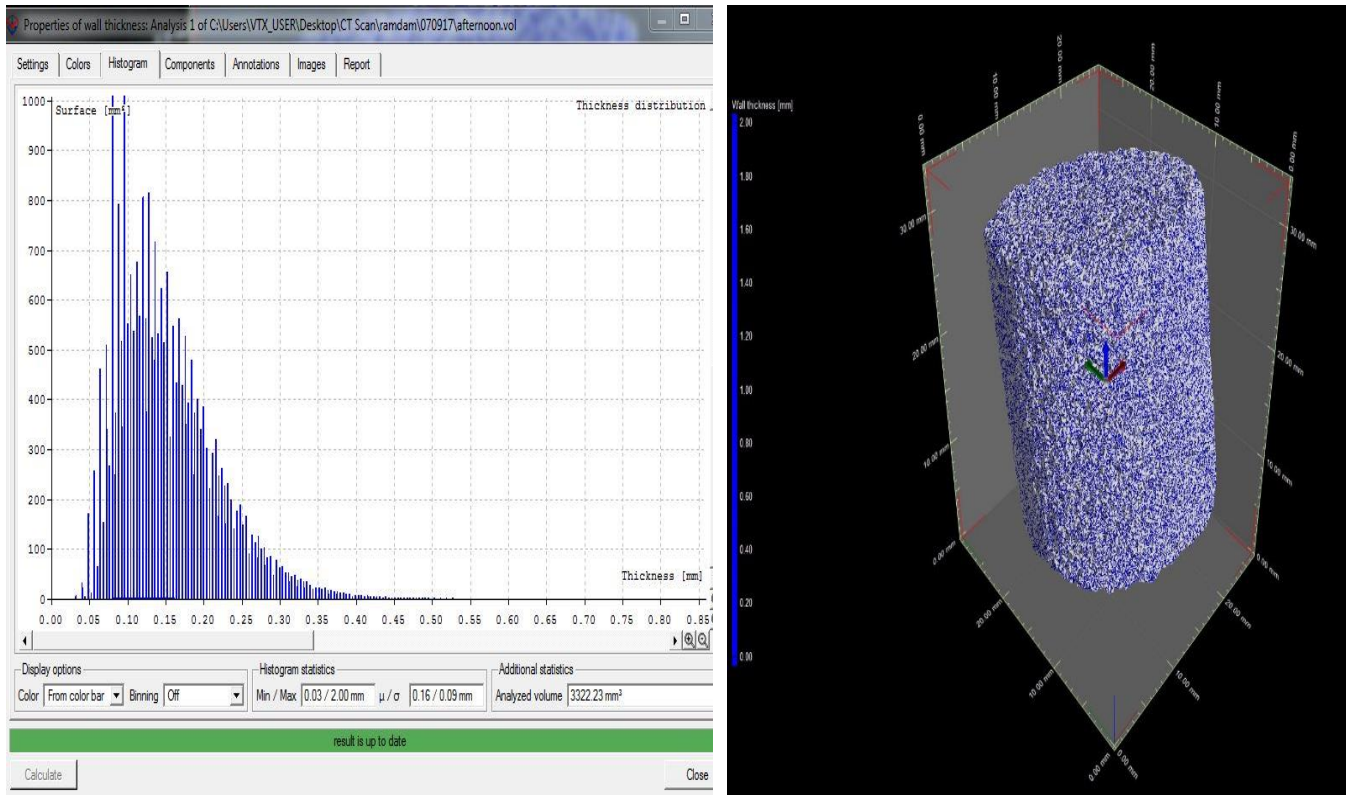


Figure 4.33: Wall thickness and 3D image of the saturated brine Idaho gray core sample

4.5.6 Porosity Determination Summary

The Table 4.32 shows the summary results of porosities determination by Helium gas porosimeter, liquid saturating method and CT scan method. All the obtained results demonstrated that the (Bentheimer, Castlegate and Idaho gray) sand stone core samples have good porosities. All the used techniques are reliable for porosity determination, and it is difficult to evaluate which method is more reliable without reference to specific interpretation problem.

Table 4.32 : Shows comparison between porosity computed by helium gas method (A), liquid saturating method (B) and CT scan method (C)

No	Core Name	Porosity (A) ϕ (%)	Porosity (B) ϕ (%)	CT Scan (C) ϕ (%)	Average ϕ (%)
1	Bentheimer	20.82	23.64	20.7	21.72
1	Cstlegate	25.62	24.41	24.3	24.77
3	Idaho gray	23.43	22.45	24.6	23.49
Average		23.29	23.5	23.2	23.33

4.6 Summary

- Measurements of the porosity and the permeability of sandstone core samples are essential
- Sandstone core samples (Bentheimer, Castlegate and Idaho gray) dimensions were recorded in Table 4.1
- Salinity, viscosity and density of the brine solutions were demonstrated, in addition to this their relationships were plotted as shown in Figures 4.1 – 4.3
- The core flooding tests results proved that the dilution of brine concentration with seawater could improve the flow rate of CO₂ in l/min for the studied core samples in sections 4.3.1 – 4.3.3; this will assist in improving the well injectivity.
- Porosity were calculated for the stated core samples, all samples showed good porosities
- The permeability damage % increases as the brine concentration (NaCl %) increases.
- The permeability alteration is defined as the ratio of gas permeability after drying with the initial one K_{g_f}/K_{g_i} . The alteration is represented versus the brine concentration for NaCl for (Bentheimer, Castlegate and Idaho gray) sandstone as shown in Figures 4.21 – 4.23.
- After drying the core samples at the temperature of 100 °C, all the core samples were visually investigated and showed that the salt precipitation was localised on the surface of the sample, this will cause pores blocking by solid salt precipitations.
- Saturating the samples with NaCl solution using sea salt (3.5 wt % concentration) assisted to dilute the brine concentration and this contributed to improve the core permeability and the injectivity as well.
- The presence of suspended solids in the injected water causes permeability damage. These objects will plug the pore spaces within the rock and therefore the flow rate of the injected CO₂ will reduce; as a result, injectivity declines if the water quality is not maintained. Seawater should be treated before it is distributed to the various CO₂ injectors. The treatment should be designed to meet the water quality standards listed in Table 3.2 to prevent and minimise formation plugging from solid particles.

- Diluting of brine concentration by seawater can eliminate or delay the onset of salt precipitation problems and assist to improve the well injectivity and avoid the pressure build up consequences during CO₂ storage in saline aquifers.
- CT scan can provide qualitative results and analysis that assist for further studies of the reservoir rocks and their characterisations.

Chapter 5: Conclusion and Recommendations

5.1 Conclusions

The following conclusions were drawn from this study:

- The core flooding tests results for the studied core samples (Bentheimer, castlegate and Idaho gray) showed that when the core samples were saturated in low salinity brine solution 3.5 wt %, the CO₂ flow rates improved, this indicates that the injectivity will increase, the differential pressure across the core sample will decrease.
- Bentheimer sandstone sample was damaged 40.5% loss in liquid permeability) due to salt precipitation in the form of NaCl around the core sample.
- Castlegate sandstone were damaged 42% loss in liquid permeability) due to salt precipitation in the form of NaCl.
- Idaho gray sandstone were damaged 47% loss in liquid permeability) due to salt precipitation in the form of NaCl around the core sample.
- It is obvious that increasing in brine concentration (NaCl) will promote the salt precipitation, and this will cause gas permeability impairment.
- Increase in permeability leads to increase the well injectivity and this will increase the CO₂ storage efficiency.
- Increase in salinity leads to decreased dissolution of CO₂ in brine; this will promote the near well bore formation dry out and salt deposition problems.
- The brine concentration (NaCl) has effect on gas permeability and tables 4.26, 4.27 and 4.28 show the gas permeability alteration for the studied sandstone core samples.
- CT scanning porosity determination showed that porosities for the studied core samples (Bentheimer, Castlegate and Idaho gray) are 20.7, 24.3 and 24.6 % respectively.

- Figures 4.30 – 4.32 show the Visualisation of the pore spaces for porosity determination of the studied sandstone core samples (Bentheimer, Castlegate and Idaho gray).

5.2 Future Work and Recommendation

- Use ECLIPSE -300 simulator and design reservoir model for the reservoir simulation to predict the saturation evolution in the wellbore investigate the alteration of permeability due to salt precipitation phenomena, throughout different salinities scenarios. The design should be used to investigate the degree at which the CO₂ would be stored without any possible eventualities (like leakage, fractures).
- Similar investigations are recommended to be conducted for limestone core samples in order to compare the effectiveness of injecting low salinity water in improving the well injectivity during CO₂ storage in geological formation.
- Two strategies are recommended to be adopted to avoid the impact with salt precipitation problems during CO₂ storage in saline aquifers:-
 - Periodic flush the formation with low salinity (Brackish water) from shallow formation water for onshore fields.
 - Periodic flush the formation with seawater for offshore fields.

Seawater is the considered the cheapest source that could be utilised for offshore fields, for the onshore fields brackish water (low salinity water from shallow formation) is reasonable source. River water can only be used if the above sources are not due to it high contents of suspended solids available. In order to achieve good water injection system the injected water should be treated properly to eliminate any unwanted contaminants that may promote the top side and down hole scale problems. If scale takes place the reservoir characteristics (porosity and permeability will be reduced, the well injectivity will be effected as well.

References

- [1] S. Bachu, "Carbon Dioxide Storage in Geological Media," 2012.
- [2] M. Sengul, "CO₂ sequestration - A safe transition technology," *8th SPE Int. Conf. Heal. Saf. Environ. Oil Gas Explor. Prod.* 2006, vol. 2, pp. 693–702, 2006.
- [3] K. Damen, A. Faaij, and W. Turkenburg, "Health, safety and environmental risks of underground CO₂ storage - Overview of mechanisms and current knowledge," *Clim. Change*, vol. 74, no. 1–3, pp. 289–318, 2006.
- [4] M. Van der Hoeven, "CO₂ Emissions from Fuel Combustion Highlights," *Int. Energy Agency*, pp. 1–134, 2011.
- [5] S. Holloway, "Carbon dioxide capture and geological storage.," *Philos. Trans. A. Math. Phys. Eng. Sci.*, vol. 365, no. 1853, pp. 1095–107, 2007.
- [6] OCP Corporate, "Fact Sheet," no. July 2011, 2014.
- [7] Iea, "World Energy Outlook 2006," *Outlook*, p. 600pp, 2006.
- [8] K. E. Trenberth and J. T. Fasullo, "An apparent hiatus in global warming?," *Earth 's Futur.*, vol. 1, no. 1, pp. 19–32, 2013.
- [9] J. Melorose, R. Perroy, and S. Careas, *climate change 2007*, vol. 1. 2015.
- [10] IPCC Working Group I, "Climate Change 2001: The Scientific Basis," *Clim. Chang. 2001 Sci. Basis*, p. 881, 2001.
- [11] D. Bennion and S. Bachu, "Dependence on Temperature , Pressure , and Salinity of the IFT and Relative Permeability Displacement Characteristics of CO₂ Injected in Deep Saline Aquifers," *SPE Annu. Tech. Conf.*, no. October, pp. 1–9, 2006.
- [12] F. Delprat-Jannaud *et al.*, "State of the Art review of CO₂ Storage Site Selection and Characterisation Methods," no. September, 2013.
- [13] a Bachu, C. Hawkes, M. Pooladi-Darvish, and E. Perkins, "CCS Characterisation Criteria," no. July, 2009.
- [14] a Busch, a Amann, P. Bertier, M. Waschbusch, and B. M. Krooss, "SPE 139588 The Significance of Caprock Sealing Integrity for CO₂ Storage," *SPE Int. Conf. CO₂ Capture, Storage, Util.*, no. November, pp. 10–12, 2010.
- [15] S. Bachu, "Screening and ranking of sedimentary basins for sequestration of CO₂ in geological media in response to climate change," *Environ. Geol.*, vol. 44, no. 3, pp. 277–289, 2003.
- [16] T. L. Watson and S. Bachu, "Evaluation of the Potential for Gas and CO₂ Leakage Along Wellbores," *SPE Drill. Complet.*, no. March, pp. 115–126, 2009.
- [17] L. Zhu, H. Gong, Z. Dai, G. Guo, and P. Teatini, "Modeling 3-D permeability distribution in alluvial fans using facies architecture and geophysical acquisitions," *Hydrol. Earth Syst. Sci.*, vol. 21, no. 2, pp. 721–733, 2017.
- [18] S. Mo and I. Akervoll, "Modeling Long-Term CO₂ Storage in Aquifer with a Black-Oil Reservoir Simulator," *SPE/EPA/DOE Explor. Prod. Environ. Conf. Galveston, Texas, USA, March 7-9, 2005*.
- [19] G. E. Pickup *et al.*, "Geological storage of CO₂: Site appraisal and modelling," *Energy*

References

- Procedia*, vol. 4, no. C, pp. 4762–4769, 2011.
- [20] S. Furnival, “Near Wellbore Drying-Out & Salt Precipitation during CO₂ Injection into a Saline Aquifer Steve Furnival , AGR Petroleum Services Agenda □ National Grid Carbon (NGC) hold UK ’ s first Carbon Storage Licence CS001 for White Rose Project □ UK SNS Saline Aq.”
- [21] W. Kleinitz, M. Koehler, G. Dietzsch, and P. E. Gmbh, “The precipitation of salt in gas producing wells,” *SPE Eur. Form. damage Conf.*, pp. 1–7, 2001.
- [22] S. M. Benson and L. Myer, “Monitoring to ensure safe and effective geologic sequestration of carbon dioxide,” *Work. Carbon Dioxide Storage, Proc.*, no. November, pp. 137–151, 2002.
- [23] a Kumar, M. Noh, G. a Pope, K. Sepehrnoori, S. Bryant, and L. W. Lake, “Reservoir Simulation of CO₂ Storage in Deep Saline Aquifers,” *SPE/DOE Symp. Improv. Oil Recover.*, 2004.
- [24] H. Ott, J. Snippe, K. De Kloe, H. Husain, and a. Abri, “Salt precipitation due to sc-gas injection: Single versus multi-porosity rocks,” *Energy Procedia*, vol. 37, pp. 3319–3330, 2013.
- [25] M. Azaroual, L. Andre, and Y. Peysson, “Behaviour of the CO₂ injection well and the near wellbore during carbon dioxide injection in saline aquifers,” *Proceedings, TOUGH ...*, pp. 1–8, 2012.
- [26] J. Ennis-King and L. Paterson, “Engineering Aspects of Geological Sequestration of Carbon Dioxide,” *SPE Asia Pacific Oil Gas Conf. Exhib.*, 2002.
- [27] D. O. Kartikasurja, H. Rds, T. G. Lin, M. W. Sukahar, and B. Viratno, “SPE 114553 Study of Produced CO₂ Storage into Aquifer in an Offshore Field , Malaysia,” *Group*, pp. 1–16, 2008.
- [28] G. Bacci, A. Korre, and S. Durucan, “An experimental and numerical investigation into the impact of dissolution/precipitation mechanisms on CO₂ injectivity in the wellbore and far field regions,” *Int. J. Greenh. Gas Control*, vol. 5, no. 3, pp. 579–588, 2011.
- [29] Y. Peysson, B. Bazin, C. Magnier, E. Kohler, and S. Youssef, “Permeability alteration due to salt precipitation driven by drying in the context of CO₂ injection,” *Energy Procedia*, vol. 4, pp. 4387–4394, 2011.
- [30] K. Pruess and N. Müller, “Formation dry-out from co₂ injection into saline aquifers: 1. effects of solids precipitation and their mitigation,” *Water Resour. Res.*, vol. 45, no. 3, pp. 1–11, 2009.
- [31] L. André, Y. Peysson, and M. Azaroual, “Well injectivity during CO₂ storage operations in deep saline aquifers - Part 2: Numerical simulations of drying, salt deposit mechanisms and role of capillary forces,” *Int. J. Greenh. Gas Control*, vol. 22, pp. 301–312, 2014.
- [32] I. W. Wright, “The in Salah Gas CO₂ storage project,” *Int. Pet. Technol. Conf. 2007, IPTC 2007*, vol. 1, no. December, pp. 658–663, 2007.
- [33] M. Zeidouni, D. Keith, and M. Pooladi-Darvish, “Sensitivity Analysis of Salt Precipitation and CO₂ -Brine Displacement in Saline Aquifers,” *2009 SPE Int. Conf. Co₂ Capture, Storage Util.*, pp. 1–16, 2009.

References

- [34] M. Delshad, M. F. Wheeler, and X. Kong, “A Critical Assessment of CO₂ Injection Strategies in Saline Aquifers,” *Conf. Pap.*, no. May, pp. 27–29, 2010.
- [35] S. S. R. Jasinski, Schlumberger Dowell, WSableolle, SPE, ShellExpro and M. Amory, “SPE-38767-MS.pdf,” in *Scale Prediction and control for Heron Cluster*, 1997.
- [36] P. R. R. C. William Ampomah, Robert S. Balch and Reid B. Grigg, “Co-optimization of CO₂-EOR and storage processes in mature oil reservoirs,” *Greenh. Gases Sci. Technol.*, vol. 2, no. 6, pp. 408–418, 2012.
- [37] P. Chiquet, D. Broseta, and S. Thibeau, “Wettability alteration of caprock minerals by carbon dioxide,” *Geofluids*, vol. 7, no. 2, pp. 112–122, 2007.
- [38] Y. Geraud, F. Surma, and F. Mazerolle, “Porosity and fluid flow characterization of granite by capillary wetting using X-ray computed tomography,” *Geol. Soc. London, Spec. Publ.*, vol. 215, no. 1, pp. 95–105, 2003.
- [39] S. Shameem and A. Khamees, “Dual-Energy CT-Scanning Applications in Rock Characterization,” *Proc. SPE Annu. Tech. Conf. Exhib.*, 2004.
- [40] D. H. Phillips and J. J. Lannutti, “Measuring physical density with X-ray computed tomography,” *Indep. Nondestruct. Test. Eval. Int.*, vol. 30, no. 6, pp. 339–350, 1997.
- [41] B. D. Nielsen, “Non-Destructive Soil Testing Using X-ray Computed Tomography,” no. November, 2004.
- [42] M. A. Bataweel, H. A. Nasr-el-din, and D. S. Schechter, “Fluid Flow Characterization of Chemical EOR Flooding : A Computerized Tomography (CT) Scan Study,” *SPE/DGS Saudi Arab. Sect. Tech. Symp. Exhib. Al-Khobar, Saudi Arab. May 15-18. SPE 149066-MS*, no. 1990, pp. 1–15, 2011.
- [43] S. A. A.M. Al-Hamad, “Factors Affecting Injectivity Decline,” *J. Chem. Inf. Model.*, vol. 53, pp. 1689–1699, 2013.
- [44] O. Izgec, B. Demiral, H. Bertin, and S. Akin, “CO₂ injection into saline carbonate aquifer formations II: Comparison of numerical simulations to experiments,” *Transp. Porous Media*, vol. 73, no. 1, pp. 57–74, 2008.

APPENDIX – A: Journal Publications